2014

FIELD-SCALE WATER AND SOLUTE TRANSPORT

Yang Yang
University of Kentucky, yangyang0524@gmail.com

STUDENT AGREEMENT:

I represent that my thesis or dissertation and abstract are my original work. Proper attribution has been given to all outside sources. I understand that I am solely responsible for obtaining any needed copyright permissions. I have obtained needed written permission statement(s) from the owner(s) of each third-party copyrighted matter to be included in my work, allowing electronic distribution (if such use is not permitted by the fair use doctrine) which will be submitted to UKnowledge as Additional File.

I hereby grant to The University of Kentucky and its agents the irrevocable, non-exclusive, and royalty-free license to archive and make accessible my work in whole or in part in all forms of media, now or hereafter known. I agree that the document mentioned above may be made available immediately for worldwide access unless an embargo applies.

I retain all other ownership rights to the copyright of my work. I also retain the right to use in future works (such as articles or books) all or part of my work. I understand that I am free to register the copyright to my work.

REVIEW, APPROVAL AND ACCEPTANCE

The document mentioned above has been reviewed and accepted by the student's advisor, on behalf of the advisory committee, and by the Director of Graduate Studies (DGS), on behalf of the program; we verify that this is the final, approved version of the student's thesis including all changes required by the advisory committee. The undersigned agree to abide by the statements above.

Yang Yang, Student

Dr. Ole Wendroth, Major Professor

Dr. Mark Coyne, Director of Graduate Studies

FIELD-SCALE WATER AND SOLUTE TRANSPORT

DISSERTATION

A dissertation submitted in partial fulfillment of the
requirements for the degree of Doctor of Philosophy in the
College of Agriculture, Food and Environment
at the University of Kentucky

By
Yang Yang

Lexington, Kentucky

Director: Dr. Ole Wendroth, Professor of Soil Physics

Lexington, Kentucky

2014

ABSTRACT OF DISSERTATION

FIELD-SCALE WATER AND SOLUTE TRANSPORT

Spatial variability of soil properties complicates the understanding of water and solute transport at the field scale. This study evaluated the impact of land use, soil surface roughness, and rainfall characteristics on water transport and Br^- leaching under field conditions by means of a new experimental design employing scale-dependent treatment distribution. On a transect with two land use systems, i.e., cropland and grassland, rainfall intensity and the time delay between Br^- application and subsequent rainfall were arranged in a periodically repetitive pattern at two different scales. Both scales were distinct from the scale of surface roughness as described by elevation variance. Nests of tensiometers and suction probes were installed at 1-m intervals along the transect to monitor matric potentials and Br^- concentrations at different depths, respectively. After rainfall simulation, soil samples were collected at every 0.5 m horizontal distance in 10 cm vertical increments down to 1 m depth for Br^- analysis. Soil Br^- concentration was more evenly distributed with soil depth and leached deeper in grassland than cropland, owing to vertically continuous macropores that supported preferential flow. Frequency-domain analysis and autoregressive state-space approach revealed that the dominant factors controlling Br^- leaching varied with depth. In shallow layers, land use was the main driving force for Br^- distribution. Beyond that, the spatial pattern of Br^- was mostly affected by rainfall characteristics. Below 40 cm, the horizontal distribution of Br^- was dominated by soil texture and to a smaller extent by rainfall intensity. Bromide concentrations obtained from soil solution samples that were collected through suction probes showed similar results with respect to the influence of rainfall intensity. The spatial variation scale of temporal matric potential change varied with both time and depth, corresponding to different boundary condition scales. Matric potential change in some cases, reflected the impact of soil properties other than the boundary conditions investigated, such as hydraulic conductivity, contributing to the scale-variant behavior of Br^- leaching. These findings suggest the applicability of scale-dependent treatment distribution in designing field experiments and also hold important implications for agricultural management and hydrological modelling.

Keywords: Bromide Leaching, Scale-Dependent Treatment Distribution, Rainfall Simulation, State-Space Model, Suction Probe

Yang Yang
Student's Signature

03/17/2014
Date

FIELD-SCALE WATER AND SOLUTE TRANSPORT

By

Yang Yang

Ole Wendroth
Director of Disseration

Mark Coyne
Director of Graduate Studies

03/17/2014
Date

ACKNOWLEDGEMENTS

This dissertation marks the end of a long and eventful journey for which I would like to acknowledge many people for their help along the way. First of all, I am deeply indebted to Dr. Ole Wendroth, my advisor, for his guidance, assistance and support on this research project. I have benefited greatly from his profound knowledge and skills in soil science during the last four years. He is not only the advisor but also a close friend of mine. We've laughed together and shared our happiness. When I get confused, I can always talk to him to "steal" his life experience. I feel incredibly privileged to work with him.

Special thanks are due to Dr. Christopher Matocha for his collaboration and advice on chemical analysis. I am sincerely grateful to my other committee members, Dr. Mark Coyne and Dr. Alan Fryar, for their expertise, suggestions and words of encouragement. I also want to thank Dr. Carl Dillon for serving as my outside examiner.

I would like to thank Riley Walton for his extreme patience and technical assistance in both field and laboratory experiments. The help of James Dollarhide, Martin Vandiviere, Sara Lawson, Jim Nelson, Michael Sama and Ann Freytag is sincerely appreciated. My gratitude is also extended to my dear colleagues and friends for their support: Sleem Kreba, Marcela Muller, Thatiana Felski, Andreas Schwen, José Beraldo, Shuang Liu, Ran Duan, Mohen Lin, and Chiyuan Miao.

The financial assistance by China Scholarship Council (CSC) is greatly appreciated. I also want to acknowledge the United States Department of Agriculture, Natural Resources

Inventory (USDA-NRI # 2008-35107-04649) and the Kentucky Water Resources Research Institute (KWRRI) 104b Student Research Enhancement Project for funding this research.

Last, but certainly not least, I must thank my parents, Zuhui Yang and Hua Chen, for their support and encouragement during my odyssey in Kentucky. I am forever grateful for their unconditional love through my entire life.

TABLE OF CONTENTS

LIST OF TABLES

LIST OF FIGURES

Chapter 1 A Review of Field-Scale Water and Solute Transport

1.1 Introduction

For at least 2000 years, farmers have employed agricultural practices to enhance water and nutrient flow in soil and plants. Virgil (70-19 BC) wrote in his second major poem "Georgics" that "it has been useful to fire barren fields and burn the light stubble" because "that heat opens fresh paths and loosens hidden pores, by which the sap may reach the tender blades" (Fairclough, 1999). This statement does not reflect our current knowledge; however, it does indicate that our ancestors have realized the importance of soil water movement and solute transport for agricultural production for a very long time (Philip, 1974).

The quantitative study of soil water flow behavior can be traced back to Buckingham (1907). In his famous report published in 1907, he originated the concept of "capillary potential" which today is commonly referred to as "matric potential", and considered it together with the gravitational potential as the forces governing water movement in soil (Philip, 1974; Nimmo and Landa, 2005). He also proposed the concept of unsaturated hydraulic conductivity and applied it in the description of water flux through unsaturated soil, which appears like a modification of Darcy's law but is believed to have been developed independently (Buckingham, 1907; Sposito, 1986; Jury and Horton, 2004). The Buckingham flux law was verified experimentally by Richards (1931) more than 20 years later, who further derived its partial differential form for transient unsaturated flow, which is now well known as Richards' equation. Another important contribution by Richards is

the development of the tensiometer, providing a simple and convenient way to measure matric potential and to describe soil water movement (Richards and Gardner, 1936; Richards, 1942). In the following several decades, the soil water flux theory has been improved in many aspects, such as introducing diffusivity function and considering capillary hysteresis (Philip, 1974).

Soil water in nature is never pure, but contains hundreds of dissolved substances and gaseous constituents (Nielsen et al., 1986). When describing the transport behavior of these solutes or evaluating the impact of fertilization or other chemical applications, the water flux theories above are obviously inadequate. In the early 1960s, Nielsen and Biggar (1961) were among the first to study miscible displacement of solutes in soil systematically (Wendroth et al., 2011c). They used Cl^- as a tracer and measured the breakthrough curves at different average flow velocities and water contents for three soils and two sizes of uniform glass beads. One year later, they generated a one dimensional convection-dispersion model (CDM) for uniform porous media (Nielsen and Biggar, 1962; Barry and Sposito, 1988). Their experiments and analyses suggested that: 1) the transport mechanisms of water and solutes can be studied through the distribution of an appropriate tracer; 2) both imposed boundary conditions, i.e., water content, and inherent soil properties, i.e., soil texture, are important factors for solute leaching.

This study and most of the subsequent ones on water and solute transport were conducted on soil columns in laboratory experiments and under steady-state flow conditions (Rao et al., 1980; Nkedi-Kizza et al., 1983), assuming that the whole column was homogeneous

and could be characterized by single values of matric potential, hydraulic conductivity, and other parameters (Jarvis, 2007). However, these results and research approaches cannot be applied in field-scale studies directly, in view of the vastly increased natural heterogeneity (Nielsen et al., 1986; Destouni and Graham, 1995; Ashraf et al., 1997). Depending on soil properties such as texture, structure, topography and spatial soil moisture distribution, the leaching behavior of water and solute is quite variable in space and time (Smith and Davis, 1974; Wendroth et al., 1999; Ersahin et al., 2002). It is critical to develop experimental approaches that allow the quantitative description of water and solute transport under field conditions.

In the current chapter, literature concerning field-scale soil water and solute transport is reviewed mainly in three aspects. First, the major tracers used to study solute leaching are introduced. Next, the important boundary conditions and soil properties that affect water and solute transport, and their associated mechanisms are described. Last but not least, field experimental designs and sampling methods are discussed.

1.2 Tracers

Depending on the question to be answered, the optimum tracer varies. For example, to study NO_3^- leaching, several scientists have used the stable isotope ^{15}N as the tracer (e.g., Di et al., 1999; Cookson et al., 2000). Here we specifically discuss conservative tracers that are not significantly absorbed by soil and not subject to chemical or biological transformations. Two typical tracers that meet these requirements are Cl^- and Br^-, both of which are commonly used in the studies of water and solute transport. Rao et al. (1982)

and Addiscott et al. (1983) adopted Br^- as the tracer to study solute diffusion in artificial and natural aggregates, respectively. Köhne et al. (2002) employed both Cl^- and Br^- to evaluate the impact of aggregate skins on the solute diffusion coefficient. On columns of porous ceramic spheres, Al-Sibai et al. (1997) applied Cl^- as the tracer and compared the breakthrough curves (BTCs) under continuous and intermittent leaching. Augustin et al. (1995) monitored Br^- transport through columns packed with soil aggregates and found that the degree of asymmetry in BTCs increased with aggregate size and pore-water velocity. Jiang et al. (1997) applied Br^- to undisturbed soil columns and analyzed BTCs as affected by water table depth and rainfall timing.

In contrast to studies on aggregates and columns in the laboratory where boundary conditions are easy to control, and both anions, i.e., Br^- and Cl^-, are equally chosen as the tracer, Br^- is usually preferred in the experiments conducted at the field scale (Bowman, 1984). The main reason is that Cl^- is a micronutrient widely required by plants (Martin, 1966), and commonly present in soils, fertilizers and precipitations; while the natural occurrence of Br^- is very low (Vinogradov, 1959; Ingram, 1976). In view of this limitation, the isotope ^{36}Cl has been employed in many solute transport studies instead of Cl^-. Pinner and Nye (1982) used ^{36}Cl to analyze solute diffusion in undisturbed and repacked soil columns as affected by water content. Nkedi-Kizza et al. (1983) measured the BTCs of ^{36}Cl displaced through packed columns under saturated conditions. However, owing to the radioactive properties, the use of ^{36}Cl is usually limited to laboratory experiments. The few field investigations on long-term solute transport were mainly conducted in the desert of Southwest America, taking advantage of the pulses of ^{36}Cl released from nuclear weapon

testing in the 1950s and 1960s (e.g., Phillips et al., 1988; Scanlon, 1992). Thus in most field experiments, Br^- has been selected to reflect water and solute transport, e.g., under different land use systems (Caron et al., 1996; Ingram, 1976), at different landscape positions (Afyuni et al., 1994; Olson and Cassel, 1999). But an additional concern should be raised when applying Br^- to large areas because it can be toxic to grazing animals (Owens et al., 1985) or result in groundwater pollution (Flury and Papritz, 1993).

Owing to anion exclusion occurring in the soil which is usually negatively charged, many experiments showed that Br^- and Cl^- moved faster than water (McMahon and Thomas, 1974), especially at high pH (Nielsen et al., 1986). Therefore, in many experiments, water molecules labeled with isotope ^2H or ^3H were preferred. De Smedt et al. (1986) studied ^3H_2O infiltration through a packed sand column and observed much larger dispersivity under unsaturated conditions compared to saturated ones. Brooks et al. (2002) applied ^2H_2O to two 1 m^2-plots to monitor water redistribution during a summer drought in Northwest America. However, neither of these tracers are appropriate for large-scale field experiments, because ^3H_2O is radioactive while the non-radioactive ^2H_2O is expensive to be enriched at required ratios (Bowman, 1984).

Dyes are another kind of tracer that have been widely used in transport studies. Unlike Cl^-, Br^-, or H_2O labeled with H isotopes, dye tracers provide direct visual traces of primary flow pathways by staining (Bouma et al., 1977; Gjettermann et al., 1997). In the late 1950s, Tamm and Troedsson (1957) adopted staining technique to determine the drainage of rainwater (Reynolds, 1966). They applied NH_4SCN on the soil surface first; and after

rainfall, they dug a pit and sprayed the profile with $FeCl_3$. Any zone in the profile containing SCN^- became deep red due to the reaction with Fe^{3+}, thereby allowing the identification of infiltration pathways. However, the chemicals used in this experiment are not safe and many trees around were killed.

One of the early experiments that applied dye tracer in vadose zone studies was conducted by Bond (1964). He dusted a pit profile with dry kaolinite containing 1% of Rhodamine B, which turned red upon contact with water, revealing wet zones in the soil profile. In this way, he was able to analyze the impact of soil water repellency on the water infiltration pattern. Later, more dyes were employed. Saffigna et al. (1976) analyzed the sources of penetration water in a potato field using Rhodamine WT. Bouma et al. (1977) described macropore flow through three types of pores with the aid of methylene blue. Flury et al. (1994) adopted Brilliant Blue ECF to investigate the water flow paths at 14 different field sites. There is no ideal conservative dye tracer in view of their sorption characteristics and biochemical properties (Davis et al., 1980). In general, Rhodamine WT and Brilliant Blue ECF are most commonly used (Flury and Wai, 2003).

1.3 Impact Factors

1.3.1 Soil Properties

It is well known that soil texture and structure play essential roles in water and solute transport (Beven and Germann, 1982; Shipitalo et al., 2000). They are the primary factors controlling soil hydraulic properties; furthermore, they interact with each other during pedogenesis, resulting in unique attributes for each soil pedon. Using computed

tomography (CT), Heijs et al. (1996) visualized the water flow paths in two distinct soils in three dimensions. In the clay soil with the presence of macropore network, soil water mainly flowed downwards with little lateral spreading; while in the water-repellent sandy soil, flow fingers were observed starting at the locations with high bulk density. More evidence for the importance of soil texture and structure has been provided by infiltration experiments employing dye tracers. Flury et al. (1994), Kulli et al. (2003) and Weiler and Naef (2003a) clearly showed in their field investigations how water and solute movement varied with soil texture and structure in both vertical and horizontal directions. Generally in fine-textured soils, vertically continuous macropores tend to conduct water and solute downwards and limit lateral mass exchange; while in sandy soils, lateral mixing is usually much stronger (Jarvis, 2007). However, exceptions may occur when horizontal cracks or root macropores develop in the plow pan, where water and solutes are mainly transported through horizontal preferential flow (Janssen and Lennartz, 2007).

Topography is another soil property that regulates solute leaching. At the landscape scale, the topography impact is exerted by the associated soil organic matter and texture, which affect solute retention and movement in soils. Olson and Cassel (1999) analyzed Br^- leaching on a Piedmont toposequence and concluded that the shallower leaching depth on linear and shoulder slopes compared to footslope was caused by the increased clay contents in the subsoil which retarded solute transport. A column experiment conducted by Clay et al. (2004) also manifested different leaching behaviors of Br^- and NO_3^- at different landscape positions.

At the small scale, topography or microrelief affects water and solute transport mainly through another mechanism. Darboux and Huang (2005) conducted rainfall simulation experiments over eight manually packed soil boxes with smooth or rough surface and found that water stored in depressions, typically under a high intensity rainfall, enhanced water infiltration and delayed runoff initiation. Based on dye tracer experiments at four sites, Weiler and Naef (2003b) further concluded that an increase in soil surface roughness fostered water and solute movement through macropores or other preferential pathways. Microrelief decides the degree of water ponding that could possibly develop in a specific rainfall event; thereby affecting the surface area and the macropores connected to and open at the surface that contribute to the initiation of preferential flow.

1.3.2 Initial and Boundary Conditions

The impact of soil water content antecedent to subsequent rainfall is complicated. A good example is the dye tracer experiment conducted by Flury et al. (1994), which manifested diverse solute transport behavior as affected by initial water content. In a soil with coarse prismatic structure, the researchers observed stained cracks only in the wet plot under unsaturated flow condition; while with flood irrigation, stained cracks appeared in both plots with even deeper ones in the dry plot. It is implied that the influence exerted by initial water content is quite dependent on the application method of irrigation and the rainfall intensity. Water starts to flow into a macropore only when the water pressure exceeds certain “water-entry” pressure, depending on the macropore size (Jarvis, 2007). When rainfall intensity is low and water slowly infiltrates into the soil matrix, the pressure generated in dry soils is obviously smaller than that in wet soils, thereby resulting in a

lower possibility of macropore flow occurrence. Under high intensity rainfall, in contrast, water ponds extensively on the surface especially when soil is dry and strongly water-repellent. Therefore, more water flows into macropores and other continuous channels under initially dry conditions, leading to deeper movement of water and solute (Weiler and Naef, 2003a). Edwards et al. (1989) obtained similar results when studying water flow through earthworm burrows under natural rainstorms. Enhanced flow in monitored burrows was observed under high intensity storms on dry soil surfaces. However, no percolate was yielded during low intensity rainfalls. White et al. (1986) also found more herbicides, i.e., napropamide and bromacil, leached from initially dry soil than prewetted soil; but they attributed this difference to the swelling of clay soil during prewetting which thereby narrowed the conducting cracks and channels. Regardless of the mechanisms responsible for this phenomenon, as initial water content increases, the displacement of resident water and the interaction between rainwater and soil matrix generally increase, which would possibly decrease the concentrations of surface-applied chemicals in leachate (Shipitalo and Edwards, 1996).

Rainfall characteristics, i.e., amount, intensity and timing, all affect water and solute transport. A larger amount of rainfall usually corresponds with deeper leaching of chemicals (Mulla and Annandale, 1990; Diez et al., 1997). However, increasing rainfall intensity may have very different effects. Keller and Alfaro (1966) and Ghuman et al. (1975) observed higher leaching efficiency at lower water application rate, when conducting miscible displacement experiments on columns packed with glass beads and sieved sandy loam soil, respectively. Yet in the rainfall simulation experiments reported by Germann et

al. (1984) and Trojan and Linden (1992), the leaching depth of Br^- increased with rainfall intensity. The preferential flow enhanced by increased rainfall intensity, typically occurring in structured soils, has been concluded as the cause (Jarvis, 2007). For a structured soil with the presence of vertically continuous macropores, surface water ponds more extensively under a heavier rainfall and preferential flow is initiated through a greater number of macropores, resulting in rapid movement of surface-applied chemicals (Gjettermann et al., 1997). This positive correlation between rainfall intensity and water and solute transport depth has been observed for a wide range of soil types and a variety of chemicals (Shipitalo et al., 2000).

Rainfall timing can have a major influence on solute leaching. Heavy rainfall shortly after surface application of chemicals often results in large leaching losses (Dekker and Bouma, 1984; Jarvis, 2007). In contrast, with a longer time delay between solute application and subsequent rainfall, more solute can move from large interaggregate pores into fine intraaggregate ones and becomes less accessible to water flow and rapid leaching; therefore, both the amount and depth of solute leaching can be considerably reduced (McLay et al., 1991; Gerke and Köhne, 2004). Evidence for this retardation phenomenon has been provided in both laboratory and field experiments (e.g., Kluitenberg and Horton, 1990; Edwards et al., 1993; Wendroth et al., 2011c).

However, a longer time delay does not always correspond with less solute leaching. In a column experiment reported by Jiang et al. (1997), extending the time delay significantly decreased NO_3^- leaching only under the wet condition when the water table was 5 cm below

the soil surface. It is implied that the impact of rainfall timing on solute transport was affected by water table depth and presumably by soil moisture. In addition, rainfall timing itself would possibly change the soil water status antecedent to subsequent rainfall. Besides solute diffusion into aggregates, increasing the time delay allows a longer time for soil water evaporation. Therefore, soil becomes drier, especially near the land surface, which under heavy rainfall favors the development of preferential flow and deep leaching of water and solutes (White et al., 1986; Edwards et al., 1989; Weiler and Naef, 2003a).

1.4 Experimental Methods

1.4.1 Experimental Designs

The first field study on solute transport was conducted by Miller et al. (1965), who measured profile distribution of Cl^- in replicated plots and concluded that intermittent ponding, compared to continuous ponding, resulted in greater leaching efficiency (Butters et al., 1989). The classic block design adopted here assumes that soil in each block is homogeneous and the distinct treatments are the only reason why observations vary. The principle is simple and its applications in many field experiments in the following decades have greatly improved our understanding of water and solute transport. However, field soils are heterogeneous in both vertical and horizontal directions. Regardless of scale dependence, this fact to some extent stands against the inherent assumption of the classic block design and the random variation of observations. As a result, the parameter or variable describing solute transport is usually obtained together with a comparable standard deviation and a large coefficient of variation (CV).

Biggar and Nielsen (1976) investigated Cl^- and NO_3^- leaching down to 1.8 m depth in a 150-ha agricultural field and obtained an average pore water velocity of 38.2 cm d^{-1} among 20 subplots, with a CV of 99.7%. Butters et al. (1989) monitored the movement of Br^- down to 4.5 m depth below soil surface in a 0.64-ha loamy sand field and found that the CV of mass recovery between replicated samplers at a given depth was close to 50%. In the field experiments conducted by Kessavalou et al. (1996) and Ottman et al. (2000), which were also based on classic block design, the standard deviations were in the same magnitude as the amounts of Br^- and ^{15}N leached below 1.2 and 4 m, respectively. The huge variability present in the set of measurements, resulting from the heterogeneity inherent in soil properties, would make it extremely difficult to quantify solute transport or to analyze treatment effects (Wendroth et al., 2011c).

To overcome this limitation and to yield a representative estimate of solute transport, many more measurements are required and the number depends on the spatial variability of the soil (Biggar and Nielsen, 1976). Accordingly, field experiments aimed to reveal the spatial structures of soil properties (Dagan, 1987) and solute transport variables (Kung, 1990), to analyze their spatial correlations (Ellsworth and Boast, 1996), or to obtain other scaling factors (Jury, 1985) are suggested. Yet until the 1990s, experimental techniques were not satisfactory for spatial analysis of soil moisture and solute concentration (Jury, 1985; Binley et al., 1996; Wendroth et al., 2011c). Van Wesenbeeck and Kachanoski (1990) installed suction probes in 20 cm intervals along two transects to calculate the variance of Cl^- travel time at different scales and found that the corresponding spatial correlation ranges were 2.8 and 3.8 m for forested and cultivated sites, respectively. Ellsworth and Boast

(1996) also quantified the spatial correlation ranges for solute leaching amount and depth based on extensive soil sampling. In addition, they concluded that the spatial variability of solute transport was quite dependent on the measuring scale. But in the field experiment conducted by Netto et al. (1999), neither spatial structure for solute concentration nor significant cross-correlation for solute concentration with water content or bulk density were observed. The primary reason was that solute transport usually varies at multiple scales and autocorrelations and semivariograms were not sufficient to reveal its spatial structure (Biggar and Nielsen, 1976; Wendroth et al., 2011c; Schwen et al., 2012).

In view of this limitation, a novel experimental design, which imposes treatments in a periodically repetitive pattern at distinct scales has been introduced. Based on Fourier transformation, the calculation of power spectra, i.e., spectral analysis, allows discrimination of soil variability over different scales (Kachanoski and De Jong, 1988). Thus, the treatment effects can be separated from the impact exerted by underlying soil processes using this technique.

The first application of spectral analysis in soil science goes back to Bazza et al. (1988), who irrigated a 6-ha field with water of cyclically changing salinity levels and detected the same periodicity in soil surface temperature (Wendroth et al., 2011b). Shillito et al. (2009) and Wendroth et al. (2011a) adopted the same technique and observed systematical responses of potato and wheat yields, respectively, to cyclically varying N rates applied at the beginning of the growing season. Later, Wendroth et al. (2011c) introduced this technique to a field-scale solute transport study. In a rainfall simulation experiment, they

arranged four levels of rainfall intensity and four levels of application time delay, i.e., the time delay between Br^- application and subsequent rainfall, along a 64-m grassland transect in cyclic layout at wavelengths of 32 and 8 m, respectively. As a result, variations at these two scales were detected in the leaching depth described by the center of Br^- mass. Adopting the same approach, Schwen et al. (2012) evaluated the impact of land use, irrigation characteristics and bulk density on water infiltration and Br^- leaching. Compared to classic block design, the scale-dependent treatment distribution design together with frequency-domain analysis, i.e., spectral and cross-spectral analyses, provide a greater opportunity to analyze water and solute transport and to identify the major factors controlling their spatial behaviors (Nielsen and Alemi, 1989).

1.4.2 Sampling Techniques

Soil coring has been the standard sampling method used to study solute transport in the vadose zone (Alberts et al., 1977). It accounts for the total resident solute concentration at the time of sampling, which quantifies the mass of solute leached to a certain volume of soil (Netto et al., 1999). However, this method is destructive and does not allow repeated sampling at the same physical location. In view of the natural heterogeneity inherent in soil properties, solute distributions may not be similar in two adjacent profiles. Therefore, it is almost impossible to analyze the temporal dynamics of solute leaching with this technique.

In contrast, a suction probe with a porous ceramic cup at the bottom can provide *in situ* samples of soil solution, once installed at a certain location and depth (England, 1974; Grossmann and Udluft, 1991). The earliest description of ceramic cup samplers appeared

in a study by Briggs and McCall (1904), who initially designed it to simulate capillary movement of soil water. Since the 1960s, the use of suction probes has become the common practice for monitoring water and solute transport in agricultural studies (Litaor, 1988). Nevertheless, other than soil coring, the volume of soil contributing to a solution sample collected by a suction probe is not strictly defined. When a vacuum larger than the matric potential is applied, the radius of influence of a suction probe can be up to several meters (Van der Ploeg and Beese, 1977). In addition, as a "point sampler", suction probes may not be able to capture the characteristics of solute transport unless adequate replicates are taken in a pattern consistent with the spatial variation (Hansen and Harris, 1975; Saffigna et al., 1976), especially when macropore flow occurs in a structured soil (Shaffer et al., 1979) or finger flow takes place due to texture change in a soil profile (Starr et al., 1978). Therefore, this sampling method is usually employed to assess soil water quality but not for evaluating the amount of water and solute moving through a soil profile (Cochran et al., 1970; Biggar and Nielsen, 1976).

Zero-tension pan lysimeters provide a means to analyze both quality and quantity of solute leaching (Jemison and Fox, 1992). They are referred to as free-drainage pan samplers in some literature (e.g., Barbee and Brown, 1986) and collect soil water drained to a certain depth driven by gravity. Haines et al. (1982) compared the composition of soil solution collected by a ceramic plate suction sampler to that by a zero-tension lysimeter, and concluded that the latter sampled more efficiently after a heavy rainfall but less efficiently under unsaturated conditions. Barbee and Brown (1986) analyzed Cl^- leaching in three different soils and found that zero-tension lysimeters generally collected larger and more

consistent samples, especially for the well-structured clay soil. However, this method is basically limited to saturated conditions and the installation is costly and time-consuming. Intercepting the leaching water at the depth where the pan sampler is inserted prevents the collection of solutes along a straight vertical line at different depths in the soil profile. Also, if the cross-sectional area of the pan is not large enough, the lysimeter can be completely circumvented by preferential flow under a heavy rainfall (Radulovich and Sollins, 1987; Jemison and Fox, 1992).

There are many other techniques for soil water and solute sampling. For example, a soil profile needs to be excavated when using a dye tracer to manifest flow pathways; and resin bags are usually installed to analyze NO_3^- leaching. No single sampling technique can perfectly describe water and solute movement under all field conditions (Litaor, 1988). But an optimal choice can be made for certain research objectives and a given study area.

1.5 Conclusions and Dissertation Overview

A precise description of water and solute transport in the vadose zone is essential for improving agricultural management and hydrological modelling. However, mainly owing to the natural soil heterogeneity, little progress has been made in quantifying solute leaching in field soils. In this review, the field experimental designs possible to overcome this limitation were discussed and the major tracers and influencing factors analyzed in previous studies were introduced. From the aspect of application, it is necessary to establish a model that incorporates spatial variability of soil properties and predicts water and solute leaching. Also, solute transport is a dynamic process both spatially and temporally. There

is a critical need in the future research to develop a field technique to describe the spatial behavior of water and solute transport evolving with time under non-equilibrium flow conditions.

In this dissertation, a rainfall simulation experiment adopting scale-dependent treatment distribution was conducted at University of Kentucky's Spindletop Research Farm to describe water transport and Br^- leaching under field conditions. In Chapter 2, the spatial structure of soil Br^- concentration is analyzed at every 10 cm from the soil surface to 1 m depth. Using spectral and cross-spectral analyses, the impact of soil surface roughness, soil texture and rainfall characteristics on Br^- leaching is evaluated. Chapter 3 applies a state-space approach to analyze the spatial associations of soil Br^- among different depths and to describe the horizontal distribution of soil Br^- concentration at each depth based on the boundary conditions investigated. Chapter 4 is an attempt to study the temporal dynamics of water transport and Br^- leaching. Matric potential changes during different periods of time and Br^- concentrations in soil solution collected through suction probes at different times are analyzed. Finally, in Chapter 5, the findings obtained in this series of analyses are presented.

Chapter 2 Field-Scale Bromide Leaching as Affected by Land Use and Rainfall Characteristics

2.1 Introduction

A precise description of water and solute transport through soil is required in calculating the fate of surface-applied nutrients and their impact on environmental quality (Feyen et al., 1998; Paramasivam et al., 2002). Many researches reveal that rainfall characteristics, i.e., rainfall amount, intensity, and the time delay relative to solute application, are important factors that influence these processes (e.g., Shipitalo et al., 2000; Jarvis, 2007).

In general, more rainfall corresponds with deeper chemical leaching (Mulla and Annandale, 1990; Diez et al., 1997). The impact of rainfall intensity on solute transport, on the contrary, is more complex. Keller and Alfaro (1966) observed higher leaching efficiency when water was applied at a lower rate on pots filled with glass beads. Ghuman et al. (1975) drew similar conclusions later from a soil column experiment: slowing down the application of water could yield deeper movement of salts immediately after infiltration. However, in a structured soil with the presence of continuous macropores, the results can be quite different. Preferential flow in macropores typically occurring at high rainfall intensity

contributes to rapid solute movement through soils (Beven and Germann, 1982; Gerke, 2006). Thus over a wide range of soil types and a variety of chemicals, positive correlations between rainfall intensity and solute leaching depth have been obtained (Shipitalo et al., 2000; Jarvis, 2007). Yet, the vertical solute distribution in a soil profile as affected by rainfall intensity is not all the same in this context. In a rainfall simulation experiment conducted by Trojan and Linden (1992), less Br^- and rhodamine dye were displaced from the soil surface as rainfall intensity increased; whereas, Germann et al. (1984) found increased downward movement of surface-applied Br^- with rainfall intensity, resulting in a lower Br^- concentration close to the soil surface and a more linear distribution of Br^- across the soil profile. Gjettermann et al. (1997) also observed a lower degree of dye tracer coverage in surface soil with increased rainfall intensity; and preferential flow initiated through an increasing number of macropores owing to the more intensive ponding at increasing intensity was considered as the reason.

Rainfall timing relative to solute application is another important factor that controls solute leaching. A heavy rainfall shortly after the surface application of solutes usually results in intensive leaching (Dekker and Bouma, 1984; Jarvis, 2007). With the increasing time delay between solute application and subsequent rainfall, the amount and depth of leaching could be considerably reduced (Edwards et al., 1993; Wendroth et al., 2011c). McLay et al. (1991) and Gerke and Köhne (2004) attributed this retardation phenomenon to the diffusion of solutes into soil aggregates. When sufficient time is allowed, solutes move from large interaggregate pores to small intraaggregate ones and become less accessible to be leached by water flow (Francis et al., 1988). Better understanding the effects of rainfall

intensity and timing on solute transport is beneficial for the management of surface-applied chemicals.

Most of the research on water and solute transport has been conducted on soil columns under laboratory conditions and steady-state flow; while at the field scale, little progress has been made, mainly owing to the natural soil heterogeneity (Nielsen et al., 1986; Ashraf et al., 1997). Depending on soil properties such as texture, structure, topography and spatial soil water distribution, solute leaching behavior is quite variable (Wendroth et al., 1999; Ersahin et al., 2002; Whetter et al., 2006). Using Br^- as a tracer in a field experiment, Ottman et al. (2000) found the average standard deviation was comparable to the amount of solute leached below 4 m depth during a growing season of irrigated wheat. To yield an effective estimate of solute transport in the field, an appropriate number of measurements have to be made and the number relies on the spatial variability of the field soil (Biggar and Nielsen, 1976). Accordingly, field experiments aimed to reveal the spatial correlation ranges of soil properties (Dagan, 1987) and solute flux (Kung, 1990) or to obtain other scaling factors (Jury, 1985) are suggested.

Nevertheless, until the mid-1990s, experimental techniques were not satisfactory for spatial analysis of soil water and solute concentration (Jury, 1985; Binley et al., 1996; Wendroth et al., 2011c). The first study detecting the spatial correlation ranges of solute concentration at the field scale was conducted by Ellsworth and Boast (1996). Netto et al. (1999) found no spatial structure in the semivariogram analysis for solute concentrations or any significant cross-correlation of solute concentration with water content or bulk density. It

is implied that semivariograms may not be sufficient to reveal the spatial structure of solute transport, which varies over different scales (Wendroth et al., 2011c). Instead, imposing treatments in cyclic layout at distinct scales, their autocorrelation functions as well as those of related processes would reflect the corresponding repetitive patterns and suggest variance decomposition in the frequency domain, i.e., spectral analysis; thereby allowing a greater opportunity to identify the major factors that affect solute transport (Nielsen and Alemi, 1989; Shillito et al., 2009). Kachanoski and De Jong (1988) applied Fourier-based transformations to decompose soil variability over different scales. Wendroth et al. (2011c) showed that arranging treatments not randomly but reoccurring and at different scales allowed the separation of small-scale processes from large-scale ones with, e.g., additive state-space approach. Therefore, large-scale variation underlying the spatial series of measurements in the present experiment would become obvious in the power spectra; while it were difficult to separate its impact on treatments in a block design.

The hypothesis of the current study is that the effects of land use and rainfall characteristics applied in the above-mentioned scale-dependent design are revealed in the spatial behavior of solute transport. Referring to the experimental design employed by Bazza et al. (1988) and Shillito et al. (2009), rainfall intensity and application time delay were arranged at different scales over a transect across two land use systems: cropland and grassland. Using Br^- as the tracer in this rainfall simulation experiment, the objectives were to: 1) assess the impact of land use and rainfall characteristics on Br^- distribution throughout the soil profile; 2) explore the spatial correlations of Br^- concentrations at different depths with these factors; and 3) identify the major factors that control solute leaching at the field scale.

2.2 Materials and Methods

2.2.1 Experimental Design

The experiment was conducted in the late spring of 2012 at the University of Kentucky's Spindletop Research Farm, Lexington, KY. The soil is a Maury silt loam, classified as a mixed, semiactive, mesic Typic Paleudalf. The average annual precipitation is 114 cm and the mean annual ambient temperature is 13 °C. From April through September, mean monthly potential evapotranspiration exceeds rainfall. On a 4125 m^2 field with established cropland and grassland, a 48-m by 3-m transect was selected (Figure 2.1). Half of the transect on the cropland used to be planted with no-till winter wheat (*Triticum aestivum L.*) had been fallowed since April 2011; and the other half on the grassland was dominated by tall fescue (*Festuca arundinacea Schreb.*), bluegrass (*Poa pratensis L.*) and red clover (*Trifolium pretense L.*). Glyphosate (Roundup, Monsanto Co.) was applied to kill all the plants prior to the leaching experiment.

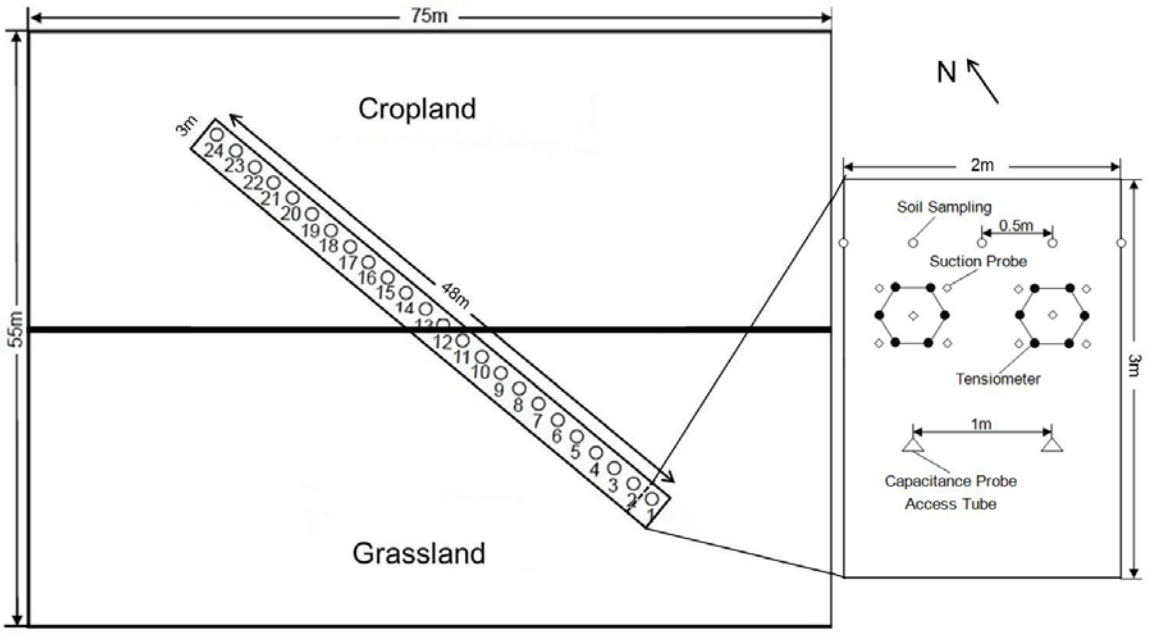

Figure 2.1 Experimental field and plot layout with soil sampling design. The Br^- leaching experiment was conducted over a 48-m by 3-m transect evenly across two land use systems: cropland and grassland. Each 2-m by 3-m plot was equipped with two sets of instruments separated by 1 m. Each set included one nest of tensiometers installed clockwise at 10, 30, 50, 70, 90 and 110 cm at the vertices of a hexagon with an edge length of 20 cm; one nest of suction probes accompanying tensiometers at 20, 40, 60, 80 and 100 cm; and one capacitance probe access tube at 1 m from the center of each tensiometer nest. Thereinto, each suction probe was installed in the middle of two tensiometers with close depths (i.e., suction probe at 20 cm installed in the middle of tensiometers at 10 and 30 cm), except the one at 60 cm, which was at the center of the nest. One day after the last rainfall simulation, soil cores of 100 cm were sampled every 0.5 m along the transect.

Along the transect, 24 plots in total were established, within which two hexagon nests of six self-manufactured tensiometers aimed to measure soil water matric potential were

installed at depths of 10, 30, 50, 70, 90 and 110 cm. Accompanied with each tensiometer nest, five suction probes used for soil water sample collection were installed as well, at 20, 40, 60, 80 and 100 cm soil depths. A parallel set of capacitance probe access tubes (Diviner 2000, Sentek Pty. Ltd., Stepney South, Australia) were installed 1 m apart to monitor soil water content in 10 cm increments down to 1 m depth (Figure 2.1). During the installation of each access tube, undisturbed soil cores down to 1 m depth were taken and divided in 10 cm increments for soil texture determination using the pipette method (Gee and Bauder, 1986). In addition, relative elevation was acquired by a Trimble SPS 930 Universal Total Station every 25 cm both along and across the transect. These measurements were averaged for every 1 m, resulting in 2 values per plot (Figure 2.2c). To better describe the complexity of topography, the corresponding elevation variance was calculated by summing up the squared differences from the neighboring relative elevations.

A constant rate of 37.5 g Br m^{-2} was adopted in this experiment, equivalent to the rate of NO_3^- in NH_4NO_3-fertilizer as recommended for no-till wheat in Kentucky (Murdock et al., 2009). Within a total of 0.9 mm of rainwater collected earlier, KBr was dissolved and applied using a regular farm sprayer. In the periodical design of rainfall characteristics, a constant rainfall amount of 44 mm, three levels of rainfall intensity, 5, 22 and 44 mm h^{-1} corresponding with the average recurrence intervals of 1, 2 and 5 years, respectively (Bonnin et al., 2006), and four levels of application time delay, 1, 4, 24 and 96 h, were distributed along the transect as shown in Figure 2.2. Thereinto, the application time delays were chosen arbitrarily to manifest the different conditions typically occurring in Kentucky during the spring season when many surface chemicals are applied in the field. Rainwater

was applied using garden sprinklers attached to a metal frame. This device allowed simultaneous irrigation of two neighboring plots. Therefore, the application of tracer was conducted at an appropriate time before the subsequent rainfall simulation on each individual plot to attain the corresponding time delay. Tarps were used to cover the plots to prevent the interference by natural precipitation and to minimize the evaporation of soil water when no rainfall simulation or tracer was applied. However, final intensities for some plots were slightly different from the ones intended as a result of natural precipitation occurring during rainfall simulation (Figure 2.2a). And owing to an accidental malfunction of the pumping system in the first day of the experiment, the actual intensity for plot 1 and 2 were about 10 mm h^{-1} higher than the one intended.

Before, during and after each rainfall simulation, soil matric potential and volumetric water content were measured at every position and depth to monitor the water status as affected by rainfall characteristics. Soil water samples were collected twice using suction probes, i.e., 1 h and 1 day after each rainfall event, respectively. One day after the last rainfall simulation, soil cores of 1 m depth were sampled at an interval of 0.5 m along the 48-m transect (Figure 2.1). They were divided in 10 cm increments for the determination of water content and Br^- concentration at each depth. An ion chromatograph (Metrohm AG, Herisau, Switzerland) was used to analyze soil Br^- concentration after the extraction of air-dried soil samples with distilled water. The minimum detection limit is 13.6 μg Br^- L^{-1}. In this study, only soil Br^- concentration data were analyzed and soil solution results will be presented in another publication.

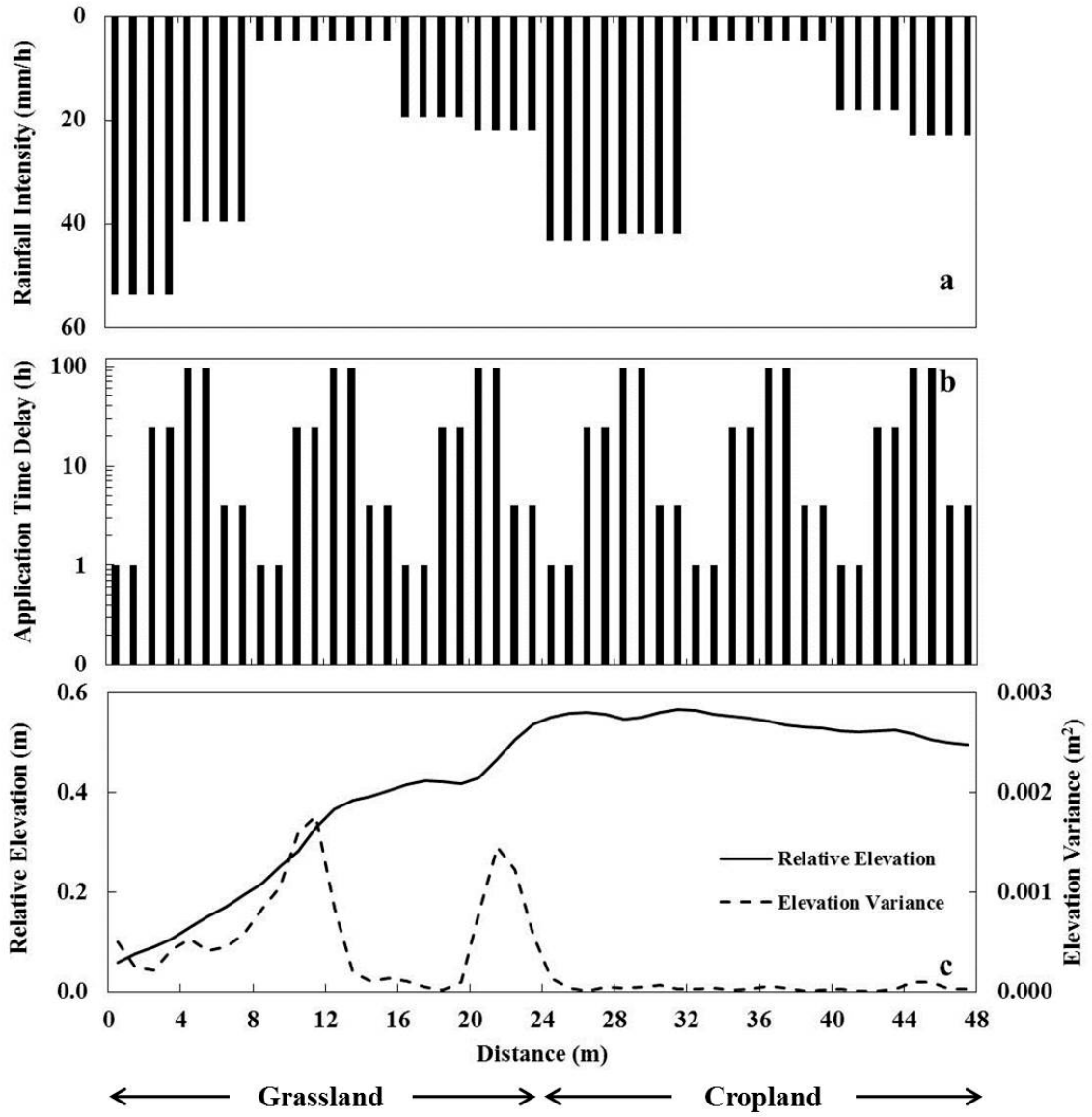

Figure 2.2 Spatial distribution of (a) rainfall intensity, (b) application time delay, and (c) relative elevation and elevation variance along the 48-m transect. Thereinto, the intensive measurements of relative elevation taken every 25 cm in both directions were averaged for every 1 m resulting in 2 values per plot; and the corresponding elevation variance was calculated as the sum of squared differences from neighboring relative elevations.

2.2.2 Spatial Analysis

Prior to spatial analysis, all the data including the measured soil Br^- concentrations at different depths, natural and imposed boundary conditions such as elevation variance and rainfall intensity, respectively, were normalized according to (Nielsen and Wendroth, 2003):

$$z_i' = \frac{z_i - (\bar{z} - 2\sigma_z)}{4\sigma_z} \tag{2.1}$$

in which z_i is the measured value at position i, $\bar{z}$ and σ_z are the mean and standard deviation of z_i, respectively. The normalized value z_i' would have a $\bar{z}$ equal to 0.5 and a σ_z equal to 0.25. The rationale behind this normalization is to avoid numerical problems that can result if two or more variables in the analysis differ by an order of magnitude or more.

The spatial variance changing with the lag distance between measurements was quantified with the experimental semivariogram $\gamma(h)$ (Matheron, 1962; Isaaks and Srivastava, 1989):

$$\gamma(h) = \frac{1}{2N(h)} \sum_{i=1}^{N(h)} [A_i(x_i) - A_i(x_i + h)]^2 \tag{2.2}$$

Thereinto, $A_i(x_i)$ is the measurement A_i at location x_i and $N(h)$ is the number of measurement pairs in lag class h. Typically with the increase of lag distance, the semivariance $\gamma(h)$ increases until it reaches a plateau, and a spatial correlation range can be generated for the corresponding measurement. However, this simple spatial behavior is not always observed for solute transport and semivariograms do not necessarily consist of only one single structure (Nielsen and Wendroth, 2003). Different plateaus can manifest different variation scales. The initial plateau indicates a landscape process at a small scale and a further change of the semivariance until another plateau at a longer lag distance can be caused by another underlying process at a larger scale (Wendroth et al., 2011c).

Landscape processes at different scales can be detected through this nested semivariance behavior (Webster and Oliver, 2001).

The spatial correlation between two variables $A_i(x_i)$ and $B_i(x_i)$ was quantified using the cross-semivariogram $\Gamma(h)$ (Yates and Warrick, 2002):

$$\Gamma(h) = \frac{1}{2N(h)} \sum_{i=1}^{N(h)} [A_i(x_i) - A_i(x_i + h)][B_i(x_i) - B_i(x_i + h)] \quad (2.3)$$

The sign of the cross-semivariance decides a positive or negative spatial correlation between the two variables and the range of the cross-semivariogram indicates up to what lag distance the two variables are spatially related.

Spectral and cross-spectral analyses were used to analyze the frequency-domain variance components (Shumway, 1988). The repetitive fluctuations implied in one data series at different scales were identified by calculating the power spectrum $S(f)$, which is based on Fourier transformation:

$$S(f) = 2 \int_0^\infty r(h) \cos(2\pi f h)\, dh \quad (2.4)$$

The autocorrelation function $r(h)$ above is integrated with respect to lag distance h. A periodicity is shown in the power spectrum as a variance peak S occurring at an associated frequency f which is the inverse of the wavelength λ reflecting the scale of variation. The synchronous periodic fluctuations in two data series were detected using the co-spectrum $Co(f)$, which integrates the cross-correlation function $r_c(h)$:

$$Co(f) = 2 \int_0^\infty r_c(h) \cos(2\pi f h)\, dh \quad (2.5)$$

The $r_c(h)$ here combines the positive and negative lags through $r_c(h) = 0.5[r_c(h < 0) + r_c(h > 0)]$, which reinforces the cyclic variations described by a cosine function and

eliminates the ones by a sine function (Nielsen and Wendroth, 2003). And the quad-spectrum $Q(f)$ in contrast, emphasizes the fluctuations described by a sine wave through $r_c'(h) = 0.5[r_c(h < 0) - (h > 0)]$ and is calculated as below.

$$Q(f) = 2\int_0^\infty r_c'(h)\sin(2\pi f h)\,dh \tag{2.6}$$

The importance of quad-spectrum mainly lies in its use to identify the phase lag $h_\emptyset$ between two data series when their maximum cross-correlation is reached (Nielsen and Wendroth, 2003; Wendroth et al., 2011c).

2.3 Results and Discussion

2.3.1 Br^- Distribution in the Soil Profile

Soil Br^- concentrations measured at five of the ten soil depths investigated along the transect are shown in Figure 2.3. Few sampling positions showed much higher Br^- concentrations relative to the others at the corresponding depth and these values were validated by duplicate analysis. In spite of some evident point-to-point fluctuations, soil Br^- concentration at the time of sampling generally decreased with soil depth. And typically higher Br^- concentrations at surface (Figure 2.3a, b) but lower ones in deep soil (Figure 2.3d) were measured in cropland, when the two land use systems were compared. Delineating the regions receiving rainfall at three levels of intensities, i.e., high, medium and low, the low intensity (Low I) corresponded with generally higher soil Br^- concentrations at surface and lower ones at greater depths. This relationship between rainfall intensity and Br^- concentration was more prominent in cropland than in grassland.

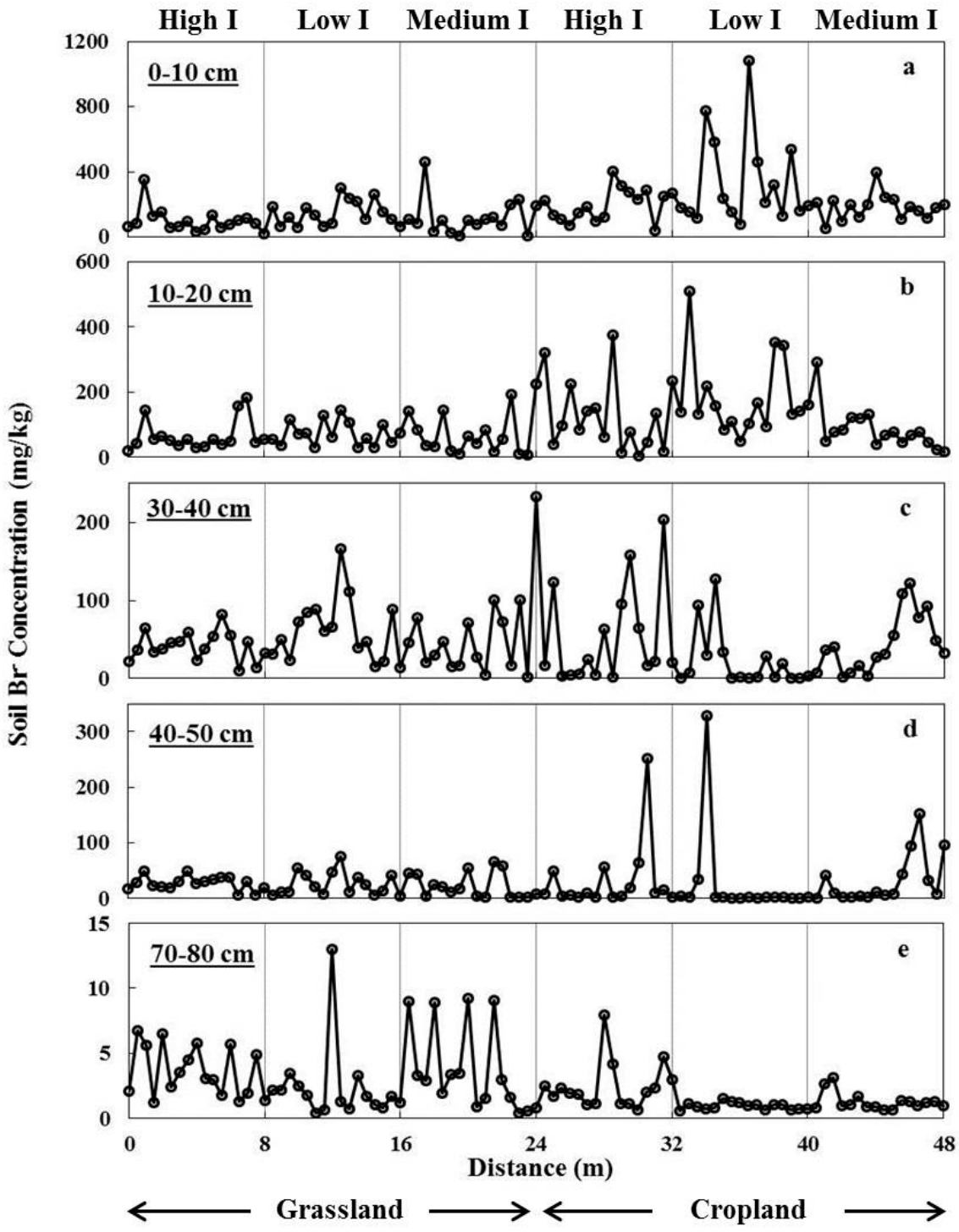

Figure 2.3 Spatial distribution of Br^- concentration measured every 0.5 m along the 48-m transect at five depths: (a) 0-10, (b) 10-20, (c) 30-40, (d) 40-50 and (e) 70-80 cm. Notice that the range of Br^- concentration varies with soil depth.

To visualize Br^- leaching patterns along the transect, a contour map based on log-transformed Br^- concentration was generated (Figure 2.4). The contrasting leaching patterns between grassland and cropland were revealed here. With less Br^- retained at shallow depths and more leached to deep soil layers, Br^- in grassland was more evenly distributed with soil depth. The probable reason was that the more developed soil structure and more continuous macropores, resulting from the typically denser root systems and higher organic matter content in grassland, caused the preferential flow and deeper leaching of Br^-. This result was in contrast to the leaching experiment in the same area without killing grasses conducted by Schwen et al. (2012) a year before, who found deeper leaching in cropland, indicating a critical impact of evapotranspiration in retarding solute leaching (Kanchanasut and Scotter, 1982).

Br^- leaching in this experiment was enhanced by increased rainfall intensity as shown in Figure 2.4. On one hand, Br^- concentrations below 60 cm were apparently lower in the regions receiving rainfall of low intensity (Low I) than those receiving medium and high intensity rainfalls in grassland. On the other hand, in cropland, relatively high Br^- concentrations in deep layers were measured sporadically and only under medium and high intensity rainfalls, referring to the existence of some preferential pathways in this soil previously managed with no-till practice. That is to say, with the increase of rainfall intensity in either land use system, soil Br^- near the surface decreased and the profile distribution of Br^- became more linear. These findings agree with those of Germann et al. (1984) and were explained by the influence of rainfall intensity and surface ponding on the

contribution of macropores to preferential flow. At higher rainfall intensity, water ponding develops more extensively and initiates preferential flow through more macropores.

Rainfall application time delay has been periodically arranged at a smaller scale (Figure 2.2) and it is not easy to identify its influence merely through the contour map. The Br^- concentrations at each depth were averaged for each plot and are presented in Figure 2.5. Apparently in cropland, Br^- concentration in the topsoil (0-10 cm) increased with application time delay (Figure 2.5d, e, f), suggesting that more solute could be protected from leaching when longer time was allowed for solute to move into aggregates. This protection effect caused by aggregates led to a lower accessibility of surface-applied Br^- by water flow. And this hypothesis is confirmed in cropland where the Br^- concentration right below (10-20 cm) showed a decreasing trend with the increase of time delay. However in grassland, this phenomenon was only obviously indicated in the plots irrigated at the low intensity (Figure 2.5b), where infiltration occurred slowly. Probably, preferential flow in those grassland plots under high and medium intensity rainfalls was strong and masked the impact of rainfall timing.

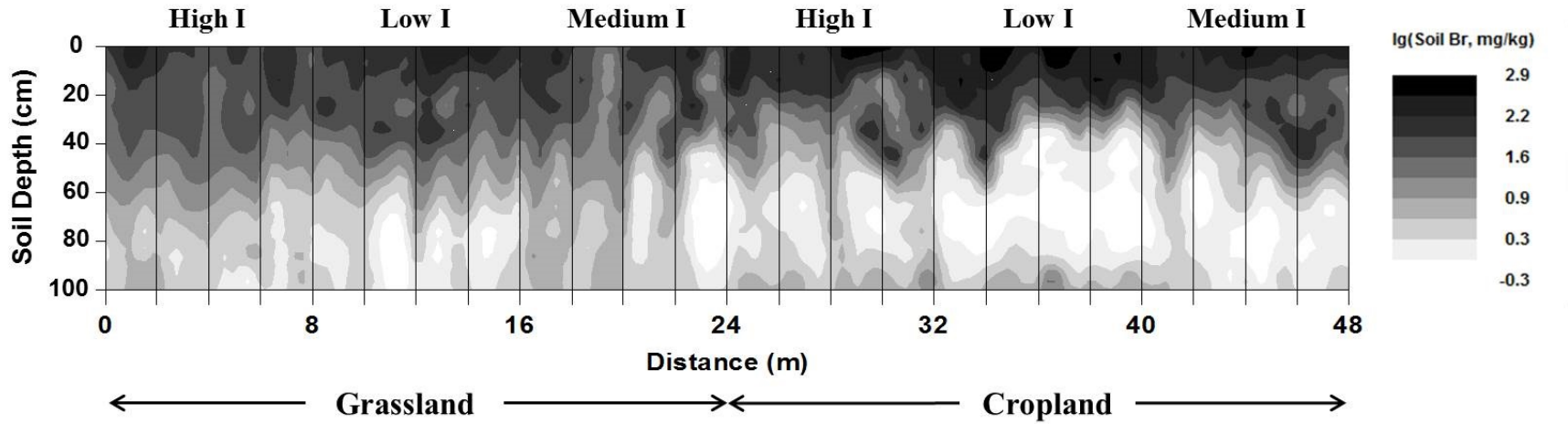

Figure 2.4 Contour map showing spatial distribution of Br^- concentration in soil profile down to 1 m depth along the 48-m transect.

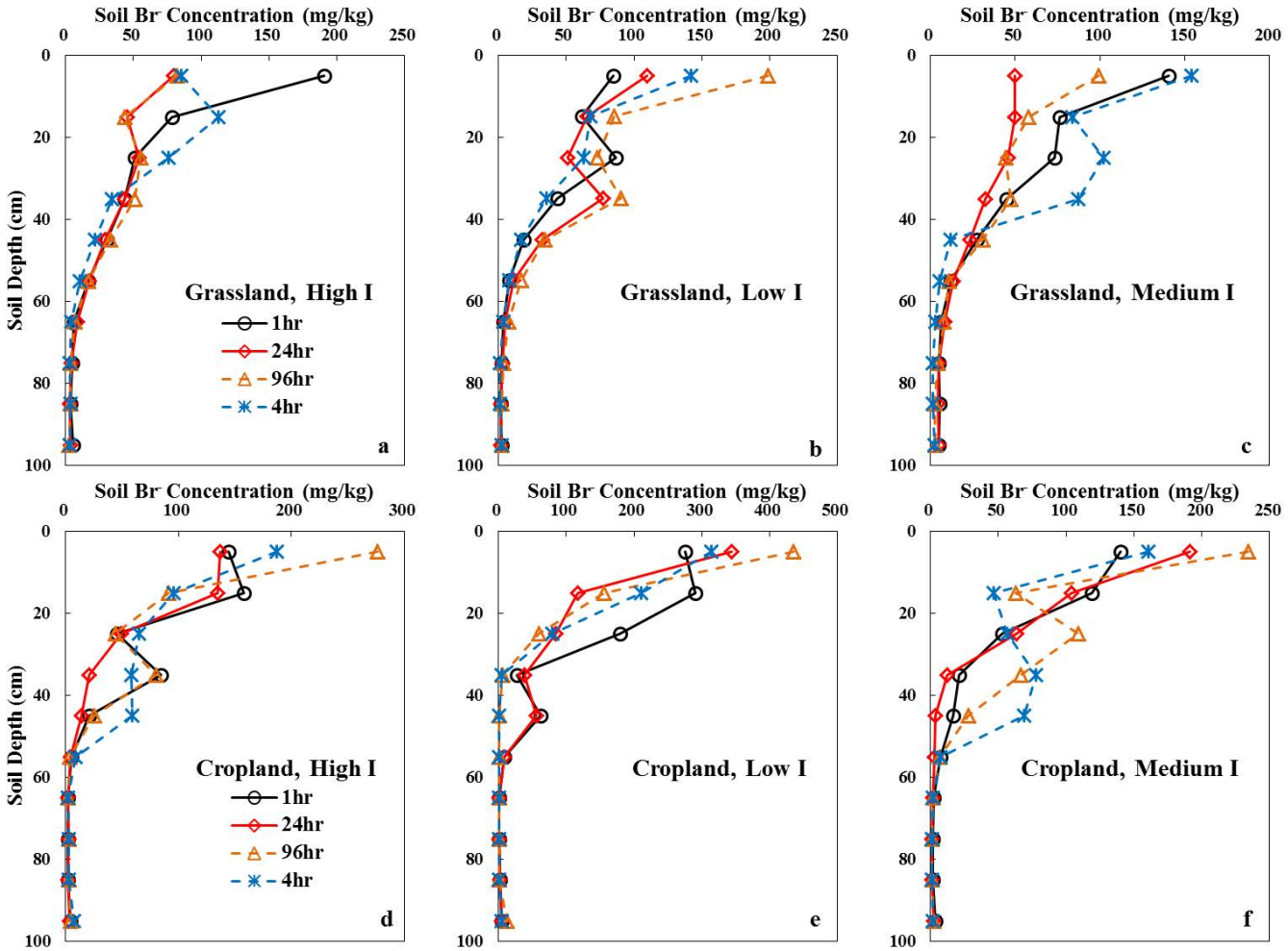

Figure 2.5 Distribution of Br^- concentration in soil profile changing with application time delay under different rainfall intensities in grassland (a, b, c) and cropland (d, e, f).

2.3.2 Spatial Correlations of Soil Br^- with Boundary Conditions

Experimental semivariograms revealing the spatial structures of boundary conditions are presented in Figure 2.6. Land use only changed once in the middle of the transect, between grassland and cropland, resulting in the appearance of semivariogram plateau at the lag distance $h \geq 24$ m (Figure 2.6a). The semivariance of rainfall intensity reached its first plateau at $h = 8$ m and decreased to the minimum at $h = 24$ m thereafter, where one cycle was completed (Figure 2.6b). The rainfall application time delay varied at a smaller scale and its semivariogram showed a short wavelength of 8 m (Figure 2.6c). It is interesting to observe the "hole effect" in the semivariogram for elevation variance (Figure 2.6d), indicating the spatial variation occurred at more than one scale (Nielsen and Wendroth, 2003). The first maximum and minimum of its semivariance appeared at $h = 8$ m and $h = 12$ m, respectively.

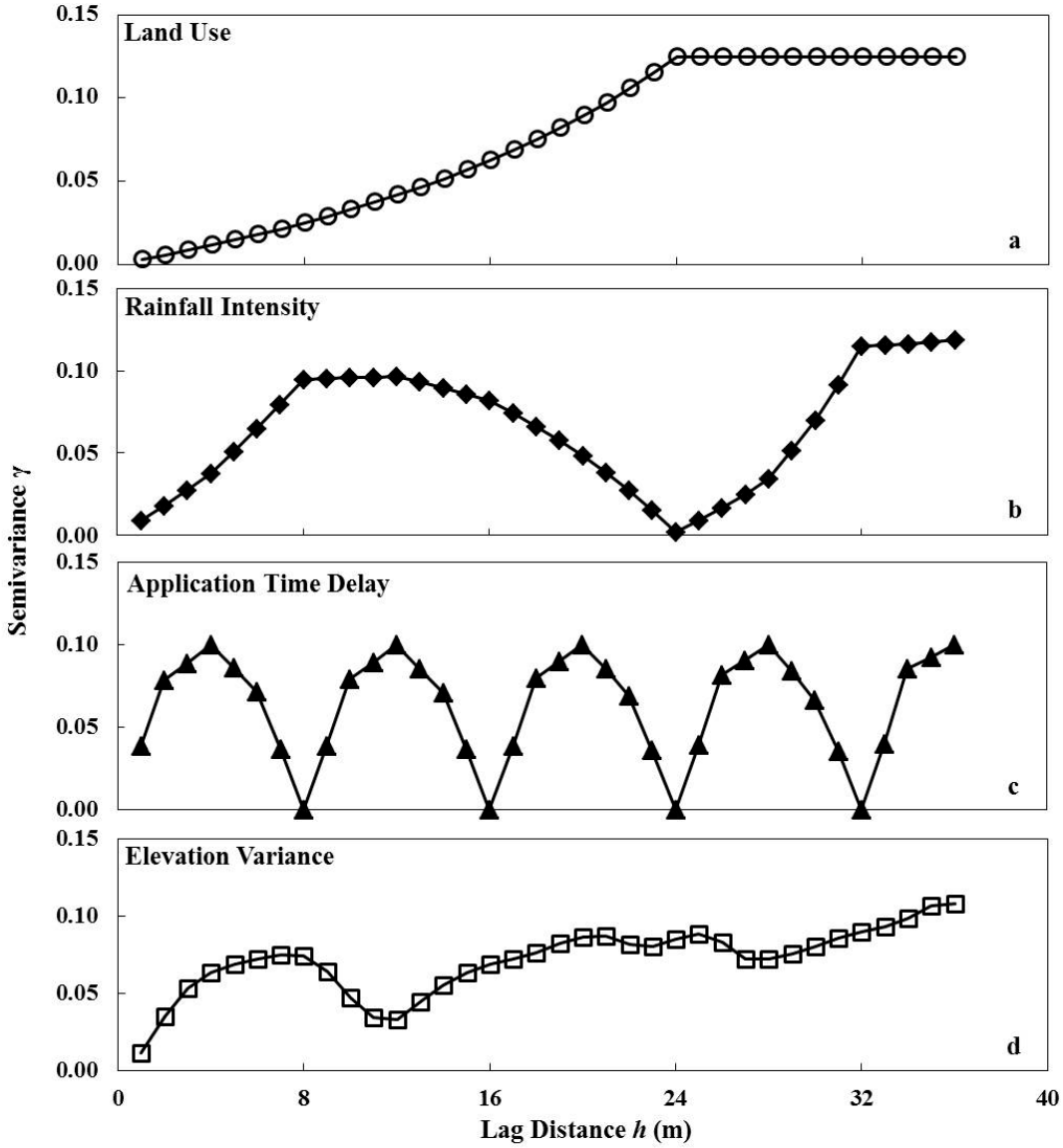

Figure 2.6 Experimental semivariograms for imposed (a) land use, (b) rainfall intensity, (c) application time delay and (d) investigated elevation variance. Note that 0 was assigned for grassland and 1 for cropland for the convenience of spatial analysis. Thus a positive correlation between land use and a specific variable indicated a larger magnitude of this variable in cropland.

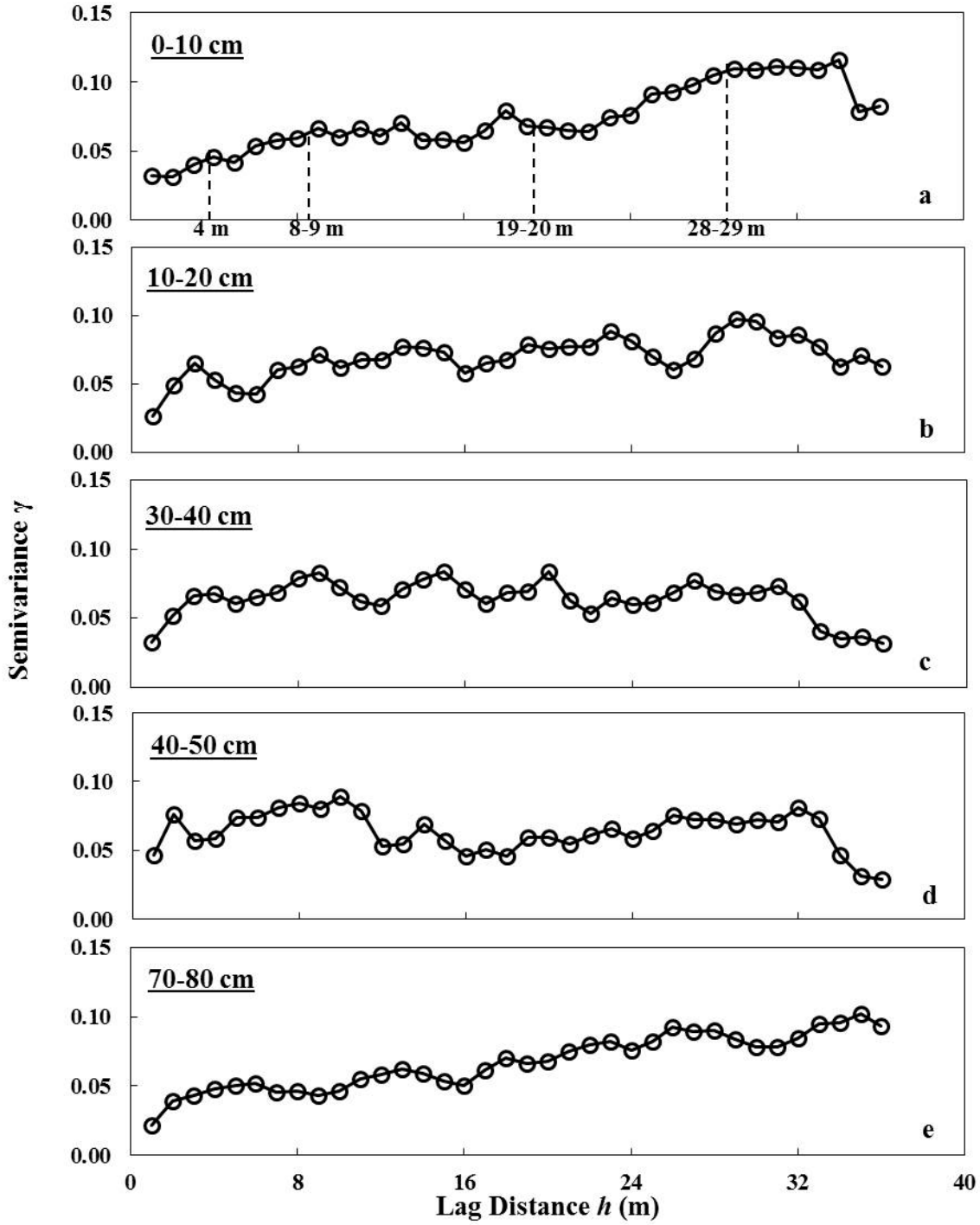

Figure 2.7 Experimental semivariograms for observed soil Br^- concentrations at five depths: (a) 0-10, (b) 10-20, (c) 30-40, (d) 40-50 and (e) 70-80 cm.

Soil Br^- concentrations at different depths were investigated at an interval of 0.5 m along the transect. These values were averaged for every 1 m resulting in 2 values per plot in each soil layer prior to normalization and spatial analysis. The semivariograms for Br^- concentrations at five depths are depicted in Figure 2.7.

In the topsoil of 0-10 cm depth, the semivariances of Br^- concentration at the first two lags were quite close, probably corresponding with the size of one plot (Figure 2.7a). At h = 4 m, at which lag distance the semivariance for application time delay achieved its first peak, a plateau was observed. The next plateau appeared at h = 8-9 m, where one cycle of application time delay was completed and the semivariance of rainfall intensity reached its first peak. The other two recognizable plateaus were observed at h = 19-20 m and h = 28-29 m, both of which were corresponding with the peak semivariances of application time delay (Figure 2.6c). At a larger scale, the semivariances at $h > 24$ m were generally greater than the ones at $h < 24$ m, which was possibly caused by the different land uses. This impact of land use attenuated in the soil layer of 10-20 cm (Figure 2.7b). The difference in the semivariances for Br^- concentration at this depth within and beyond h = 24 m was not as distinct as in the topsoil. Instead of the spatial variation at various scales, repetitive fluctuations at a wavelength of 8 m were easily identified in the semivariogram (Figure 2.7b). When the soil depth increased to 30-40 cm, besides the further weakening of land use effect, semivariance of Br^- concentration cycling at every 5-6 m and 11-12 m were observed (Figure 2.7c). Hardly could any spatial structure be detected in the semivariogram for Br^- concentration at 40-50 cm (Figure 2.7d); however below 50 cm, the generally higher semivariance at $h \geq 24$ m appeared again, which was obviously shown at 70-80 cm (Figure

2.7e). In addition, a wavelength of 8 m was recognized in the semivariogram for Br^- concentration in this layer.

To further analyze how these boundary conditions affected Br^- transport, the experimental cross-semivariances between Br^- concentrations at ten depths and the underlying boundary conditions were calculated and plotted against lag distance. Figure 2.8 shows these cross-semivariograms at five soil depths. Br^- concentration was spatially positively correlated with land use at 0-10 and 10-20 cm (Figure 2.8a, e), suggesting more Br^- retained near surface in cropland relative to grassland. At 30-40 cm, a negative spatial correlation was observed between Br^- concentration and land use (Figure 2.8i), suggesting that the more developed macropore system in grassland was able to conduct more solute into subsoil. The spatial correlation of Br^- concentration with land use was close to 0 at 40-50 cm (Figure 2.8m) and became strongly negative in deeper layers (e.g., Figure 2.8q). These findings were consistent with the more linear Br^- distribution along soil profile in grassland concluded in Section 2.3.1. The absence of spatial correlation at 40-50 cm was probably correlated to a plow pan with very low sand content (data not shown) resulting from tobacco planting and intensive tillage several years ago.

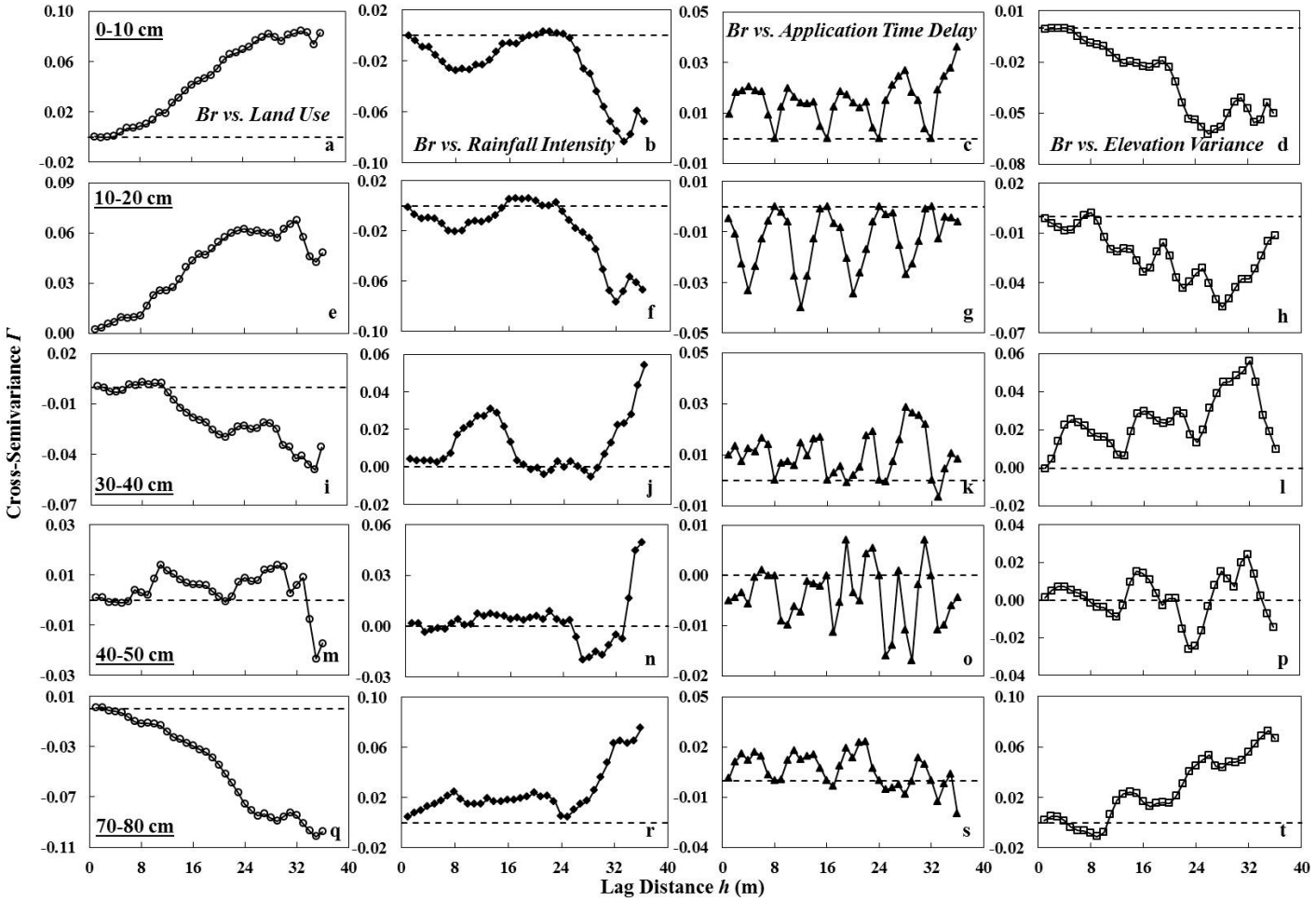

Figure 2.8 Experimental cross-semivariograms between soil Br^- concentration and imposed land use (a, e, i, m, q), rainfall intensity (b, f, j, n, r), application time delay (c, g, k, o, s) and investigated elevation variance (d, h, l, p, t) at five depths.

The spatial correlations between rainfall intensity and Br^- concentration at different depths, to some extent, confirmed the existence of the plow pan. Increased rainfall intensity was more capable of transporting surface-applied solute downwards, which was impeded by the plow pan at 40-50 cm, leading to the decrease of Br^- concentration at the surface (Figure 2.8b, f) and the accumulation of Br^- at 30-40 cm (Figure 2.8j). Water and solute may have redistributed over the plow pan through more developed lateral flow, and tended to be rapidly leached under high intensity rainfall wherever macropores were present (Janssen and Lennartz, 2007), which thereby resulted in a positive spatial correlation between intensity and Br^- concentration in deeper layers (Figure 2.8r). Bromide concentration was spatially positively correlated with application time delay in topsoil (Figure 2.8c) but negatively in the soil layer right below, 10-20 cm (Figure 2.8g). It is indicated that the time delay between solute transport and subsequent rainfall somehow decided the amount of Br^- protected by aggregates in topsoil and available for downward movement. Yet, it was unexpected to observe a positive spatial correlation between application time delay and Br^- concentration in deep soil (Figure 2.8s), although the magnitude of Br^- concentrations here was much smaller than that near soil surface. More complicated topography corresponded with deeper leaching of solute, implied in the negative spatial correlations of elevation variance with Br^- concentration in surface layers (Figure 2.8d, h) and a periodically positive one at 30-40 cm (Figure 2.8l).

2.3.3 Spectral Analysis of Soil Br^- and Boundary Conditions

Spectral and cross-spectral analyses were applied to identify the major factors that caused the spatial behaviors of soil Br^- concentration at each depth. The power spectra for

boundary conditions and soil Br^- concentration at five depths are presented in Figure 2.9. Distinct peaks in the power spectra for imposed rainfall intensity and application time delay appeared at the frequencies f = 0.0391-0.0469 and f = 0.125, corresponding to the wavelengths λ = 21.3-25.6 m and λ = 8 m, respectively (Figure 2.9a). The power spectra for elevation variance in Figure 2.9a manifested a major peak at f = 0.0781-0.0859 (λ = 11.6-12.8 m) and a minor one at f = 0.1719 (λ = 5.8 m). Comparing these power spectra to the ones for soil Br^- concentrations, the periodic variations of the boundary conditions contributing to the spatial distribution of Br^- concentration at each depth were revealed. The major peak in the power spectra for Br^- concentration at 0-10 cm occurring at the frequency f = 0.0313-0.0469 (λ = 21.3-32 m) might be correlated with rainfall intensity; while the minor one at the frequency f = 0.125 (λ = 8 m) with application time delay (Figure 2.9b). In this way, rainfall intensity probably exerted important influence on Br^- concentration at 10-20 and 30-40 cm since distinct peaks at the frequencies close to f = 0.0391-0.0469 were present in their power spectra (Figure 2.9c, d); whereas, the power spectra for Br^- concentration at 10-20 cm rather than the one at 30-40 cm, had a minor peak at the frequency of 0.125 (λ = 8 m), indicating that the influence of application time delay diminished with soil depth. Meanwhile, an obvious peak at the frequency f = 0.0859 (λ = 11.6 m) was manifested in the power spectra for Br^- concentration at 30-40 cm, revealing the contribution of topography complexity described by elevation variance (Figure 2.9d). At the soil depth of 40-50 cm, few periodic variations in Br^- concentration were found at the same frequencies with boundary conditions except a minor peak at f = 0.1719 (λ = 5.8 m) correlated with the small-scale fluctuation of elevation variance (Figure 2.9e). The redistribution of water and solute by lateral flow due to the fine soil texture here (data not

shown) was possibly the reason. The boundary conditions might affect the spatial distribution of solute leached to deep layers, since a major peak at f = 0.1172-0.125 (λ = 8-8.5 m) correlated with application time delay and a minor peak at f = 0.0391 (λ = 25.6 m) with rainfall intensity existed in the power spectra for Br^- concentration at 70-80 cm (Figure 2.9f).

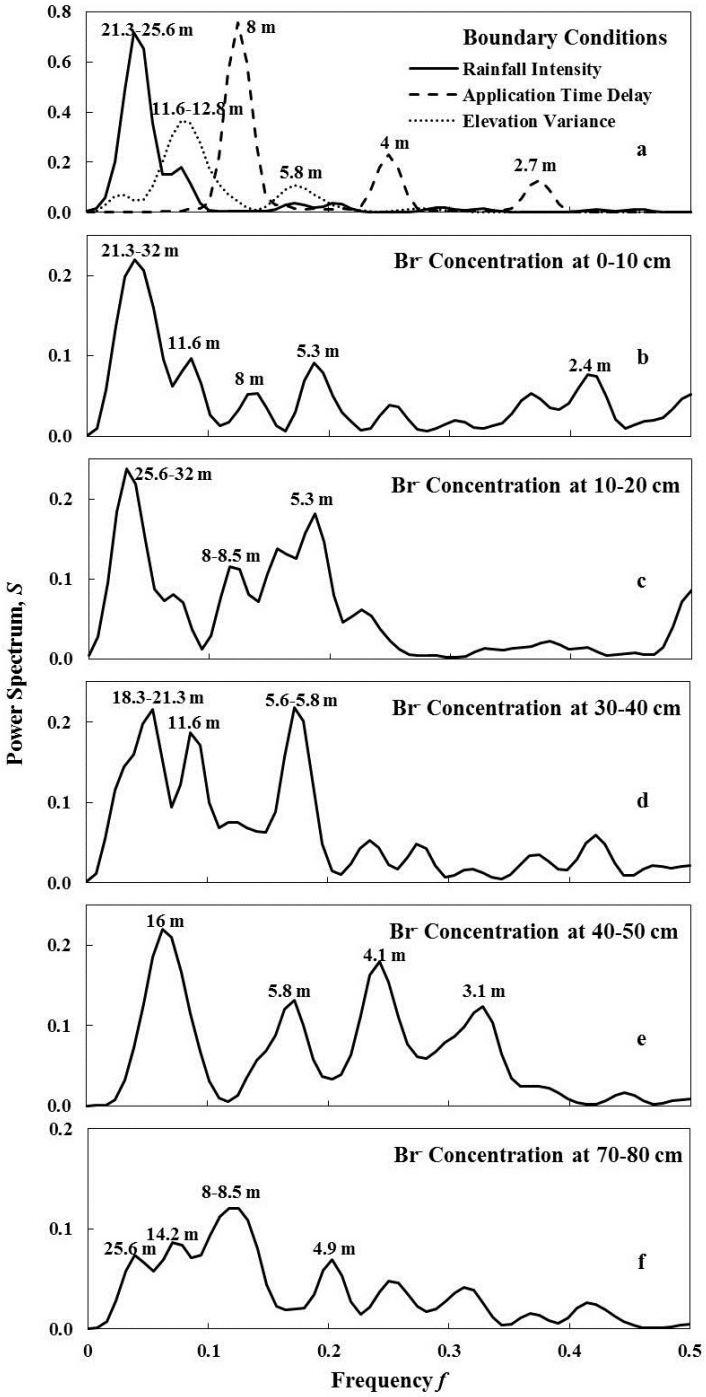

Figure 2.9 Power spectra for (a) boundary conditions (rainfall intensity, application time delay and elevation variance) and for soil Br^- concentration at five depths: (b) 0-10, (c) 10-20, (d) 30-40, (e) 40-50 and (f) 70-80 cm. The numbers above the peaks indicate the wavelengths λ at corresponding frequencies f.

Co- and quad-spectra based on normalized data revealed how the boundary conditions affected Br^- leaching and their relative importance. The spatial associations between each boundary condition and Br^- concentration were manifested by the peaks at one or several common frequencies in the co-spectra. With normalizations of all the data series, the magnitude of each peak indicated the degree of corresponding spatial correlation. The greater the peak, no matter positive or negative; the more strongly the boundary condition was correlated with the Br^- concentration. Figure 2.10 shows the co- and quad-spectra between soil Br^- concentration and the boundary conditions under investigation at five depths.

Rainfall intensity was the dominant factor that affected the spatial distribution of Br^- concentration in the topsoil of 0-10 cm, since the corresponding co-spectra showed the highest peak of -0.25 at the frequency f = 0.0469 (λ = 21.3 m) (Figure 2.10a). This strongly negative spatial correlation indicated that the increase in rainfall intensity resulted in more surface-applied Br^- transported downwards. A positive peak in the co-spectra between Br^- and clay content at f = 0.0313 (λ = 32 m) manifested their positive spatial correlation (Figure 2.10d). This might be explained by the low hydraulic conductivity as a result of increased clay content that slowed down Br^- leaching. The highest peak in the co-spectra for Br^- concentration at 10-20 cm occurred with application time delay at f = 0.125 (λ = 8 m), indicating the main influence by rainfall timing (Figure 2.10f). The pronounced negative peak here, in contrast to the slightly positive spatial correlation of application time delay with Br^- concentration in the soil layer above (Figure 2.10b), resulted in a negative peak at f = 0.125 (λ = 8 m) present in the co-spectra of Br^- concentration between these two

soil layers (Figure 2.11). At 30-40 cm, positive peaks around 0.2 were observed in the co-spectra for Br^- concentration versus rainfall intensity, elevation variance and clay content at different frequencies (Figure 2.10i, k, l). However, in the next soil layer of 40-50 cm, the distribution of Br^- was mainly affected by clay content as reflected by the highest peak in the co-spectra at f = 0.0469 (λ = 21.3 m) (Figure 2.10p). The positive peaks appearing in the co-spectra for Br^- concentration at 70-80 cm with rainfall intensity and application time delay revealed the importance of these two rainfall characteristics on the spatial behavior of Br^- leached to deep soil (Figure 2.10q, r). Compared to the experiments conducted by Wendroth et al. (2011c) and Schwen et al. (2012), in which the scale-dependent treatment was adopted to explore the influence of rainfall characteristics on solute leaching depth as well, the spatial analysis of Br^- concentration at every 10 cm down to 1 m depth provided a more comprehensive basis for the management of surface-applied chemicals. Furthermore, the investigations of elevation and soil texture in addition to rainfall characteristics, and their spatial correlations with Br^- concentration to some extent explained the large-scale processes underlying the Br^- leaching. Nevertheless, except the boundary conditions imposed (i.e., rainfall intensity, application time delay) or inherent spatial processes observed (i.e., elevation variance, clay content) in this study, there existed some other soil properties that affected Br^- leaching and contributed to its scale-variant spatial behavior (Figure 2.9).

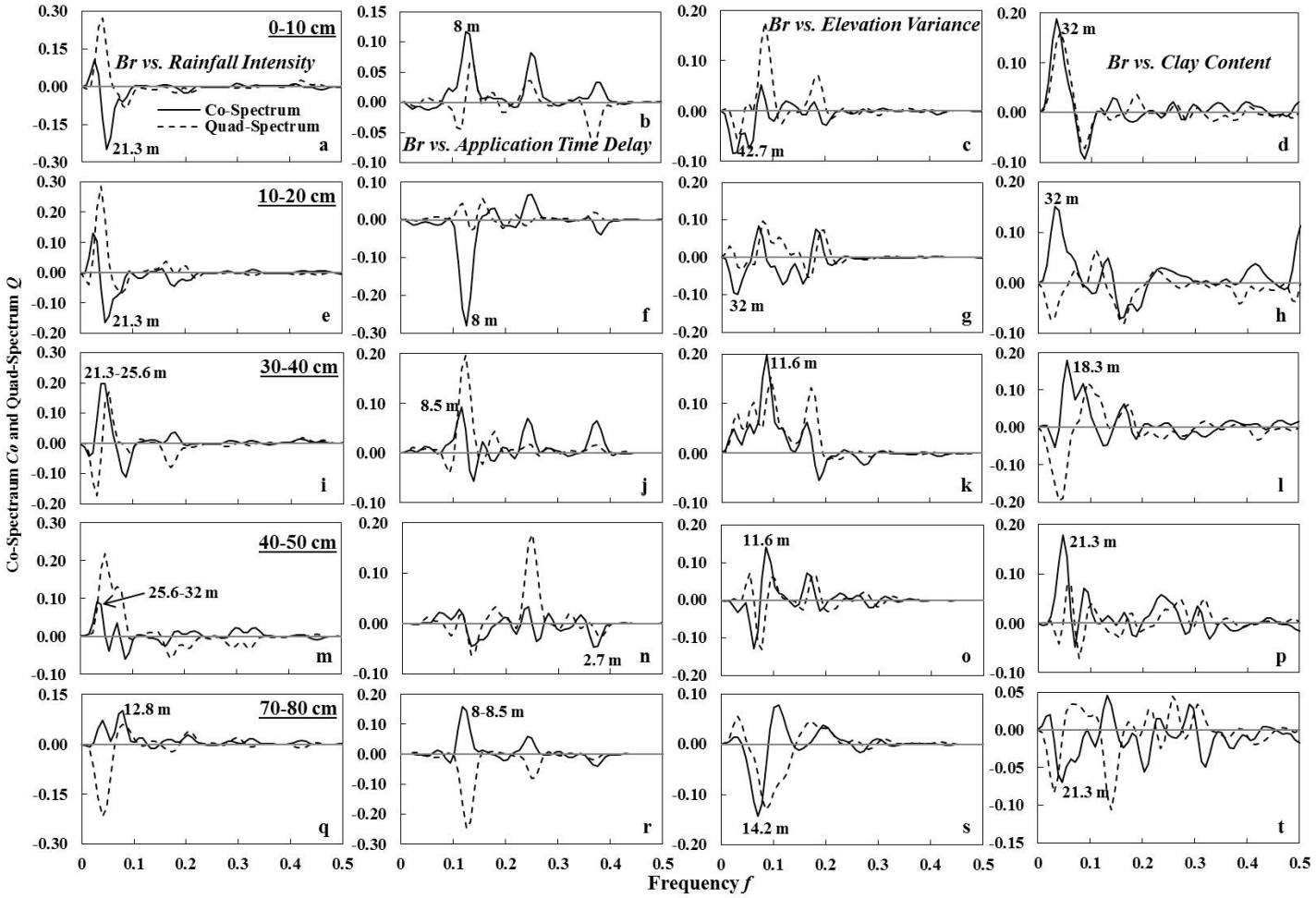

Figure 2.10 Co- and quad-spectra between soil Br^- concentration and imposed rainfall intensity (a, e, i, m, q), application time delay (b, f, j, n, r), investigated elevation variance (c, g, k, o, s) and soil clay content (d, h, l, p, t) at five depths.

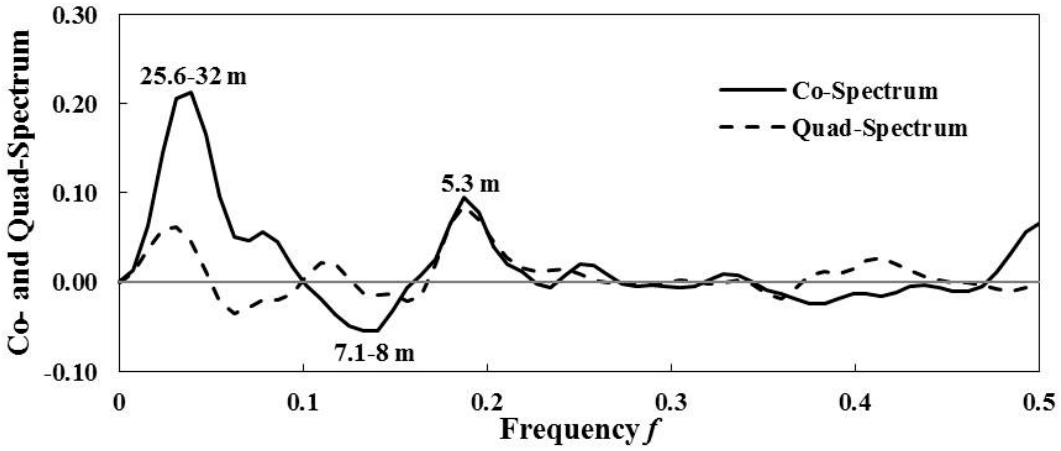

Figure 2.11 Co- and quad-spectra of soil Br^- concentration between 0-10 and 10-20 cm.

2.4. Conclusions

A new approach arranging treatments in a cyclic pattern at distinct spatial scales was used in this study to evaluate the impact of land use, rainfall intensity and the time delay relative to solute application on Br^- leaching. In this rainfall simulation experiment, more Br^- was leached from the soil surface in grassland, resulting in more even distribution of Br^- with soil depth than in cropland. The preferential flow developed through the continuous macropores in grassland was probably the reason. Furthermore, the preferential flow increased with rainfall intensity as manifested in both land use systems.

The dominant factor controlling the spatial distribution of Br^- varied with depth. In the top layer of 0-10 cm, spectral analysis showed that soil Br^- was mainly affected by rainfall intensity and to a smaller extent by soil clay content. Although the influence of application time delay was not obvious in the topsoil, the strongest spatial correlation with Br^- concentration in the soil layer right below as revealed in spectral analysis demonstrated its importance. Allowing longer time for solute to move into aggregates, less solute would be

accessible and leached down by rainfall subsequently, suggesting the use of non-equilibrium approaches based on hierarchical pore system geometry for the numerical description of transport processes. As soil depth increased, the impact of rainfall characteristics diminished; instead, the soil properties such as topographic complexity and soil texture became the major driving forces. Especially at 40-50 cm where a plow pan was believed to be present as a result of tobacco management several years ago, the spatial behavior of soil Br^- was mainly correlated with clay content. However, a positive spatial correlation was detected between rainfall intensity and Br^- concentration in deep soil, indicating the risk of groundwater contamination under heavy rainfall. The usefulness of the experimental design with scale-dependent treatment distribution used in this study suggested its applicability in studying hydrological processes at the field or even larger scales.

Chapter 3 State-Space Approach to Analyze Field-Scale Bromide Leaching

3.1 Introduction

A precise description of water and solute transport in the vadose zone is essential for the management of surface-applied chemicals, which in sustainable agriculture aims to improve crop productivity and food quality while minimizing the groundwater contamination through leaching (Russo, 1991; Corwin et al., 1999; Paramasivam et al., 2002). Many studies have been conducted on soil columns under laboratory conditions and steady-state flow; however, at the field scale, little progress has been made in characterizing the processes of water flow and solute transport, probably owing to the challenge of inherent soil spatial and temporal heterogeneity (Nielsen et al., 1986; Destouni and Graham, 1995; Ashraf et al., 1997). Affected by soil properties such as topography, soil texture, structure and spatial soil water distribution, the spatial transport behavior of water and solute is quite variable (Wendroth et al., 1999; Ersahin et al., 2002; Whetter et al., 2006).

In their field experiments based on classic block design, Kessavalou et al. (1996) and Ottman et al. (2000) used Br^- and ^{15}N as tracers and found the standard deviations were in

the same magnitude as the amounts of solutes leached below 1.2 and 4 m depths, respectively. When such a large inherent variability is present in the set of measurements, it becomes extremely difficult to quantify solute transport and to analyze treatment effects afterwards (Wendroth et al., 2011c). In order to yield a representative estimate of solute transport, field experiments aimed at the spatial structures of solute transport variables and their spatial correlations with soil properties have been established since mid-1990s (Ellsworth and Boast, 1996). Nevertheless in many cases, a single spatial range of an individual observation on solute transport could hardly be derived (Netto et al., 1999; Schwen et al., 2012), as it usually varies over different scales (Biggar and Nielsen, 1976; Wendroth et al., 2011c). In view of this limitation, a novel experimental design, arranging treatments in cyclic layout at distinct scales has been introduced (Bazza et al., 1988; Shillito et al., 2009). Using frequency-domain analysis, i.e., spectral and cross-spectral analyses, the variances of treatments as well as the related processes can be decomposed among different scales (Kachanoski and De Jong, 1988; Wendroth et al., 2011c); thereby allowing identification of the major factors and inherent soil variability-related processes that take effect (Nielsen and Alemi, 1989; Shillito et al., 2009). Thus a field study applying land use and two rainfall characteristics, i.e., rainfall intensity and the time delay between solute application and subsequent rainfall (application time delay), at different scales was conducted earlier (Yang et al., 2013). Including topography complexity and soil texture as boundary conditions, the dominant factors controlling Br^- leaching were found to vary with soil depth.

Spectral analysis and the scale-dependent treatment distribution mentioned above provide an effective way to characterize the spatial associations between boundary conditions and solute transport variables. However, when two boundary conditions, e.g., topography and soil texture, interact, which are typically present between inherent soil processes on which the varying scale-dependent treatments could not be imposed arbitrarily, the implications of spatial correlations between solute transport and either boundary condition to chemical management are prone to be impaired. Moreover, spectral analysis alone is not able to simulate or forecast the fate of surface-applied chemicals quantitatively, which could be applied in precision agriculture and site-specific solute transport modeling (Loague and Green, 1991; Van Alphen and Stoorvogel, 2000). To further interpret the causes of solute leaching behaviors and to describe their spatial patterns thereafter, the application of state-space technique was suggested (Wendroth et al., 2011c; Schwen et al., 2013).

The state-space methodology was introduced by Kalman (1960) and Kalman and Bucy (1961) to filter noisy electrical time series; and then extended to analyze economic series by Shumway and Stoffer (1982) and soil properties by Morkoc et al. (1985). In an autoregressive multivariate state-space model, the variable of interest is related to the same variable and other related variables at the previous location (Shumway and Stoffer, 1982; Nielsen and Wendroth, 2003); and the regression coefficient of each variable reflects the degree of its spatial correlation with the outcome (Morkoc et al., 1985). In the state-space approach, the same variables can be employed as in a classical linear regression analysis. However, the principles behind these two approaches differ conceptually. Assuming that all the observations are independent from each other, the classical statistical method

generates an overall response function between two variables. This attempt often fails at the field scale because the observations are commonly spatially correlated (Nielsen and Alemi, 1989) and the underlying processes that are not included in the investigation could modify the response manner across the field. On the contrary, the autoregressive state-space approach takes advantage of the spatial dependence inherent in observations and analyzes the correlations of spatial point-to-point processes between two variables. The change in one variable from one location to the next is related to the change in the other variable. Based on the spatial correlations between point-to-point changes, the state-space model is able to estimate even missing data as well as to forecast the ones outside the domain of observation (Morkoc et al., 1985; Wendroth et al., 2003) while standard error intervals of the estimation increase with increasing distance from a point with an observation. Timm et al. (2004) described the spatial distribution of soil water content in a sugarcane field by clay content, soil organic matter and aggregate stability; and found that compared to multiple regression equations, the estimates based on state-space model by far better agreed with the measured data. Leaving out one third of the measurements along a sorghum transect, Morkoc et al. (1985) successfully estimated the water content by soil surface temperature using state-space model; and for the fifteen omitted locations, the resulting estimates were all within one standard error except for only two locations. Moreover, in contrast to classical statistics, the state-space technique considers the observations as a limited reflection of the real process. With given equipment, sampling volume and analytical device, observations cannot be equivalent to the “true state” but only provide an indirect measure with an unidentified “noise” (Nielsen and Wendroth, 2003). Moreover, inasmuch as the form of a first-order autoregressive model implies limits in the

description of the process, the model uncertainty is included in the process description as well. Accordingly, a mathematical algorithm is included in the state-space approach to filter these uncertainties. In view of these merits, this spatial analysis tool has been widely used to quantify the spatial correlations between soil water and temperature (Morkoc et al., 1985; Dourado-Neto et al., 1999), among soil physical and chemical properties (Timm et al., 2004; Wendroth et al., 2006), as well as to predict crop yields based on soil properties (Cassel et al., 2000; Li et al., 2002) or nutrient status (Wendroth et al., 1992) or both (Wendroth et al., 2003). However, few state-space models of solute transport have been developed and presented.

Most researches incorporating the spatial variability of soil properties to analyze water and solute transport only consider the horizontal variation, but ignore the soil heterogeneity in the vertical direction (Russo, 1991; Russo and Bouton, 1992; Vanclooster et al., 1995; Netto et al., 1999). Field soils, however, are often layered and more homogeneous in the horizontal than the vertical direction (Porro et al., 1993). This vertical heterogeneity, typically in soil texture and structure (Butters and Jury, 1989; Heijs et al., 1996; Kulli et al., 2003), exerts an important impact on lateral water flow and solute mixing; thereby affecting solute distribution in both horizontal and vertical directions (Vanclooster et al., 1995; Flühler et al., 1996). Using Brilliant Blue ECF as a dye tracer, Kulli et al. (2003) investigated the stained infiltration patterns at 25 plots over 8 sites and discovered that besides soil texture and structure, the characteristics of the overlying soil layers could also influence the solute distribution in a given layer and subsequently through the soil profile. With distinct layers above, which control the solute input together with experimental setup

(e.g., the amount of solute applied, rainfall intensity) and other boundary conditions (Trojan and Linden, 1992), even similarly textured soil layers are prone to exhibit quite different flow patterns of water and solute (Kulli et al., 2003). Therefore, it would be helpful to involve the solute concentrations and soil properties of the overlying layers into the spatial description of field solute transport.

The hypothesis of the present study is that subsequent to the diagnosis of cyclic variation sources using frequency-domain analysis, the state-space approach more comprehensively characterizes the spatial processes of Br^- leaching in the field experiment conducted earlier by Yang et al. (2013), when natural boundary conditions are taken into account. Adopting autoregressive state-space models, the objectives were to: 1) analyze the spatial correlations of soil Br^- among different depths; 2) describe the horizontal distribution of soil Br^- at each depth based on the boundary conditions investigated; and 3) identify the main driving forces, either imposed treatments or natural processes or both, that control Br^- leaching and its spatial distribution at a particular soil depth.

3.2 Materials and Methods

3.2.1 Experimental Design

The field experiment was conducted in the late spring of 2012 at the University of Kentucky's Spindletop Research Farm, Lexington, KY. Along a 48-m transect evenly laid out across two land use systems: cropland and grassland, 24 plots each 2 m in length and 3 m in width were established. As a result, half of the plots were located on cropland, which is normally planted with no-till winter wheat, and the other half on grassland, dominated

by tall fescue, bluegrass and red clover. In a sampling campaign, undisturbed soil cores of 1 m depth were collected every 1 m along the transect and divided in 10 cm increments for soil texture determination using the pipette method (Gee and Bauder, 1986). The contour maps of sand and clay content along the transect are presented in Figure 3.1. Meanwhile, relative elevation at an interval of 25 cm, both along and across, the transect in a 197×13 grid was measured and then averaged for every 1 m (Figure 3.2c). As an indicator of topographic complexity, the corresponding elevation variance was calculated as the sum of squared differences from the neighboring relative elevations.

One and a half months before the Br^- leaching experiment, glyphosate (Roundup, Monsanto Co.) was applied to kill all the plants. KBr solution was applied to the transect at a constant rate of 37.5 g Br m^{-2} with a regular farm sprayer. Using garden sprinklers attached to a metal frame, rainwater collected earlier was applied along the transect at a constant amount of 44 mm, at three levels of intensity, 5, 22 and 44 mm h^{-1}, and with four levels of application time delay, 1, 4, 24 and 96 h, in a repetitive pattern at distinct scales (Figure 3.2a, b). As a result of the natural precipitation occurring during rainfall simulation, final amounts and intensities at some plots were slightly different from the ones intended; and the about 10 mm h^{-1} higher intensity at plot 1 and 2 than the one intended was due to an accidental malfunction of the pumping system. After rainfall simulation, soil cores down to 1 m depth were sampled at an interval of 0.5 m along the 48-m transect and then divided in 10 cm increments for Br^- analysis. For more details, the reader is referred to Yang et al. (2013).

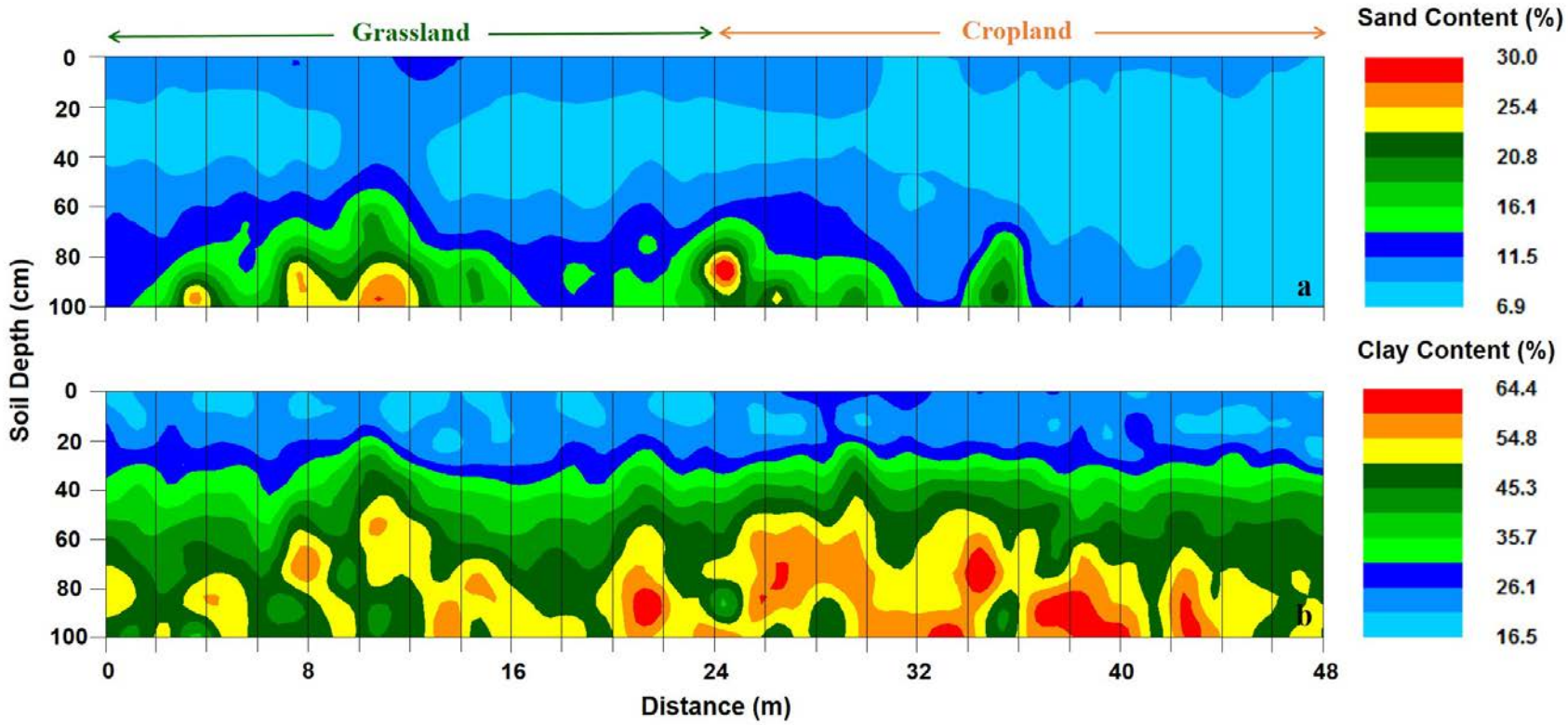

Figure 3.1 Contour maps showing spatial distribution of (a) sand content and (b) clay content in the soil profile down to 1 m depth along the 48-m transect.

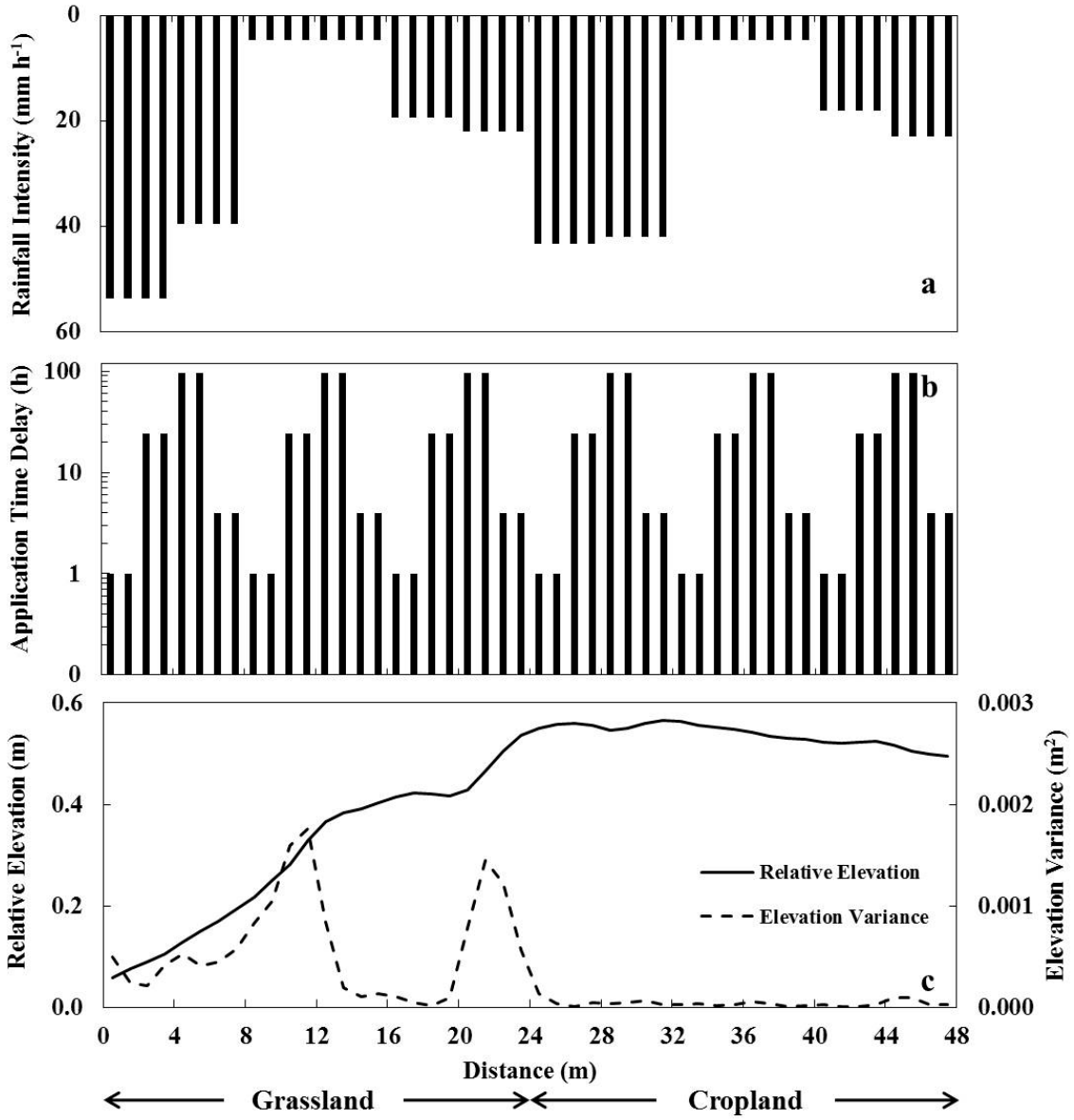

Figure 3.2 Spatial distribution of (a) rainfall intensity, (b) application time delay, and (c) relative elevation and elevation variance along the 48-m transect. Thereinto, the intensive measurements of relative elevation taken every 25 cm in both directions were averaged for every 1 m resulting in 2 values per plot; and the corresponding elevation variance was calculated by summing up the squared differences from the neighboring relative elevations.

3.2.2 Theory of State-space Model

Allowing measurement uncertainty as well as model error (Nielsen et al., 1999; Nielsen and Wendroth, 2003), the autoregressive state-space models consist of an observation equation and a state equation (Shumway and Stoffer, 1982). In the observation equation

$$Y_i = \mathrm{M}_i Z_i + v_i \tag{3.1}$$

the observed vector Y_i is related to the true state vector Z_i through a measurement matrix M_i and an uncorrelated mean zero observation error vector v_i (Shumway, 1988; Cassel et al., 2000).

The state equation, in a commonly used first-order autoregressive state-space model, considers the state of a variable or a set of variables at location i with respect to the state at location $i-1$ (Shumway, 1988):

$$Z_i = \Phi Z_{i-1} + \omega_i \tag{3.2}$$

in which Z_i is the state vector, i.e., a set of p variables at location i, Φ the $p \times p$ transfer matrix consisting of autoregressive coefficients and ω_i the uncorrelated zero mean model error vector. The state-space models, in this study, were solved using Kalman filtering (Kalman, 1960) and the EM algorithm within an iterative procedure (Shumway and Stoffer, 1982), during which the iteration was terminated once the relative convergence limit of 0.005 was reached.

Prior to state-space analysis, all the data including boundary conditions (e.g., sand content, rainfall intensity) and soil Br^- concentration at each depth, were scaled by the equation below (Nielsen and Wendroth, 2003).

$$x_i' = \frac{x_i - (\bar{x} - 2\sigma_x)}{4\sigma_x} \tag{3.3}$$

Hereby, x_i denotes the observed value at location i, $\bar{x}$ and σ_x are the mean and standard deviation of x_i, respectively. After normalization, the data series x_i' would have a mean of 0.5 and a standard deviation of 0.25. The rationale behind this scaling procedure is to avoid numerical problems that can arise if two or more variables differ by orders in their magnitude. Furthermore, when the variables are in the same order of magnitude through normalization, their contributions to the estimate can be reflected in their transition coefficients in the corresponding state-space model. However, when the variables are applied in different models, the transition coefficients themselves are not sufficient. And the relative contribution of each variable is calculated, by dividing the corresponding transition coefficient over the sum of coefficients in the respective state equation.

The average of the residuals between observations and estimations, RSS_{avg}, which is often used to evaluate the prediction quality of a regression model is calculated according to:

$$RSS_{avg} = \frac{1}{N}\sum_{i=1}^{N}(y_i - y_i^*)^2 \tag{3.4}$$

in which N is the number of observations, y_i and y_i^* are the observation and estimation at location i, respectively. For autoregressive model selection, Akaike (1969) developed an information criterion, AIC, accounting for the effect exerted by the number of regression variables k (Shumway and Stoffer, 2000).

$$AIC = lnRSS_{avg} + \frac{2k}{N} \tag{3.5}$$

The lower the AIC, the better the goodness of fit . When the number of observations is small compared to the number of regression variables selected in the state-space model, e.g., $N/k < 40$, the corrected AIC, AIC_c, is recommended (Nielsen and Wendroth, 2003).

$$AIC_c = lnRSS_{avg} + \frac{N+k}{N-k-2} \tag{3.6}$$

3.2.3 Spectral Analysis

Since the experiment was laid out in a spatially cyclic arrangement of treatments, spectral and cross-spectral analyses were used to analyze the frequency-domain variance components (Shumway, 1988; Nielsen and Wendroth, 2003). Based on Fourier transformation, in which a data series is considered as an infinite combination of sine and cosine waves, the power spectrum $S(f)$ was calculated by integrating the autocorrelation function $r(h)$ with respect to lag distance h:

$$S(f) = 2\int_0^\infty r(h)\cos(2\pi f h)\,dh \tag{3.7}$$

A periodicity implied in a data series is exhibited in the power spectrum as a variance peak S plotted against the associated frequency f, which is the inverse of the wavelength λ reflecting the scale of variation. The occurrence of several peaks on $S(f)$ indicates that the data series varies at more than one scale.

Integrating the cross-correlation function $r_c(h)$, the co-spectrum $Co(f)$ detects at what scales two data series have common variations:

$$Co(f) = 2\int_0^\infty r_c(h)\cos(2\pi f h)\,dh \tag{3.8}$$

where the $r_c(h)$ combines the positive and negative lags through $r_c(h) = 0.5[r_c(h<0) + r_c(h>0)]$. This averaging procedure emphasizes the cyclic variations described by a

cosine wave but eliminates the ones by a sine wave. And the quad-spectrum $Q(f)$ reinforces the periodic fluctuations by a sine function:

$$Q(f) = 2\int_0^\infty r_c'(h)\sin(2\pi f h)\,dh \tag{3.9}$$

in which $r_c'(h) = 0.5[r_c(h<0) - (h>0)]$. The main importance of quad-spectrum lies in its use to identify the phase lag $h_\emptyset$ at which two data series reach their maximum cross-correlation (Nielsen and Wendroth, 2003; Wendroth et al., 2011c).

3.3 Results and Discussion

Spatial series of soil Br^- concentrations at five out of the ten measured depths are shown in Figure 3.3. In general, soil Br^- concentration decreased with depth at the time of sampling. These values investigated at an interval of 0.5 m along the 48-m transect were averaged for every 1 m, resulting in 2 values per plot in each soil layer. After normalization with respect to the mean and standard deviation, soil Br^- concentration series observed at each depth were analyzed with state-space models.

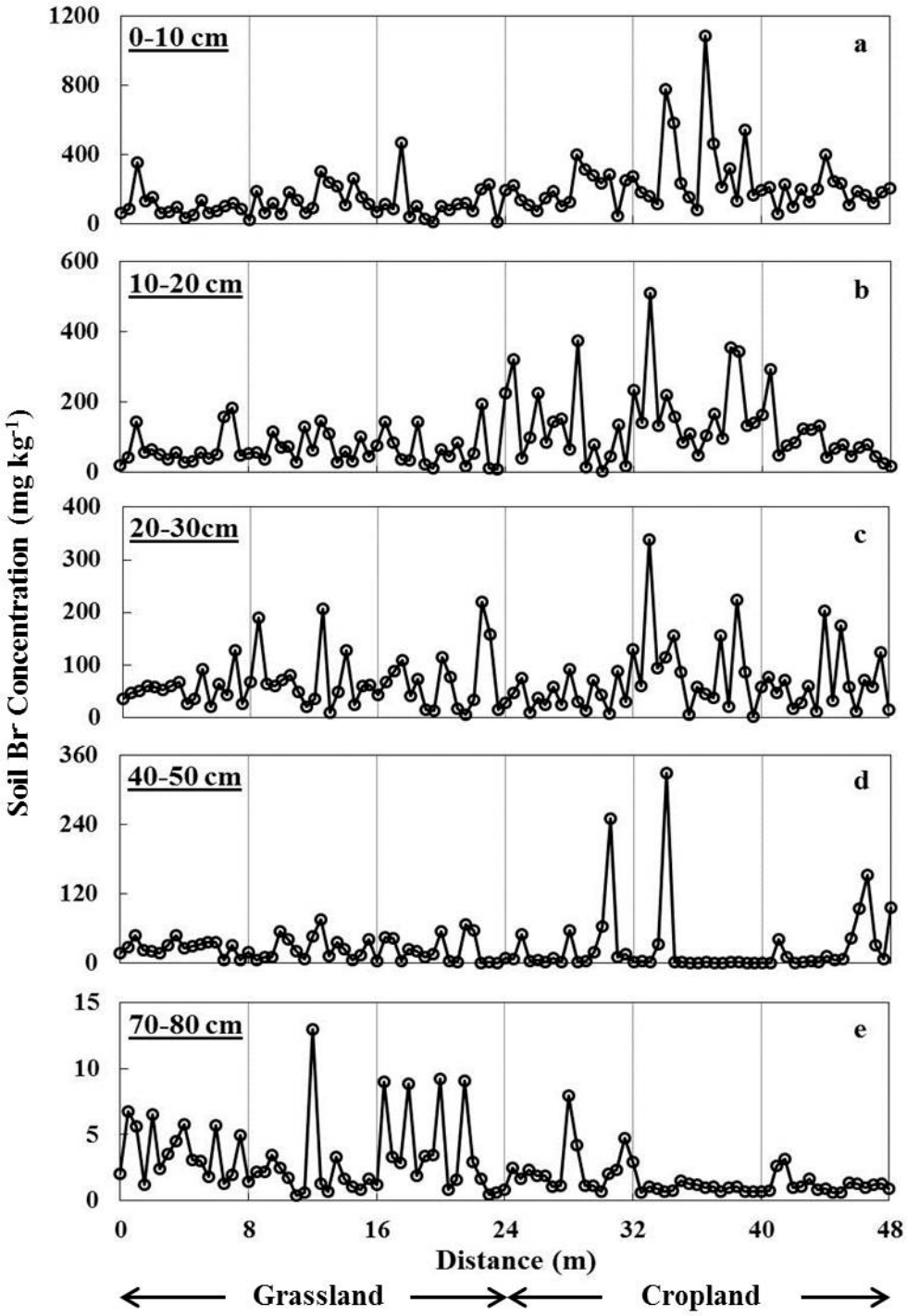

Figure 3.3 Spatial distribution of Br^- concentration measured every 0.5 m along the 48-m transect at five depths: (a) 0-10, (b) 10-20, (c) 20-30, (d) 40-50 and (e) 70-80 cm. Note that the range of Br^- concentration varies with soil depth.

3.3.1 Spatial Associations of Soil Br^- across Different Soil Depths

Soil Br^- concentration in each 10-cm layer except the top 0-10 cm was analyzed using a bivariate state-space model based on the Br^- concentration in each of its overlying layers. Table 3.1 shows the state-space equation giving the best prediction as indicated by the smallest RSS_{avg} and AIC_c. For three of the soil layers at 10-20, 50-60 and 60-70 cm, the spatial process of soil Br^- was better described in the state-space model based on the Br^- concentration in the above layer, i.e., 0-10, 40-50 and 50-60 cm, respectively, compared to other overlying soil layers. Yet this result was not found in other layers. Instead, the spatial process of Br^- concentration at 0-10 cm depth affected the spatial Br^- behavior in several layers. Using Br^- concentration in the top soil of 0-10 cm resulted in the best prediction of soil Br^- at 20-30, 30-40 and 40-50 cm; while for the soil layers of 70-80, 80-90 and 90-100 cm, the best estimations were obtained with state-space models based on Br^- concentrations at 50-60 cm. This is explained in more details with an example below.

Table 3.1 Optimal bivariate state-space equation for soil Br^- concentration in each soil layer below 10 cm depth and its RSS_{avg} and AIC_c. The number following Br indicates the center depth of the corresponding soil layer. For example, $Br15_i$ denotes soil Br^- concentration in the soil layer of 10-20 cm at location i.

Depth (cm)	Autoregressive State-Space Equation	RSS_{avg}	AIC_c
10-20	$Br15_i = 0.542Br15_{i-1} + 0.421Br5_{i-1} + w_i$	0.0009	-5.92
20-30	$Br25_i = 0.497Br25_{i-1} + 0.447Br5_{i-1} + w_i$	0.0009	-5.85
30-40	$Br35_i = 0.830Br35_{i-1} + 0.132Br5_{i-1} + w_i$	0.0042	-4.34
40-50	$Br45_i = 0.760Br45_{i-1} + 0.206Br5_{i-1} + w_i$	0.0205	-2.75
50-60	$Br55_i = 1.101Br55_{i-1} - 0.198Br45_{i-1} + w_i$	0.0051	-4.14
60-70	$Br65_i = 0.903Br65_{i-1} + 0.042Br55_{i-1} + w_i$	0.0003	-6.98
70-80	$Br75_i = 0.177Br75_{i-1} + 0.786Br55_{i-1} + w_i$	0.0001	-8.71
80-90	$Br85_i = 0.375Br85_{i-1} + 0.591Br55_{i-1} + w_i$	0.0017	-5.26
90-100	$Br95_i = 0.840Br95_{i-1} + 0.146Br55_{i-1} + w_i$	0.0345	-2.23

Figure 3.4 shows the comparison between state-space models using the Br^- concentration in the adjacent layer and in the optimal layer as presented in Table 3.1. Based on soil Br^- at 10-20 cm ($Br15$), the bivariate state-space model for Br^- concentration at 20-30 cm ($Br25$) resulted in a $RSS_{avg}$of 0.0051 and an average estimation standard error of 0.095 (Figure 3.4a). The estimation of $Br25$ at location i ($Br25_i$) was primarily relying on the value of $Br25$ at location $i-1$ ($Br25_{i-1}$), indicated by the greater transition coefficient of 0.610 compared to that of $Br15_{i-1}$ in the state equation. When applying $Br5$ in the bivariate analysis, both the resulting RSS_{avg} and standard error decreased considerably, to 0.0009 and 0.076, respectively, manifesting a better estimation result of $Br25$ with this model (Figure 3.4b). To compare the ability of $Br15$ and $Br5$ in explaining the spatial process of $Br25$, the relative contribution of $Br25_{i-1}$ was calculated and found to be

reduced from 0.656 to 0.527 when using $Br5$ instead of $Br15$. This comparison indicated a stronger spatial association of $Br25$ with $Br5$ than with $Br15$.

The situation was a little different when comparing the two bivariate state-space models for Br^- concentration at 40-50 cm ($Br45$). As shown in Figure 3.4c and d, adopting $Br5$ better described the spatial processes of $Br45$, as implied in a lower RSS_{avg} and a smaller contribution of $Br45_{i-1}$ than those in the state-space model involving Br^- concentration in the adjacent layer of 30-40 cm ($Br35$). However, the standard errors of the estimates have more than doubled for most locations probably because of the larger point-to-point fluctuations that can be more difficult to capture (Vachaud et al., 1985) than longer local trends. This model behavior reflects that rather than $Br35$, $Br5$ better revealed the general trends of $Br45$. The accompanied greater uncertainty might have resulted from the local small-scale variations in soil properties which affected water and solute transport behavior and was not captured by $Br5$ (Kachanoski and De Jong, 1988).

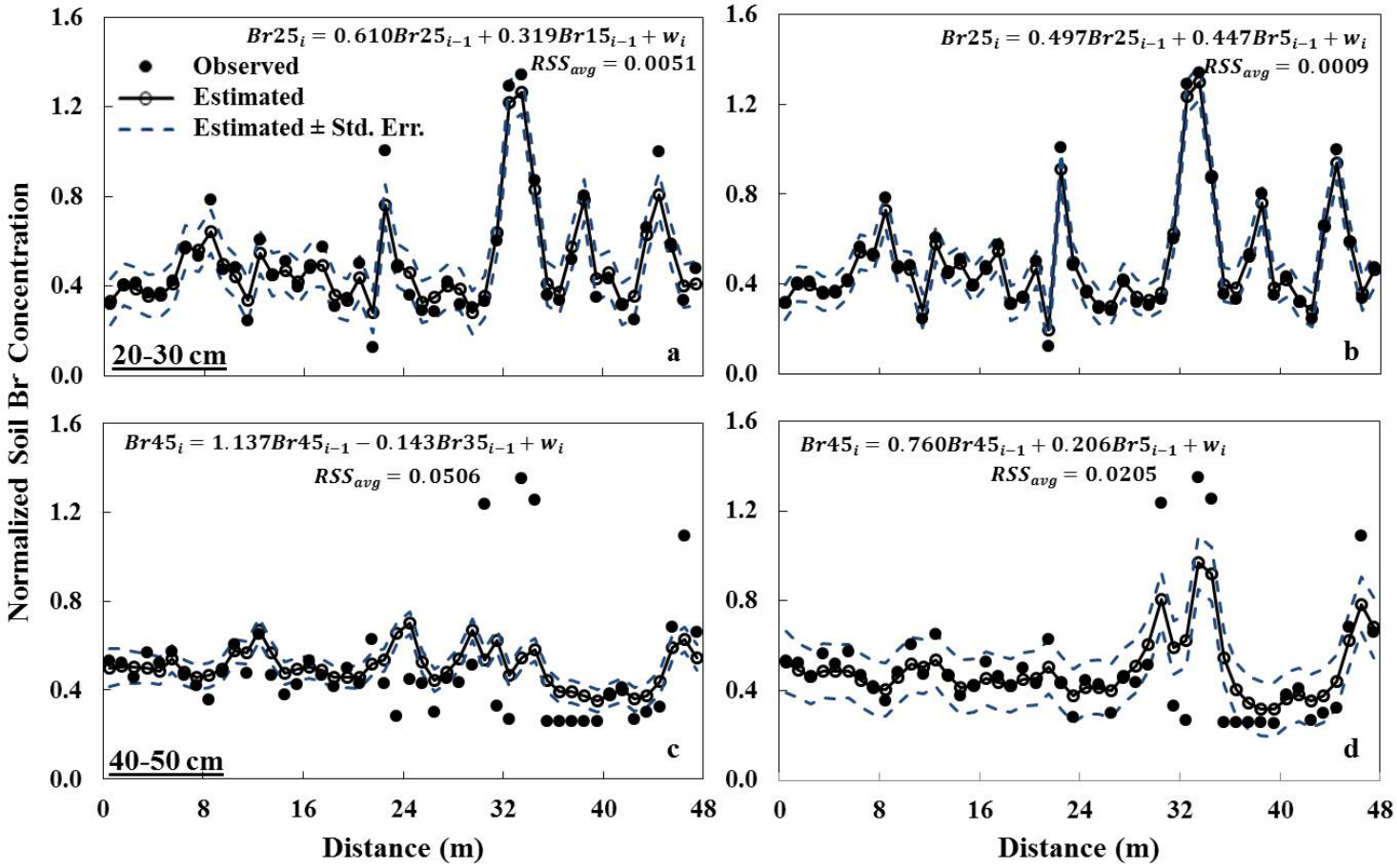

Figure 3.4 Spatial processes of soil Br^- at 20-30 and 40-50 cm described in the bivariate state-space models based on Br^- concentration (a, c) in the adjacent layer and (b, d) in the optimal overlying layer. The respective state-space equations and the values of RSS_{avg} are given.

Spectral and cross-spectral analyses based on normalized data were conducted to explore the variation scales these Br^- concentrations were correlated at. As shown in Figure 3.5a, a distinct peak in the power spectra for $Br5$ appeared at the frequency f = 0.0391, corresponding to the wavelength λ = 25.6 m. More than one distinct peak was revealed in the power spectra for Br^- concentration at the lower two depths. For $Br35$, the peaks at f = 0.0547 (λ = 18.3 m) and f = 0.1719 (λ = 5.8 m) were the highest and a smaller variance component was revealed at f = 0.0859 (λ = 11.6 m) (Figure 3.5b); while for $Br45$, besides the major one at f = 0.0625 (λ = 16 m), three minor peaks occurred at the frequencies of 0.2422 (λ = 4.1 m), 0.1719 (λ = 5.8 m) and 0.3281 (λ = 3.1 m), following the descending order of peak magnitude (Figure 3.5c). Obviously, $Br45$ and $Br35$ exhibited the same variation scale of 5.8 m. On the other hand, comparing the power spectra for $Br5$ with the one for $Br45$, the common periodicities were not clearly manifested. To further analyze the spatial correlations between $Br45$ and $Br35$, and between $Br45$ and $Br5$, the corresponding co-spectra were calculated and presented in Figure 3.5d. A major peak in the co-spectra between $Br45$ and $Br35$ was revealed at the frequency f = 0.1719, corresponding to the wavelength λ = 5.8 m, and reflecting the scale of dominant synchronous variations. In contrast, the only distinct peak appeared at f = 0.0547 (λ = 18.3 m) in the co-spectra between $Br45$ and $Br5$, indicating that the Br^- concentrations at these two depths were spatially correlated at a larger scale. These results confirmed that $Br5$ rather reflected the overall distribution of $Br45$ but not the small-scale fluctuations, which could be a major source of the relatively higher model uncertainty.

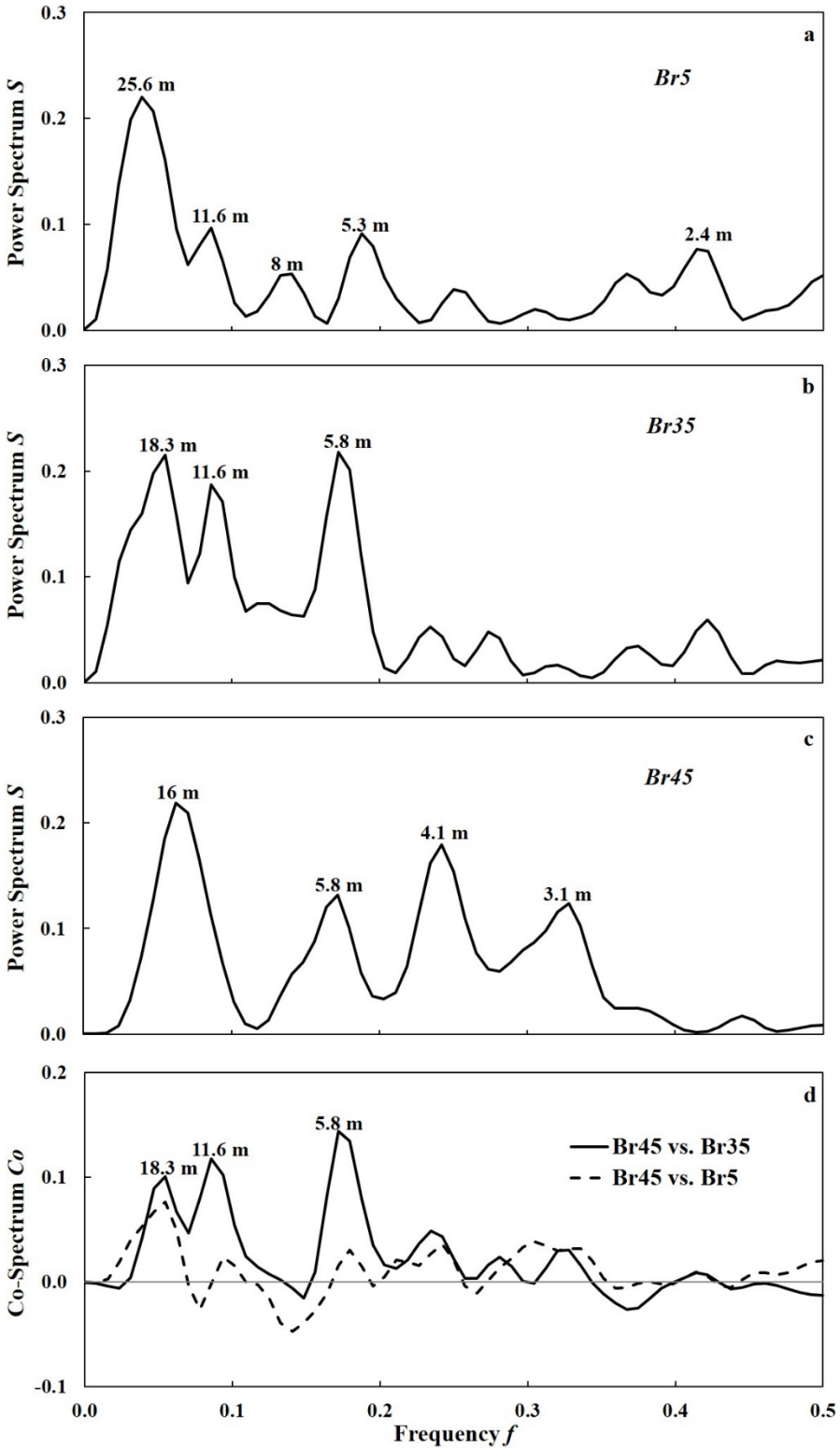

Figure 3.5 Power spectra for soil Br^- at (a) 0-10 cm ($Br5$), (b) 30-40 cm ($Br35$), (c) 40-50 cm ($Br45$), and (d) co-spectra for $Br45$ with $Br35$ and $Br5$.

The involvement of $Br5$ in the bivariate state-space analyses for $Br25$, $Br35$ and $Br45$ not only resulted in smaller RSS_{avg} and AIC_c values; but also decreased the relative impact of Bro_{i-1} , except that for 30-40 cm (Figure 3.6a, b), in comparison to the state-space models adopting the Br^- concentration in the adjacent layer above. Hereby, Bro_{i-1} is the soil Br^- concentration in the objective layer at location $i-1$. For example, in a state-space model for $Br25$, Bro_{i-1} refers to $Br25_{i-1}$. It was implied that $Br5$ better explained the spatial variations in $Br25$, $Br35$ and $Br45$. In other words, in these three layers, spatial Br^- processes were more strongly associated with $Br5$ than with the Br^- concentration in the respective neighboring layer. A possible explanation for this phenomenon is that the characteristics of the boundary conditions applied on the soil surface, such as rainfall intensity and timing, were best reflected in the distribution of Br^- concentration in the top layer of 0-10 cm among all the ten layers investigated. The spatial analysis conducted earlier in Yang et al. (2013) revealed strong spatial correlations for $Br5$ with land use, rainfall characteristics and elevation variance. Accordingly, the spatial processes of the Br^- concentrations in the layers below 0-10 cm depth showed the greatest association with $Br5$ if they were mainly affected by these imposed boundary conditions rather than the inherent soil properties like sand and clay content. With increasing distance apart from the top soil layer, the influence of surface-applied boundary conditions diminished; and employing $Br5$ in the estimation was less able to manifest the variations in soil Br^- concentration. As shown in Figure 3.6a, the value of AIC_c for the state-space model based on $Br5$ increased with soil depth until 40-50 cm, although $Br5$ remained the most helpful spatial process in describing Br concentrations at these depths. In addition, with the involvement of $Br5$, the average standard error of estimation was smaller for $Br25$, but larger for $Br45$, compared

to the values resulting from the bivariate state-space models that were based on the Br^- concentration in the neighboring layers, i.e., $Br15$ and $Br35$, respectively (Figure 3.6c).

When water and solute reached the soil layer of 40-50 cm, where sand content was very low (Figure 3.1a) and a plow pan was believed to be present resulting from tobacco production several years ago, they tended to mix more thoroughly through the more developed lateral flow. Because of this lateral redistribution, a different flow regime was introduced and the Br^- concentrations at 70-80, 80-90 and 90-100 cm were most strongly correlated with the Br^- concentration at 50-60 cm ($Br55$) (Figure 3.6a, b), which was right below the plow layer. However, the prediction quality of the state-space model based on $Br55$ did not monotonically decreased with soil depth. With the involvement of $Br55$, the Br^- distribution at 70-80 cm was better described than that in the soil layer above, 60-70 cm, indicated by a more negative AIC_c and a smaller standard error. Also at 70-80 cm, the estimation at location i ($Br75_i$) largely depended on $Br55$ rather than $Br75$ at $i-1$ (Table 3.1). The transition coefficients were 0.786 and 0.177, respectively. Therefore in this lower flow regime, another reason may also account for the greatest impact exerted by $Br55$ on the Br^- concentrations one and several layers below, which is the incomplete solute mixing in the horizontal direction due to the variations in soil properties such as soil texture and structure (Kulli et al., 2003; Jarvis, 2007). This reasoning was to some extent supported by the preferential flow pathways observed below the plow pan in the contour map of Br^- concentration generated in Yang et al. (2013). If water and solute accumulate on the plow pan quickly, usually under high intensity rainfall, preferential flow could be initiated once cracks or continuous macropores were present (Janssen and Lennartz, 2007).

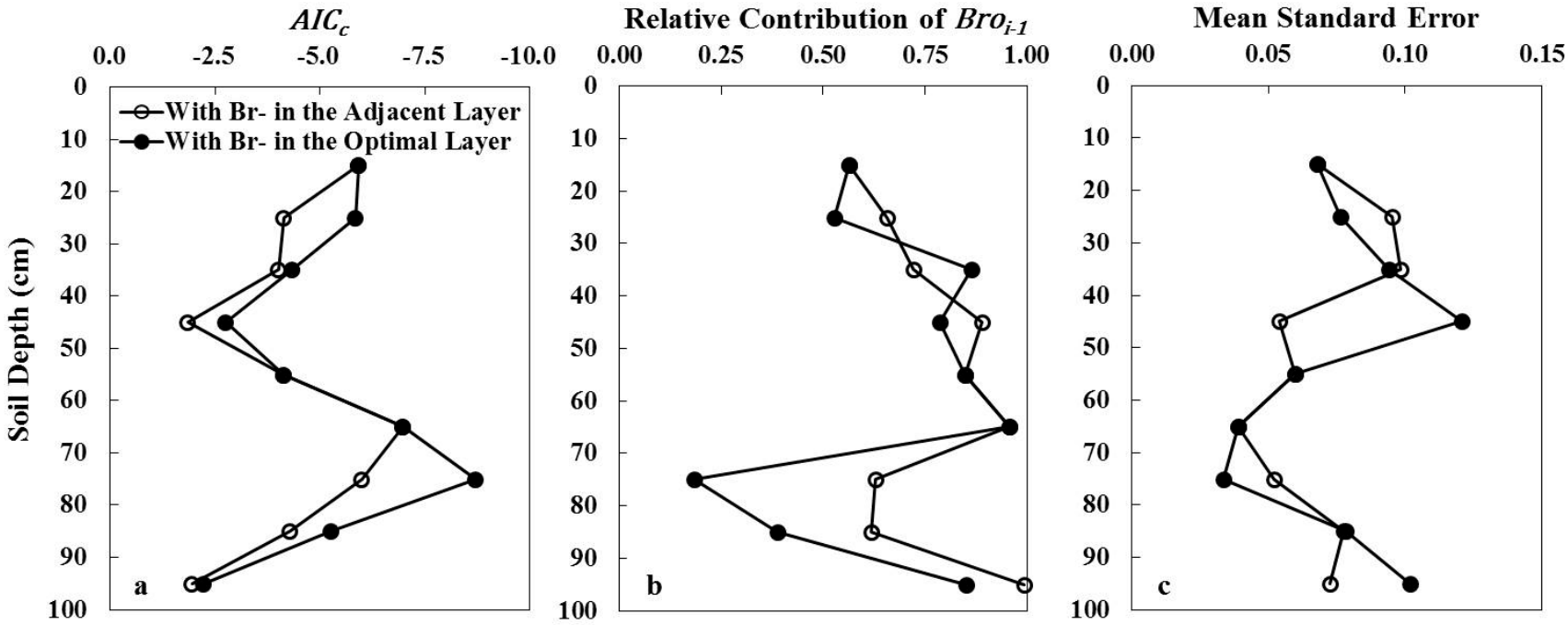

Figure 3.6 Comparison between bivariate state-space models of soil Br^- at each depth with the Br^- concentration in the adjacent layer and with that in the optimal layer indicated in Table 3.1, through (a) AIC_c, (b) relative contribution of Bro_{i-1} and (c) the mean standard error of estimation. Thereinto, Bro_{i-1} denotes the soil Br^- concentration in the objective layer at location $i-1$. For example, in a state-space model for $Br25$, Bro_{i-1} refers to $Br25_{i-1}$.

3.3.2 Spatial Processes of Soil Br^- Described by Boundary Conditions

Autoregressive state-space models considering up to 3 boundary conditions, either natural or imposed, were applied to describe the spatial processes of soil Br^- at each depth and to explore the major influencing factors. According to RSS_{avg} and AIC_c, the latter taking the number of regression variables into account, the optimal state-space equations can be derived from Table 3.2. The precision of the state-space models in describing Br^- concentration varied with soil depth, based on the boundary conditions investigated in this field experiment. The state-space models for soil Br^- at 40-50 and 60-70 cm yielded the most negative AIC_c, -10.58 and -10.20, respectively, indicating the best prediction quality compared to those for Br^- concentration at other depths.

Table 3.2 Transition coefficients for the optimal state-space equation of soil Br^- concentration in each soil layer as well as respective RSS_{avg} and AIC_c, based on the imposed boundary conditions, i.e., land use (LU), rainfall intensity (I) and application time delay (D), and inherent spatial processes, i.e., elevation variance (EV), sand content (S) and clay content (C). Note that 0 was assigned for grassland and 1 for cropland for the convenience of state-space analysis. Bro_{i-1} denotes the soil Br^- concentration in the objective layer at location $i-1$, same with Figure 3.6.

Depth (cm)	RSS_{avg}	AIC_c	Transition Coefficients						
			Bro_{i-1}	LU_{i-1}	I_{i-1}	D_{i-1}	EV_{i-1}	S_{i-1}	C_{i-1}
0-10	0.01364	-3.06	0.576	0.260				0.085	0.084
10-20	0.00002	-9.74	0.458	0.273					0.253
20-30	0.00112	-5.61	0.514	0.261				0.198	
30-40	0.00003	-9.24	0.589	0.002	0.133	0.235			
40-50	0.00001	-10.58	0.397		-0.007		-0.244	0.790	
50-60	0.00004	-8.79	0.500	-0.0003	-0.051			0.506	
60-70	0.00001	-10.20	0.702		-0.041			0.317	
70-80	0.00007	-8.36	0.625		0.135		0.126		0.080
80-90	0.00482	-4.15	0.673		0.127				0.178
90-100	0.00812	-3.58	0.339		0.077			0.328	0.248

Based on the magnitudes of transition coefficients in each state equation, the underlying processes that affected Br^- leaching can be identified. In addition, to compare the impact of each boundary condition on the spatial distribution of soil Br^- at different depths, the relative contributions were calculated and presented in Figure 3.7. The impact of land use (LU) was included in describing the spatial patterns of soil Br^- in the upper three layers. The corresponding weights ranged from 0.260 to 0.273, greater than the other boundary conditions considered. However, as the soil depth increased, the influence of land use diminished, only contributing little to the state-space models for Br^- at 30-40 and 50-60 cm. The major effect exerted by land use at shallow depths was probably related to soil

structural differences between cropland and grassland, which can be expected to become most apparent near the soil surface. It is interesting to observe the contribution of rainfall intensity (I) to the spatial description of soil Br^- in deep layers, whether large or small, for its important implications to chemical application and irrigation. The positive transition coefficients in the state equations for Br^- below 70 cm indicated increased risk of deep leaching and groundwater contamination under heavy rainfall (Table 3.2). The influence of application time delay (D) and elevation variance (EV) was limited to one and two soil depths, respectively. Considering both sand content (S) and clay content (C), soil texture affected Br^- leaching throughout the 1-m deep soil profile investigated in this study. Especially at 40-50 and 90-100 cm, where the relative contributions of sand and clay content were the largest among the ten depths, the weights of Br^- concentration at the objective layers at location $i-1$ (Bro_{i-1}) were less than 0.5. The results of state-space analysis for the soil layers below 40 cm corresponded to those found earlier based on frequency-domain analysis (Yang et al., 2013), which concluded that the spatial behavior of Br^- in deep soil layers was mainly controlled by soil properties like soil texture; while rainfall intensity could also exert some influence.

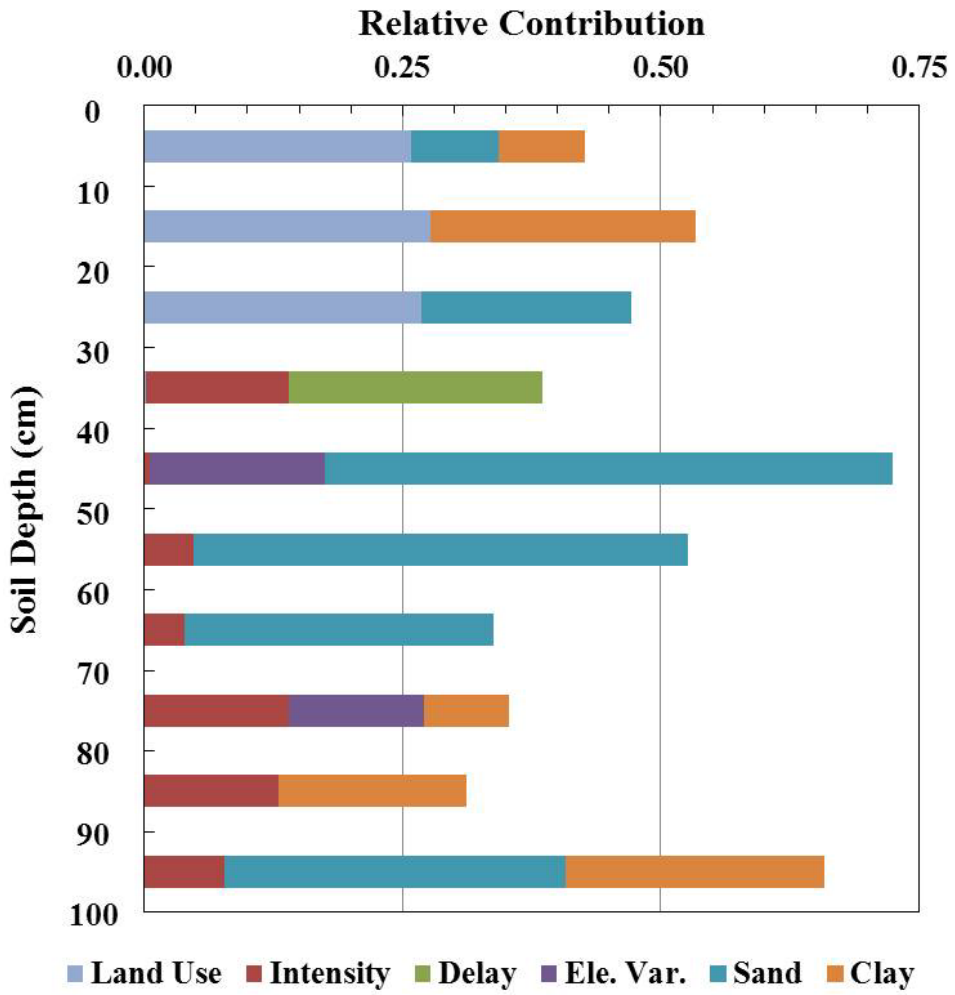

Figure 3.7 Relative contribution of each boundary condition in the optimal state-space model for Br^- concentration at each depth.

Land use only changed once in the middle of the transect; so it is not appropriate to treat it as a typical repetitive pattern and to analyze its common periodicity with soil Br^-. In the spectral and cross-spectral analyses by Yang et al. (2013), land use was not taken into account. Therefore, to compare the results for shallow depths, where land use was obviously important as shown in Table 3.2 and Figure 3.7, state-space analysis was conducted based on boundary conditions other than land use. Similarly, all combinations

of up to 3 boundary conditions were evaluated in this analysis and the resulting state-space model yielded the most negative AIC_c. Figure 3.8 compares the optimal state-space models with and without land use.

For the upper two layers, removing land use did not much reduce the prediction quality of state-space models according to AIC_c, which has been increased by only 6.2% and 4.9%, respectively. However, with the exclusion of land use, the weights of Bro_{i-1} were greatly increased, from 0.576 to 0.730 for 0-10 cm (Figure 3.8a, b) and from 0.458 to 0.621 for 10-20 cm (Figure 3.8c, d). Scaling to relative contribution for the purpose of comparing different depths, the increase rates for Bro_{i-1} were 27.8% and 35.5%, respectively. It is implied that the impact of land use could be integrated in the Br^- concentration at previous location, which to a very large extent determined the spatial behavior of soil Br^- at either depth. Without considering land use, clay content became the only boundary condition taken in the state-space model giving the best estimate of Br^- concentration at 0-10 cm. The corresponding RSS_{avg} and AIC_c were 0.018 and -2.87, respectively (Figure 3.8b). While in the spectral analysis (Yang et al., 2013), clay content was identified as the second most important factor behind rainfall intensity controlling the spatial Br^- distribution; state-space analysis revealed the same two variables as the most important ones, however, clay content had a slightly larger impact than rainfall intensity. The state-space model based on rainfall intensity resulted in a good estimation with the RSS_{avg} of 0.019 and the AIC_c of -2.83. At 10-20 cm, the influence of application time delay became obvious after removing land use (Figure 3.8d), which was consistent with the result of spectral analysis.

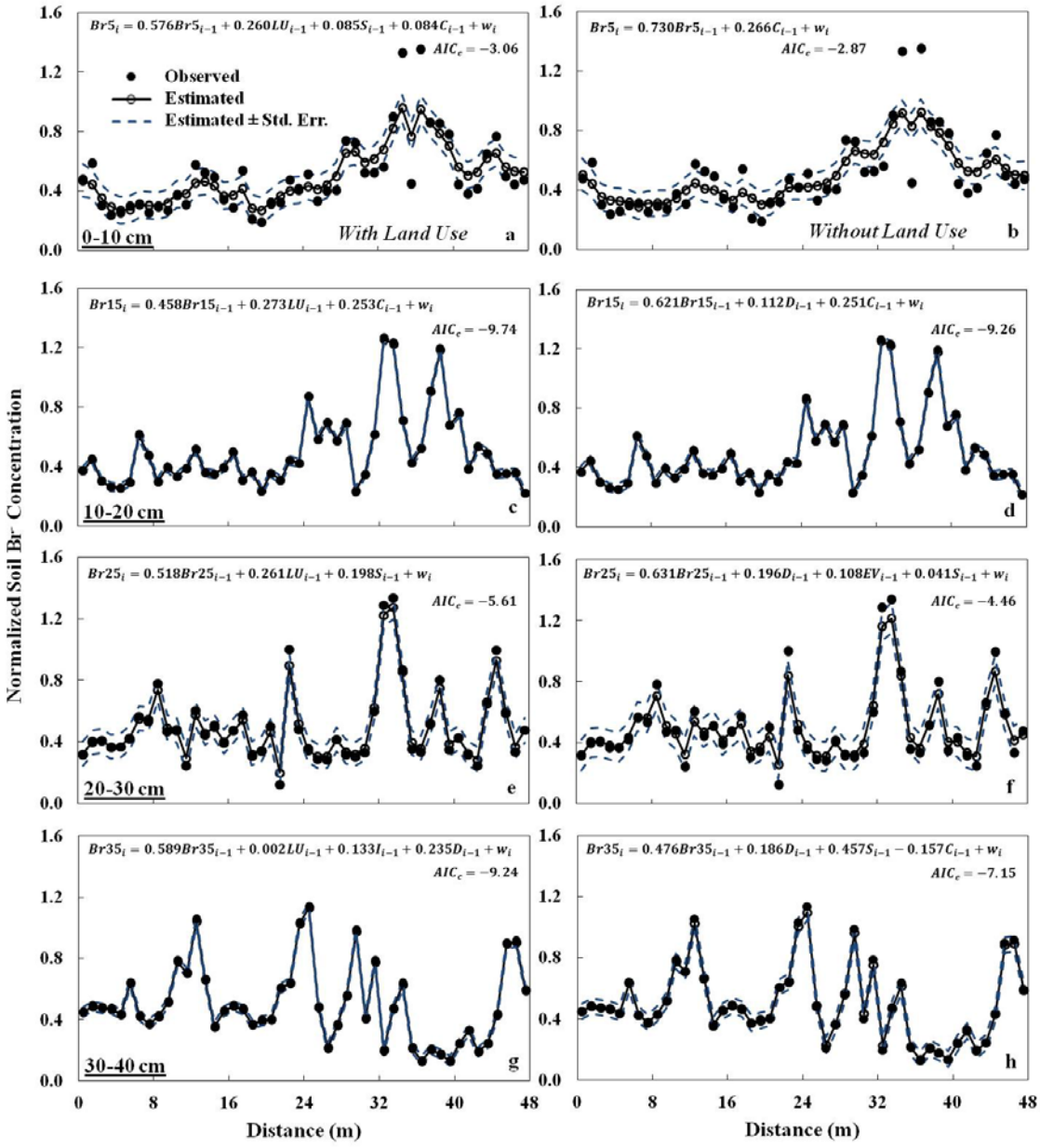

Figure 3.8 Spatial processes of soil Br^- in four upper layers described in the optimal state-space models based on boundary conditions (a, c, e, g) with and (b, d, f, h) without land use. The respective state equations and the values of AIC_c are given.

Without land use, the state-space models derived to describe the spatial processes of soil Br^- at 20-30 and 30-40 cm did not perform as well as those including land use in the analysis. The values of AIC_c were increased by 20.5% and 22.6%, respectively; and the mean

standard errors of the estimation increased (Figure 3.8e, f, g, h). At 20-30 cm, the relative contribution of Bro_{i-1} slightly increased, when land use was replaced by the other boundary conditions. More importantly, application time delay and elevation variance turned into the most relevant boundary conditions affected Br^- concentration at this depth, when land use was removed from the state-space model (Figure 3.8f), which agreed with the earlier conclusion by Yang et al. (2013). However, the state-space model for Br^- concentration at 30-40 cm exhibited the impact of soil texture only after removing land use (Figure 3.8h), which was only one of the three main driving factors identified in spectral analysis (Yang et al., 2013). Interestingly, the contribution of Bro_{i-1} at this depth was not increased but reduced by 39.3%, despite the small weight of 0.002 for land use in the optimal state-space model as shown in Figure 3.8g. These results indicated an important influence of land use on the spatial distribution of soil Br^- at 30-40 cm. The probable reason was that for a given rainfall intensity and application time delay, the different soil structures typical for grassland and cropland resulted in distinct flows reaching this depth.

The influence of both Br^- concentration and soil textural state variables in the adjacent overlying layer was examined by state-space analysis in the next step. For soil Br^- in each layer except the top one of 0-10 cm, Br^- concentration, sand and clay content in the neighboring layer above were added to the boundary conditions and subject to the exploration of the optimal state-space model, while considering no more than 3 variables besides Bro_{i-1}, and held the most negative AIC_c. As displayed in Figure 3.9, the addition of these variables mainly improved the prediction of soil Br^- at the soil depth below 60 cm, accompanied with the decrease of relative contribution of Bro_{i-1}.

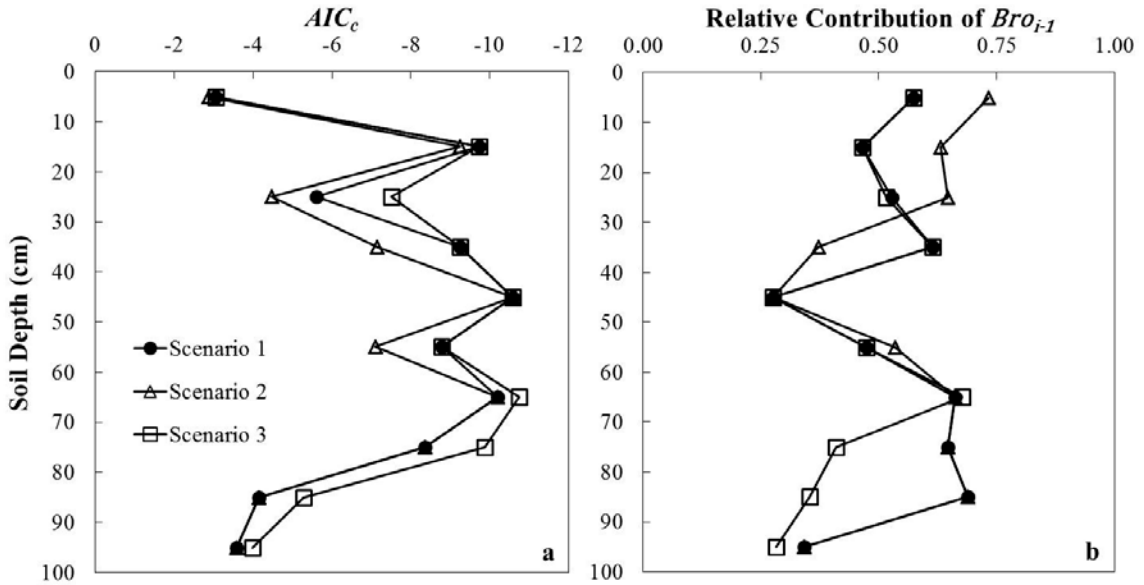

Figure 3.9 (a) AIC_c and (b) relative contribution of Br^- concentration in the objective layer at location $i-1$ (Bro_{i-1}) of the optimal state-space models based on all the boundary conditions investigated (scenario 1), all the boundary conditions except land use (scenario 2) and all the boundary conditions with the addition of Br^- concentration, sand and clay contents in the adjacent layer above (scenario 3).

Figure 3.10 compares the state-space models for soil Br^- at 70-80 and 90-100 cm based on the boundary conditions, with and without Br^- concentration and soil texture in the overlying layer. Including these variables decreased the values of AIC_c by 18.1% and 11.1%, respectively. Besides reducing the weight of $Br75_{i-1}$ from 0.625 to 0.393, the involvements of $Br65$ and the clay content at 60-70 cm ($C65$) in the state-space model for Br^- at 70-80 cm precluded the contributions of rainfall intensity and elevation variance. The overlying distribution of clay could possibly affect the topography but not the rainfall intensity, which was manually imposed. Therefore the rainfall intensity effect was probably integrated in $Br65$; yet it was hard to partition the impact of elevation variance or the

decreased contribution of $Br75_{i-1}$ into $Br65$ and $C65$. In describing the spatial processes of Br^- concentration at 90-100 cm ($Br95$), the relative contributions of $Br95_{i-1}$, rainfall intensity and clay content under scenario 1 and 3 were very close; while sand content at this depth was replaced by the one in the upper neighboring layer of 80-90 cm ($S85$) and their relative contributions in the respective state-space models were both around 0.334. In view of the high value of AIC_c, no matter under which scenario, soil properties other than the ones investigated in this study may also have impact on the spatial distribution of $Br95$.

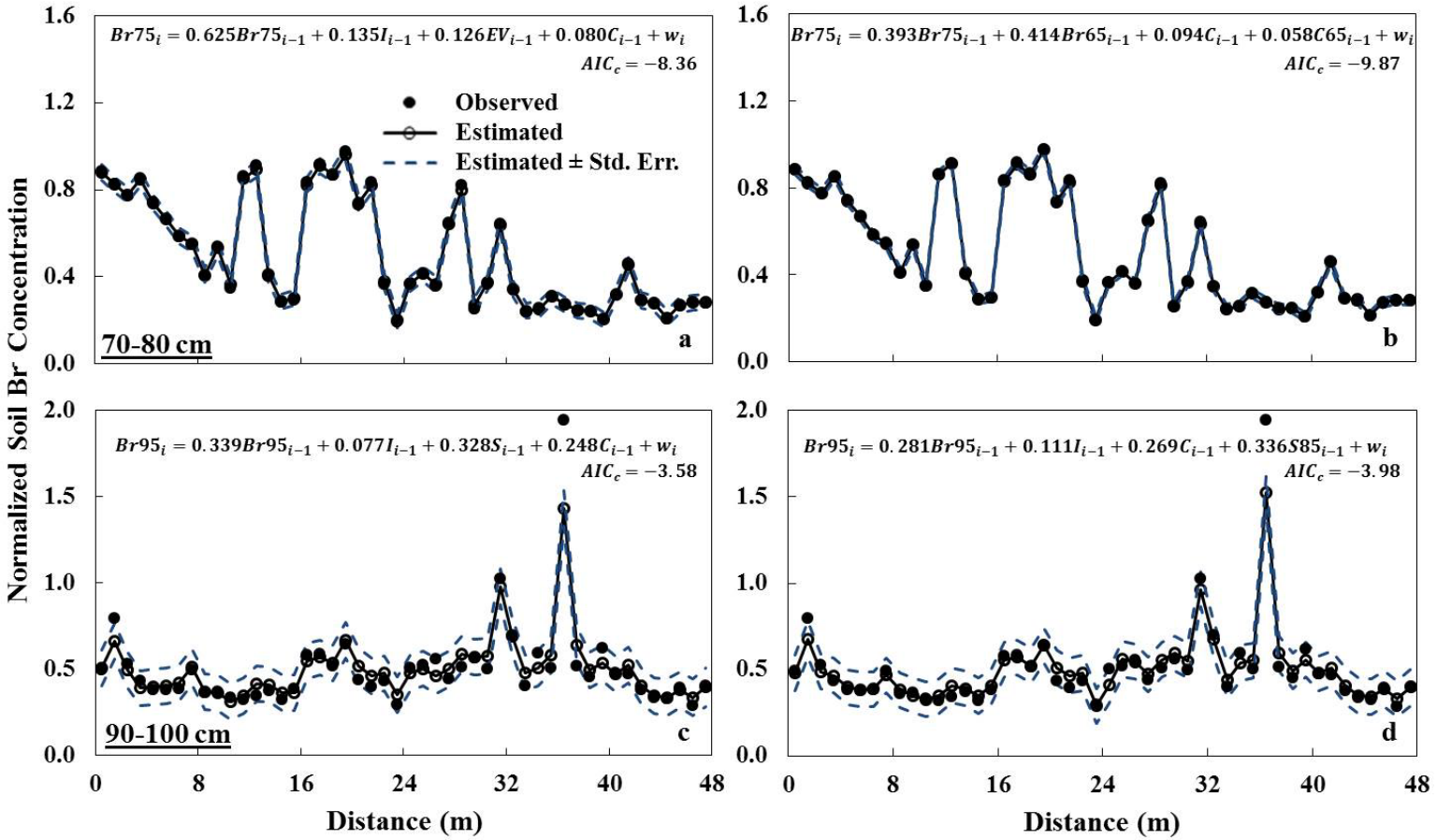

Figure 3.10 Spatial processes of soil Br^- at 70-80 and 90-100 cm described in the optimal state-space models based on boundary conditions (a, c) with and (b, d) without Br^- concentration, sand and clay content in the corresponding overlying layer. The respective state-space equations and the values of AIC_c are given.

3.4 Conclusions

State-space analysis was used in this study to characterize the spatial behavior of Br^- leaching and resulting horizontal distribution in different layers in a field experiment conducted earlier. Br^- concentration at 20-30, 30-40 and 40-50 cm were most strongly correlated with that in the top soil of 0-10 cm, rather than in the respective adjacent soil layer above. Using $Br5$ in the state-space model well reflected the large-scale variations in Br^- concentration below; however, the small-scale fluctuations were usually neglected, especially at greater depth. Similar phenomena were observed below the plow pan at 40-50 cm, where a flow regime different from the above was introduced. Soil Br^- at 70-80, 80-90 and 90-100 cm had the strongest spatial associations with Br^- concentration at 50-60 cm.

The optimal state-space models relying on no more than three boundary conditions were derived for Br^- concentration at each depth. According to the weight and relative contribution of each variable, land use was the dominant factor that controlled the horizontal distribution of soil Br^- in the upper three layers. At 30-40 cm, land use was not weighted the most; however, the prediction quality of the state-space model decreased a lot when land use was not involved. For the soil layers below 40 cm, sand and clay content were the main driving factors and rainfall intensity ranked the second. Excluding land use and reanalyzing the state-vectors for Br^- concentration in upper layers, the importance of rainfall characteristics were revealed, which was similar to the previous findings acquired from frequency-domain analysis (Yang et al., 2013). In contrast to land use, involving Br^- concentration and soil texture of the overlying adjacent layer mainly improved the prediction quality of soil Br^- in deep soils below 60 cm. The state-space approach provided

a comprehensive description of Br^- leaching site-specifically and illustrates the impact of soil variations at shallow depths and experimental boundary conditions on the hydrologic responses and solute distribution.

Chapter 4 Field-Scale Water and Bromide Transport During and After Irrigation

4.1 Introduction

A detailed knowledge of water flow and solute transport in the vadose zone is of great importance for improving agricultural management and maintaining environmental quality (Ahuja et al., 1993; Paramasivam et al., 2002). The first systematic study of solute transport was conducted by Nielsen and Biggar (1961), who investigated the miscible displacement of Cl^- in three soils and two sizes of uniform glass beads (Wendroth et al., 2011c). In the following decades, both inherent soil properties, e.g., soil texture and structure, and imposed boundary conditions, e.g., irrigation intensity and the timing relative to solute application, have been identified as important factors for solute leaching (Shipitalo et al., 2000; Jarvis, 2007; Schwen et al., 2012).

For a structured soil with vertically continuous macropores, higher irrigation intensity usually causes deeper leaching of chemicals. Gjettermann et al. (1997) attributed this behavior, which can be observed in a wide range of soil types and for many chemicals (Shipitalo et al., 2000), to the influence of intensity on the development of preferential flow. At a high irrigation intensity, a ponding water head develops at the surface and preferential flow is initiated through macropores, resulting in fast leaching of surface-applied chemicals (Beven and Germann, 1982; Gerke, 2006). Similarly, soil surface roughness reflects the number of local depressions and determines the degree of water ponding that would possibly develop in a certain irrigation event and thereby cause preferential flow initiation and affect solute transport (Weiler and Naef, 2003b).

Irrigation timing affects solute transport mainly through another mechanism. With a longer time delay between solute application and subsequent irrigation, more solute is able to move from large interaggregate pores to small intraaggregate ones and becomes less accessible to leaching (Francis et al., 1988; McLay et al., 1991; Gerke and Köhne, 2004). Evidence for this retardation phenomenon was provided in both laboratory and field experiments (Kluitenberg and Horton, 1990; Edwards, et al., 1993; Wendroth et al., 2011c). Nevertheless, a longer time delay does not always result in less leaching or shorter leaching depth. Jiang et al. (1997) found in their column experiment that the influence of irrigation timing was affected by soil moisture. Only under the wet condition when the water table was 5 cm below the soil surface, was significantly weaker nitrate leaching observed with longer time delay. Furthermore, the irrigation timing itself would possibly impact the soil water status antecedent to irrigation. Extending the time delay could not only promote solute diffusion into aggregates, but also allow longer time for soil water evaporation. As a result, soil, especially on the surface, is expected to be drier and more water-repellent; which favors the development of preferential flow and deep leaching of water and solute (White et al., 1986; Shipitalo and Edwards, 1996; Weiler and Naef, 2003a; Jarvis, 2007).

Most of the published research on water infiltration and solute transport has been conducted under laboratory conditions; while at the field scale, little progress has been made, mainly owing to the inherent heterogeneity of soil properties (Nielsen et al., 1986; Butters et al., 1989). Since Miller et al. (1965) first studied solute transport on replicated plots outside the laboratory (Butters et al., 1989), classic block design has been widely applied in field-scale experiments. Yet the resulting standard deviations are usually comparable to or even

greater than the values of corresponding solute transport variables (Biggar and Nielsen, 1976; Kessavalou et al., 1996; Netto et al., 1999; Ottman et al., 2000). To overcome this huge variability and to yield a representative estimate, field studies aimed to derive the spatial correlation ranges of solute transport variables have been conducted since the mid-1990s (Ellsworth and Boast, 1996). However, solute transport, affected by many factors, usually varies over several scales (Biggar and Nielsen, 1976) and a single spatial range could hardly be acquired. In view of this limitation, the scale-dependent treatment distribution has been introduced, which imposes treatments in a repetitive pattern at distinct scales (Bazza et al., 1988; Shillito et al., 2009; Wendroth et al., 2011c). With the aid of frequency-domain analysis, i.e., spectral and cross-spectral analyses, the variances of treatments and solute transport variables can be decomposed among different scales (Kachanoski and De Jong, 1988); thereby allowing a greater opportunity to identify the major factors controlling the spatial behavior of solute leaching (Nielsen and Alemi, 1989; Wendroth et al., 2011c).

Soil coring has been the standard sampling method in studying solute transport (Alberts et al., 1977; Netto et al., 1999). However, it is time-consuming and destructive; and does not allow repeated sampling at the same physical location. In contrast, a suction probe with a ceramic cup at the bottom can provide *in situ* samples of soil water, once installed at a specific location and depth (England, 1974; Hansen and Harris, 1975; Grossmann and Udluft, 1991). Although problems exist that impair the representativity of soil water samples, such as soil heterogeneity (Barbee and Brown, 1986) and finger flow induced by the suction exerted for solution sampling (Starr et al., 1978), the use of suction probes can

sometimes be preferred to soil coring when analyzing the temporal change of solute leaching.

In the current study, irrigation intensity and application time delay were applied in a cyclic layout at two different scales distinct from the one for surface roughness along a transect evenly across grassland and cropland. We hypothesized that the effects of these boundary conditions were manifested in the spatial behavior of water infiltration and solute transport. Bromide was used as the tracer, and tensiometers and suction probes were employed to monitor soil water status and Br^- concentrations, respectively, during and after simulated irrigation. The objectives were to: 1) describe the spatial patterns of matric potential change and Br^- concentration at each depth during different periods of time; and 2) explore the major factors controlling the spatial behaviors of water infiltration and Br^- leaching.

4.2 Materials and Methods

4.2.1 Experimental Design

The field experiment was performed in the late spring of 2012 over a 48- by 3-m transect at University of Kentucky's Spindletop Research Farm, Lexington, KY. Along this transect, 24 plots were established, each 2 m in length and 3 m in width. Half of the plots were located on cropland formerly planted with no-till winter wheat and the other half on grassland dominated by tall fescue, bluegrass and red clover. In each plot, two hexagon nests of six self-manufactured tensiometers used for soil water matric potential measurements were installed clockwise at depths of 10, 30, 50, 70, 90 and 110 cm. The centers of the two nests were located at uniform distances of 0.5 and 1.5 m within each 2-

m long plot, resulting in a 1-m interval between tensiometer nests along the transect. Accompanying each nest of tensiometers, five suction probes aimed to collect soil water samples were installed at 20, 40, 60, 80 and 100 cm depths. Details of the plot layout were described in Yang et al. (2013).

Prior to the Br^- leaching experiment, glyphosate (Roundup, Monsanto Co.) was applied to kill all the plants. Using a regular farm sprayer, 37.5 g Br m^{-2} were applied as KBr with a total of 0.9 mm of previously collected rainwater. In the scale-dependent design of irrigation characteristics, rainwater was irrigated along the transect at a constant amount of 44 mm, at three levels of intensity, i.e., 5, 22 and 44 mm h^{-1}, and with four time delays after KBr application, i.e., 1, 4, 24 and 96 h, in a cyclic pattern at distinct spatial scales (Figure 4.1a, b). All the irrigations were conducted using garden sprinklers attached to a metal frame. Tarps were used to cover the whole transect until three days after the last irrigation, which on one hand prevented the influence of natural rainfall and on the other hand minimized the evaporation of soil water when no irrigation or tracer was applied. However, owing to the natural rainfall occurring during irrigation, final intensities at some plots were slightly different from those intended. And the approximately 10 mm h^{-1} higher irrigation intensity at plots 1 and 2 was the result of an accidental malfunction of the pumping system in the first day of the experiment.

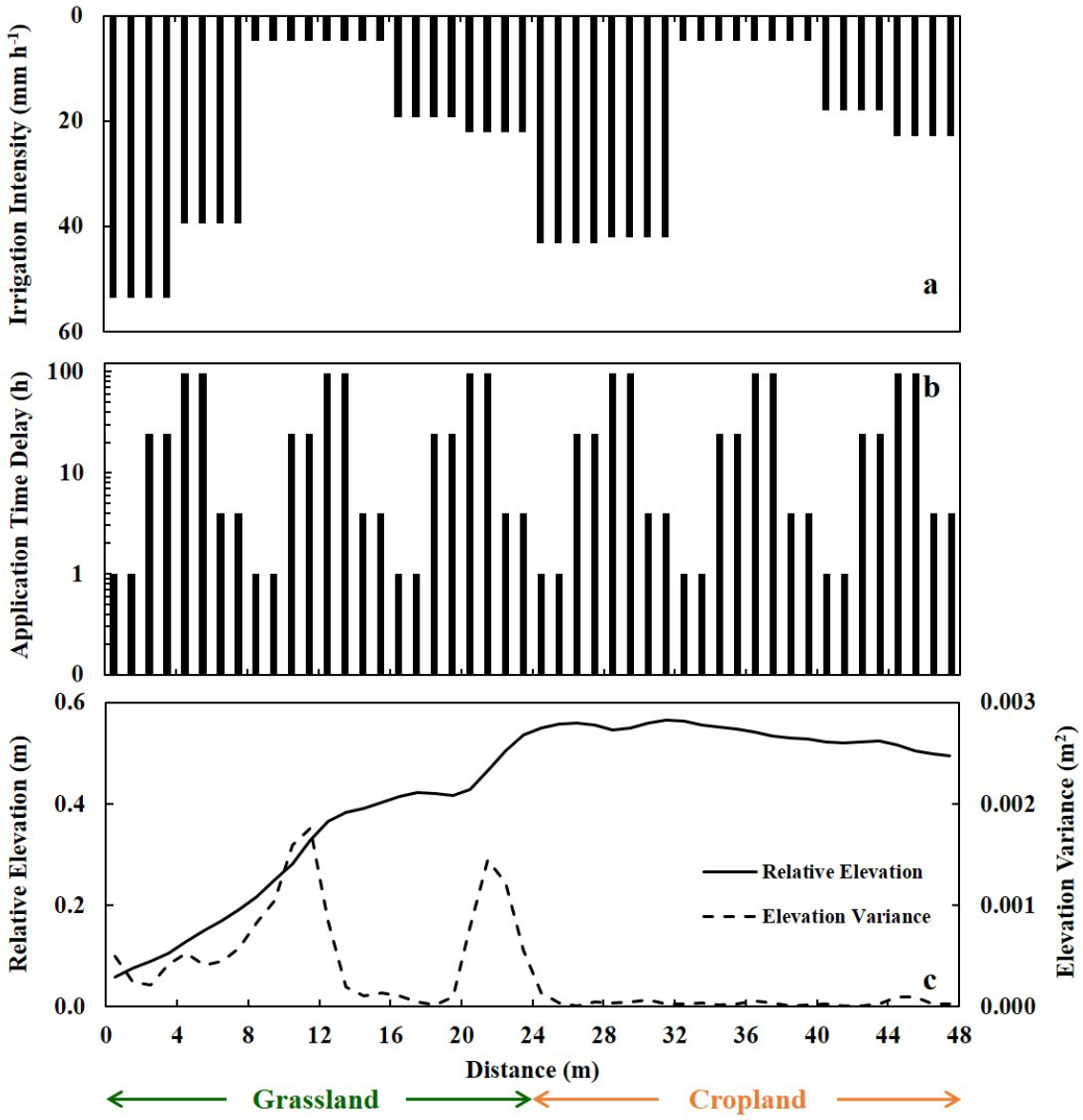

Figure 4.1 Spatial distribution of (a) irrigation intensity, (b) application time delay, and (c) relative elevation and elevation variance along the 48-m transect. Intensive measurements of relative elevation taken every 25 cm in both directions were averaged for every 1 m resulting in 2 values per plot; and the corresponding elevation variance was calculated as the sum of the squared differences from the neighboring relative elevations.

Immediately before and after irrigation, matric potentials were measured with the tensiometers at every location and depth. The difference with time was calculated to evaluate the soil water status change as affected by irrigation. One and three days after the end of irrigation, matric potentials were measured again to monitor the post-irrigation movement of soil water during different periods of time. Soil water samples were collected twice in this experiment. After each irrigation, a suction of 50 cm was applied to corresponding suction probes and maintained for about 1 h. Soil water within the suction probes was sampled using a vacuum pump. Originally, a suction was planned to apply at a magnitude 30% more than the average of matric potential readings at the two tensiometers above and below the sampling depth. For example, for a suction probe installed at the depth of 40 cm, the intended suction would be calculated based on the tensiometric measurements at 30 and 50 cm depths. However, matric potential was close to water saturation; a vacuum of 50 cm was selected as this appeared to be sufficient to collect solution from the surrounding soil. Right after the first sampling, another suction of 50 cm was applied again and a second set of soil water samples was taken after one day. Both samples were analyzed for Br^- concentration using an ion chromatograph (Metrohm AG, Herisau, Switzerland).

In addition to land use and irrigation characteristics, soil texture and topography were also considered in this study to explore their influences on water infiltration and Br^- leaching. In a soil sampling campaign, undisturbed soil cores down to 1 m depth were collected in an interval of 1 m along the transect and divided in 10 cm increments for soil texture determination using the sieving and pipette method (Gee and Bauder, 1986). Relative elevation at every 25 cm both along and across the transect in a 197×13 grid was acquired

by a Trimble SPS 930 Universal Total Station. These measurements were averaged for every 1 m along the transect, resulting in two values per plot (Figure 4.1c). To describe the soil surface roughness, the corresponding elevation variance was calculated by summing up the squared differences from the neighboring relative elevations.

4.2.2 Spectral Analysis

Prior to spectral analysis, all the data including boundary conditions (e.g., irrigation intensity, elevation variance), matric potential change, and Br^- concentration in soil water at each depth, were scaled by the following equation (Nielsen and Wendroth, 2003):

$$x_i' = \frac{x_i - (\bar{x} - 2\sigma_x)}{4\sigma_x} \quad (4.1)$$

where x_i is the observed value at location i, $\bar{x}$ and σ_x are the mean and standard deviation of x_i, respectively. The resulting data series x_i' would be dimensionless, and have a mean of 0.5 and a standard deviation of 0.25. This normalization procedure was conducted to avoid numerical problems that can arise if variables differ by an order of magnitude or more.

Spectral and cross-spectral analyses were used to identify the frequency-domain variance components (Shumway, 1988; Nielsen and Wendroth, 2003). Based on Fourier transformation, the power spectrum $S(f)$ integrates the autocorrelation function $r(h)$ with respect to lag distance h:

$$S(f) = 2\int_0^\infty r(h)\cos(2\pi f h)\, dh \quad (4.2)$$

A periodicity implied in a data series is shown in the power spectrum as a variance peak S versus the associated frequency f, which is the inverse of the wavelength λ reflecting the

scale of variation. The appearance of several relative maxima or peaks on $S(f)$ indicates more than one scale at which the data series varies.

The co-spectrum $Co(f)$ identifies the fluctuating scales at which two data series are correlated with each other. Integrating the cross-correlation function $r_c(h)$, $Co(f)$ is calculated with:

$$Co(f) = 2\int_0^\infty r_c(h)\cos(2\pi fh)\,dh \quad (4.3)$$

where the $r_c(h)$ combines the positive and negative lags through $r_c(h) = 0.5[r_c(h < 0) + r_c(h > 0)]$. This averaging procedure emphasizes the periodic fluctuations by a cosine wave but eliminates the ones by a sine wave. On the contrary, the quad-spectrum $Q(f)$ reinforces the cyclic variations described by a sine function:

$$Q(f) = 2\int_0^\infty r_c'(h)\sin(2\pi fh)\,dh \quad (4.4)$$

where $r_c'(h) = 0.5[r_c(h < 0) - (h > 0)]$. Relative to $Co(f)$, $Q(f)$ identifies the phase lag $h_\emptyset$ between two data series at which their maximum cross-correlation is reached (Nielsen and Wendroth, 2003; Wendroth et al., 2011c). The phase lag $h_\emptyset$ between two data series at a given frequency f is calculated as below:

$$h_\emptyset(f) = \frac{1}{2\pi f} tan^{-1}[\frac{Q(f)}{Co(f)}] \quad (4.5)$$

4.3 Results and Discussion

4.3.1 Water Infiltration and Br^- Leaching Patterns During and After Irrigation

The change in matric potential over a time increment was calculated as the difference between the beginning and ending potential values. For example, the matric potential change during irrigation (RB) was the potential measured immediately after minus the one

before irrigation. As shown in Figure 4.2, the values of RB were positive along the transect at all the six depths measured, except a slightly negative one at the depth of 90 cm and the distance of 15 m. The increase in matric potential during irrigation was relatively greater near the soil surface, i.e., at 10 and 30 cm; and among the other four depths, no significant difference was observed. The difference of RB between the two land use systems was mainly manifested at the three shallow depths, i.e., 10, 30 and 50 cm (Figure 4.2a-c). Significantly more potential increase was observed in cropland, especially at the distance from 30 to 38 m, which probably resulted from the relatively high clay content and low matric potential before irrigation (data not shown). Also at these three depths, smaller RB was observed in the regions receiving irrigation at high intensity (High I). This influence of irrigation intensity was more obvious in grassland than in cropland.

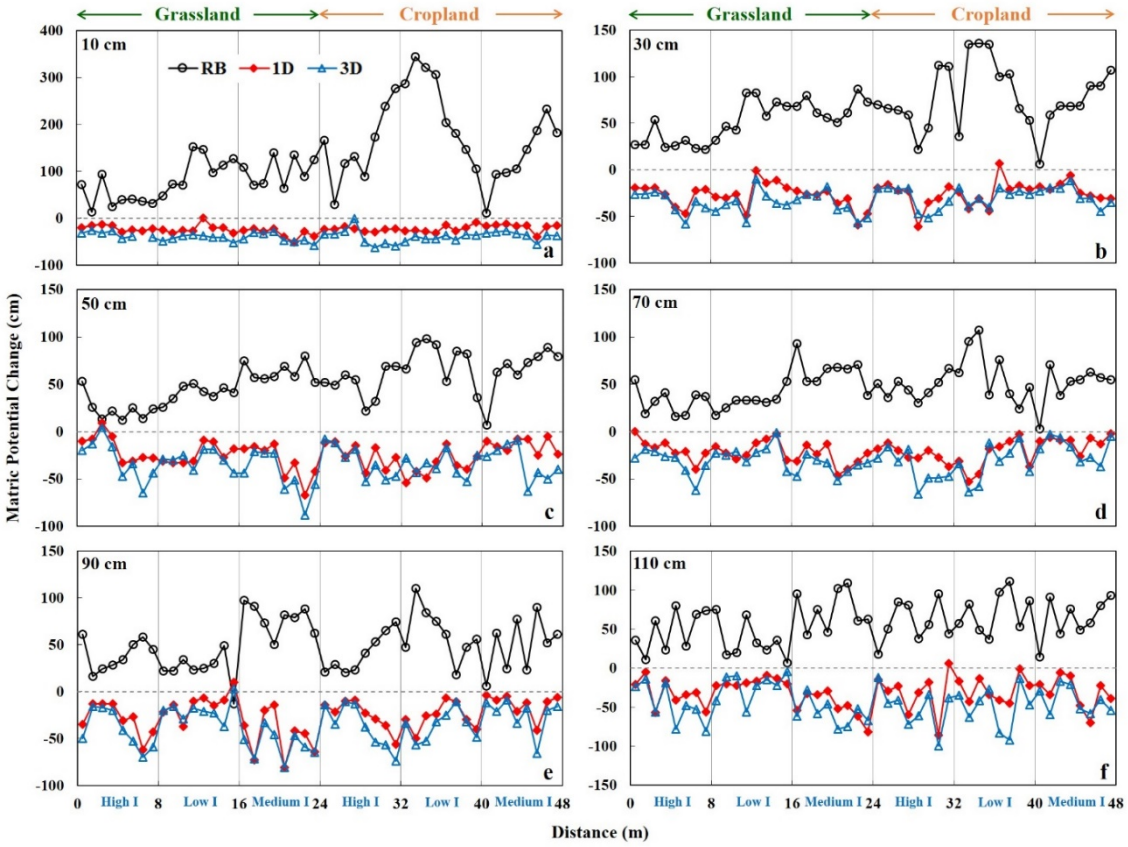

Figure 4.2 Spatial distribution of matric potential changes from the beginning to the end of irrigation (RB), and from the end of irrigation to one day (1D) and three days after irrigation (3D) at six depths: (a) 10, (b) 30, (c) 50, (d) 70, (e) 90, and (f) 110 cm. Each matric potential change value was calculated as the difference between the potential at the end of a specific period and that at the beginning. Notice that the range of matric potential change varies with soil depth.

According to the hydraulic gradients (data not shown), water was generally moving downwards, from wet zones near soil surface to drier ones below during the first few days of redistribution following irrigation. For all the six depths investigated along the transect, matric potential decreased with time and water drained off at most locations, indicated by

the negative matric potential changes over one day (1D) and three days (3D) since the cessation of irrigation (Figure 4.2). Furthermore, without more irrigation, soil became drier with time, resulting in generally lower 3D than 1D. However, in the process of post-irrigation redistribution, wetting occurs at the same time as drying (Bresler et al., 1969). The positive 1D or 3D or both at several spots typically obtained below 10 cm could possibly be explained by the prevalence of wetting during a specific period.

To better visualize the water infiltration patterns in the soil profile along the 48-m transect, contour maps of RB, 1D and 3D were drawn and presented in Figure 4.3. In general, irrigation increased the matric potential in cropland to a greater extent than in grassland, especially at shallow depths (Figure 4.3a); yet for the water redistribution afterwards, no contrasting patterns of matric potential change were observed between these two land use systems (Figure 4.3b, c). The response of matric potential to irrigation intensity was also more evident during irrigation (Figure 4.3a). In grassland, with lower RB at shallow depths, matric potential increase was distributed more evenly with soil depth in the regions under high intensity (High I) irrigation. On the contrary, more water was retained in surface layers in the regions receiving irrigation at low intensity (Low I). The preferential flow reinforced by increased irrigation intensity was probably the reason. Trojan and Linden (1992) concluded from their lab experiment that increasing the intensity of simulated rainfall caused an increase in water transport through earthworm burrows. In a structured soil, preferential flow typically could be initiated through macropores open at the surface when water ponds at the soil surface under a high intensity rainfall/irrigation (Gjettermann et al., 1997). Compared to grassland, where the denser root systems and higher organic matter

content resulted in more developed soil structure and more continuous macropores, the relationship between irrigation intensity and RB distribution was not as obvious in cropland.

During the redistribution process, a generally larger decrease in matric potential and presumably in soil water content at the bottom of the investigated 110-cm profile occurred in the regions receiving irrigations at high and medium intensity, especially in grassland (Figure 4.3b, c). Besides, hardly any water movement pattern could be related to the diverse irrigation intensities.

Soil water samples were taken at five depths along the transect one hour and one day after irrigation; and their Br^- concentrations are shown in Figure 4.4. Limited by the length and volume of suction probes installed at 20 cm, the vacuum applied inside vanished very soon once a small amount of soil water entered through the ceramic walls. At five locations, soil water samples of this depth did not have sufficient volumes for Br^- analysis for the one-hour sampling. During the second sampling campaign one day later, when matric potentials were more negative, Br^- concentration data at 20 cm depth were not available at almost half of the 48 locations. Despite this lack of data, Br^- concentrations in soil water sampled at all the five depths one hour after irrigation were consistently higher than those obtained in the later sampling. In view of the general matric potential decreases and implying water losses one day after the cessation of irrigation, a certain amount of Br^- was believed to move below 100 cm, which was the lowest depth for soil water sampling in this experiment.

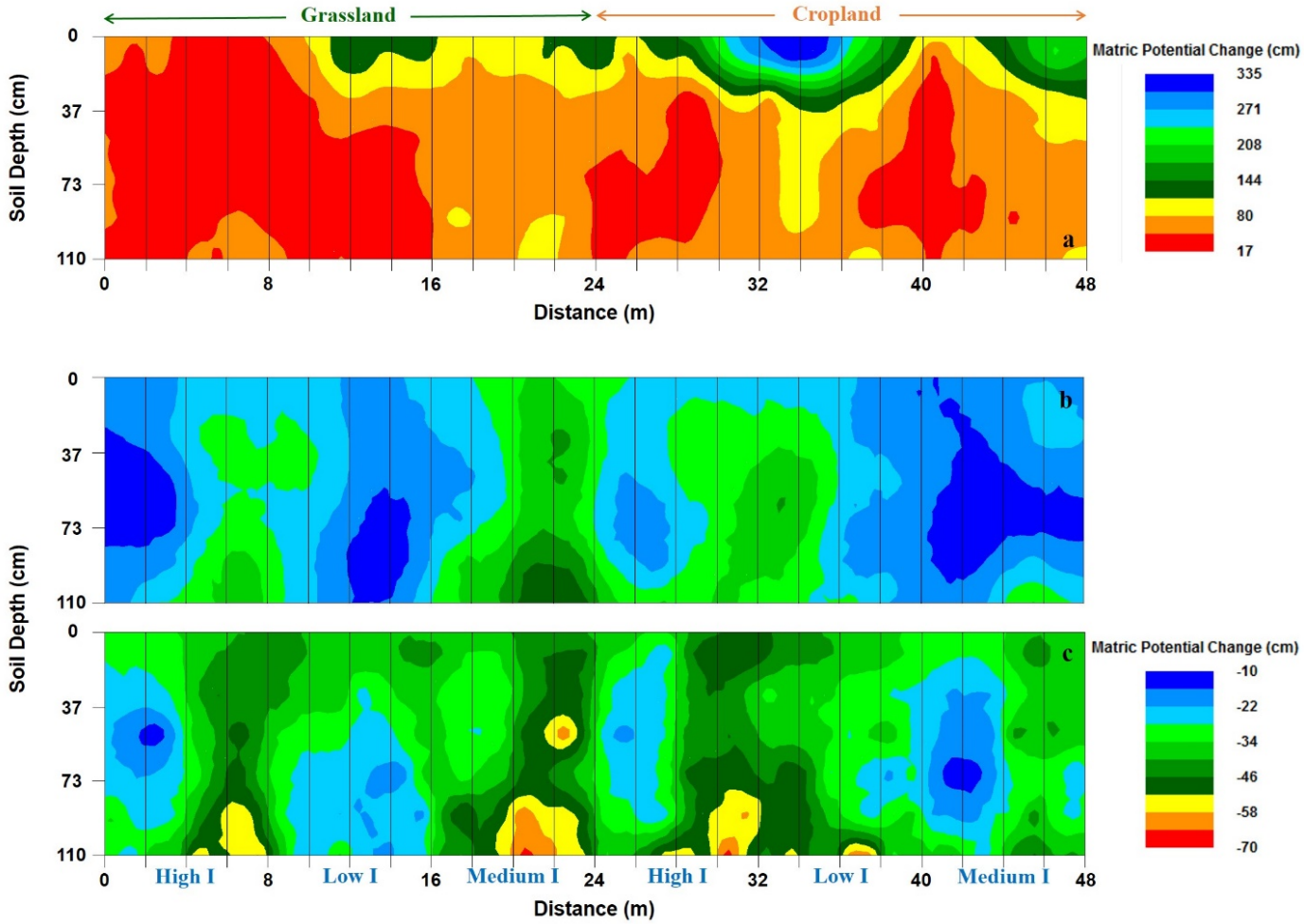

Figure 4.3 Contour maps showing spatial distribution of matric potential changes (a) from the beginning to the end of irrigation (RB), and from the end of irrigation to (b) one day (1D) and (c) three days after irrigation (3D).

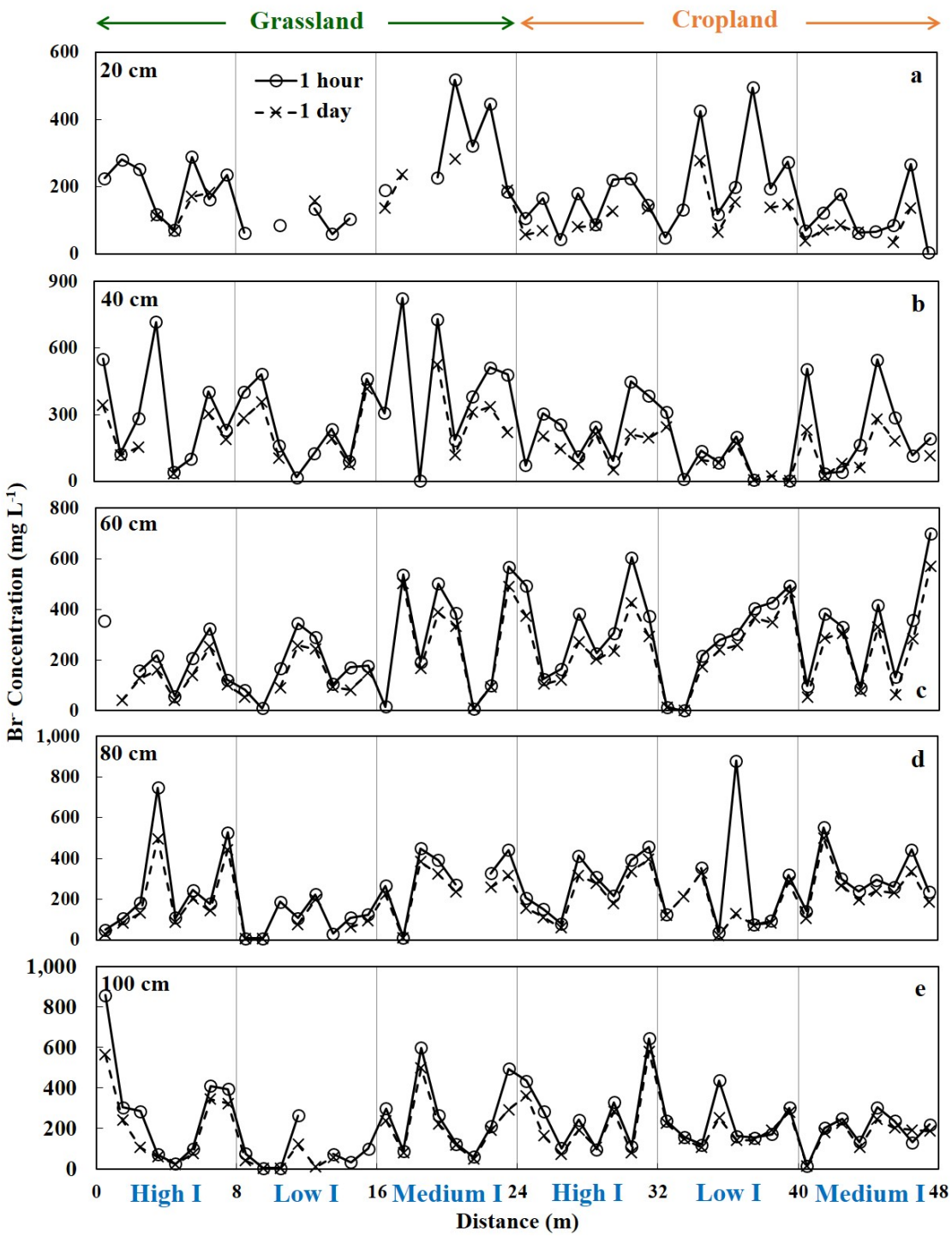

Figure 4.4 Spatial distribution of Br^- concentration in soil water sampled one hour and one day after irrigation at five depths: (a) 20, (b) 40, (c) 60, (d) 80, and (e) 100 cm. Notice that the range of Br^- concentration varies with soil depth.

In general, Br^- concentrations at 20 cm were lowest; and there was no significant difference among the other soil depths. When comparing Br^- concentrations at each depth between the two land use systems, no significant difference was detected. The distribution of Br^- concentration corresponded with the arrangement of irrigation intensity at some depths. Typically higher concentrations at 40 cm were measured in the regions receiving high and medium intensity irrigations, especially for the samples taken one hour after irrigation. This relationship between soil water Br^- concentration and irrigation intensity was also observed at 80 and 100 cm but not at 60 cm.

Contour maps were also generated for Br^- concentrations in soil water sampled at both times (Figure 4.5) to analyze the solute leaching patterns. For the sampling conducted one hour after irrigation, Br^- in grassland was typically higher and more evenly distributed with soil depth in the regions under high and medium intensity irrigations. The leaching patterns persisted after one day of drainage; but the contrast among different intensities was not as distinct. The Br^- distribution was more variable in cropland, especially in the regions receiving irrigation at low intensity (Low I). Under high and medium intensity irrigations, the Br^- concentrations below 60 cm were typically higher compared to the upper layers.

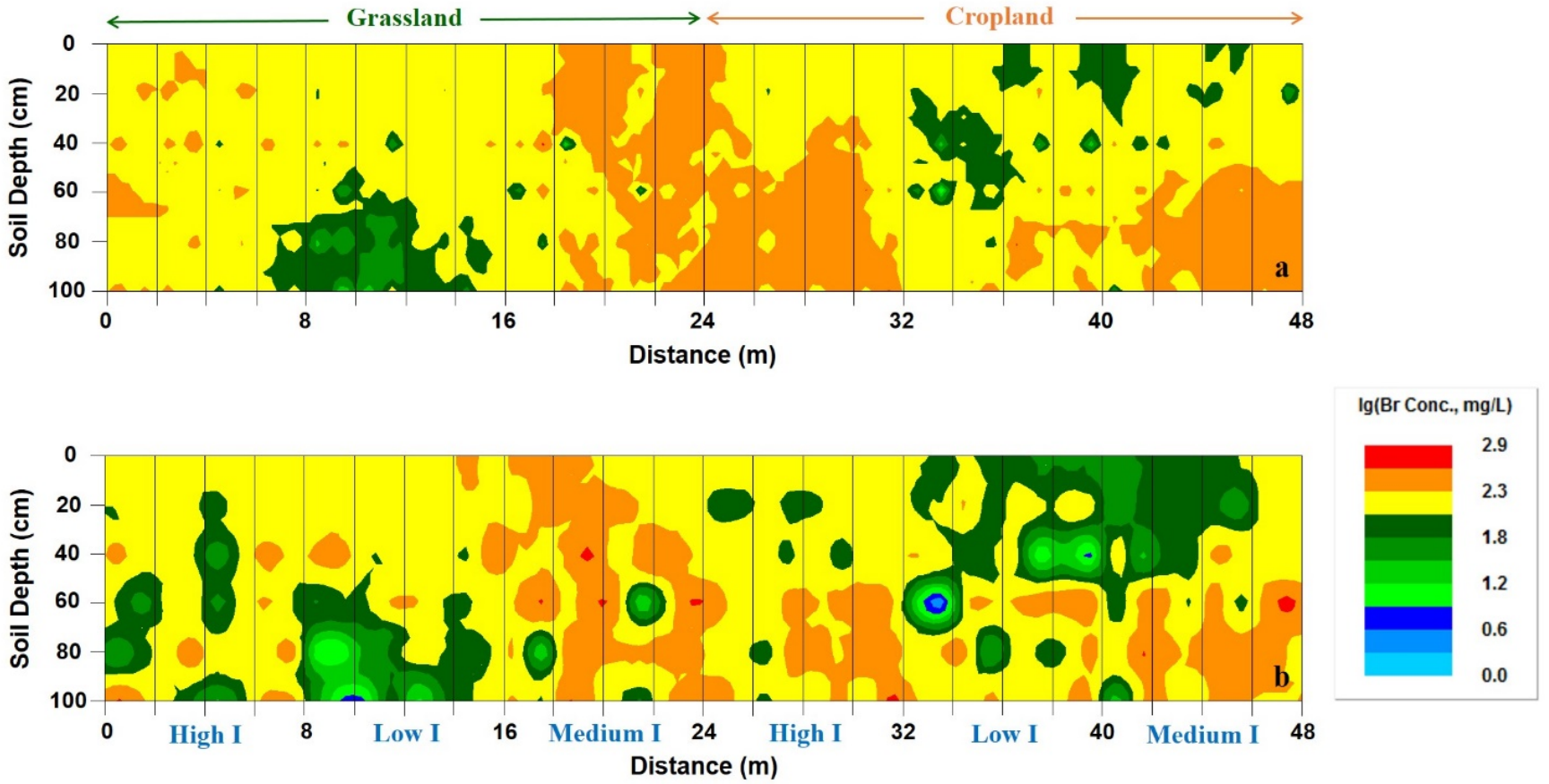

Figure 4.5 Contour maps showing spatial distribution of Br^- concentration in soil water sampled (a) one hour and (b) one day after irrigation.

The influence of intensity on the profile distributions of both matric potential increase and soil water Br^- concentration immediately after irrigation was consistent with the results found in soil coring samples analyzed earlier in Yang et al. (2013). As the irrigation intensity increased, more surface-applied Br^- moved downwards together with water, resulting in more linear distribution and deeper leaching of Br^-, especially in grassland. These findings, to some extent, reconfirmed that analyzing soil water sampled by suction probes could be an effective way to study *in situ* solute transport under field conditions.

4.3.2 Spatial Scales of Matric Potential Change and Boundary Conditions

The power spectra for the three boundary conditions are presented in Figure 4.6. A distinct peak appeared in the power spectra for irrigation intensity at the frequency f = 0.0391-0.0469, corresponding to the wavelength λ = 21.3-25.6 m. The power spectra for application time delay and elevation variance had more than one distinct peak. For the former, the major peak was manifested at f = 0.125 (λ = 8 m) and the minor one at f = 0.25 (λ = 4 m); while for the later boundary condition, the major and minor peaks occurred at f = 0.0781-0.0859 (λ = 11.6-12.8 m) and f = 0.1719 (λ = 5.8 m), respectively. The power spectra here, compared to those for matric potential changes displayed in Figure 4.7, provided a basis for identifying which of the three boundary conditions may have contributed to the spatial behavior of water infiltration.

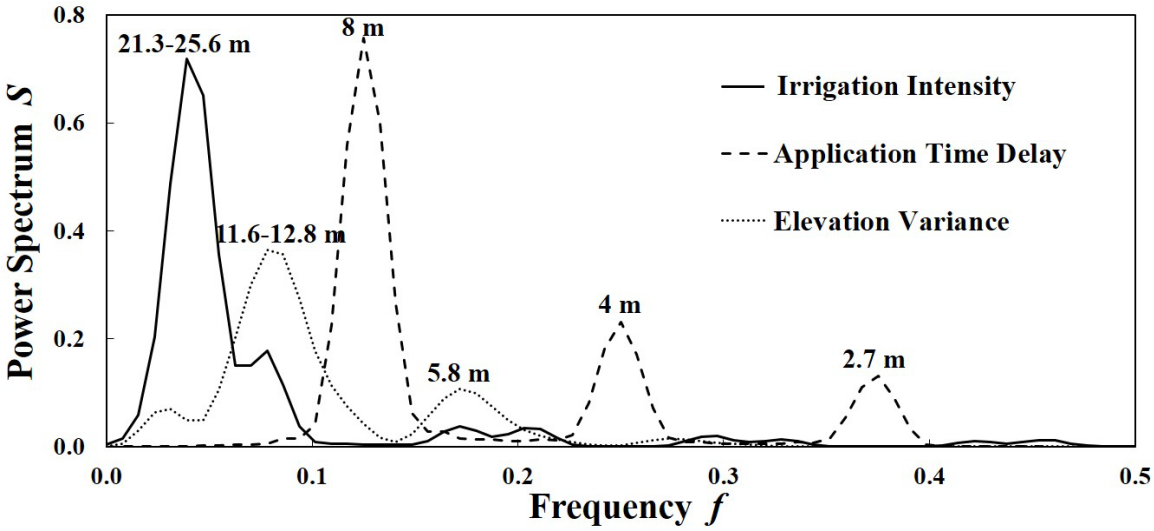

Figure 4.6 Power spectra for irrigation intensity, application time delay and elevation variance. The numbers above the peaks indicate the wavelengths λ at corresponding frequencies *f*.

The matric potential increase (RB) at 10 cm during irrigation might be mainly affected by irrigation intensity, since a single peak appeared at a frequency quite close to 0.0469 in its power spectra. In the water redistribution afterwards, the dominating process has changed at this depth. The major peaks were manifested at the frequencies $f = 0.0781$ ($\lambda = 12.8$ m) and $f = 0.125$ ($\lambda = 8$ m) in the power spectra for matric potential decreases during the drainage for one day (1D) and three days (3D), indicating the primary effects exerted by elevation variance and application time delay, respectively (Figure 4.7a). The controlling boundary conditions for RB, 1D and 3D at 30 cm were the same with those at 10 cm (Figure 4.7b). A slight difference was that the major peak in the power spectra for 1D appeared at $f = 0.1719$ ($\lambda = 5.8$ m) correlated with the small-scale fluctuation of elevation variance instead of the large-scale one.

The spatial scales of matric potential change at these two shallow depths varied among different periods of time; this temporal feature became weaker at the soil depth immediately below (Figure 4.7c). At 50 cm, both RB and 1D were mainly influenced by elevation variance; while application time delay dominated the spatial distribution pattern of 3D, same with the ones at 10 and 30 cm. However, at 70 cm depth, three primary wavelengths: 16, 12.8 and 32-42.7 m, were revealed in the power spectra for RB, 1D and 3D, respectively (Figure 4.7d), indicating that three different factors accounted for the spatial distributions of matric potential change during the three periods studied. The periodic variations in 1D were correlated with elevation variance and in 3D with irrigation intensity; while the primary fluctuation scale of 16 m was distinct from those for the boundary conditions manifested in Figure 4.6. When including soil texture in the analysis, this periodicity might be correlated with sand content at 60-70 cm, which will be further discussed later in the cross-spectral analysis. At the lowest two depths investigated in this experiment, i.e., 90 and 110 cm, the spatial scale of matric potential change was more constant with time. The major peaks in the power spectra for RB, 1D and 3D at 110 cm all occurred at $f = 0.4375$ ($\lambda = 2.3$ m), probably correlated with the plot length of 2 m (Figure 4.7f). And except for RB, which periodically varied at the wavelength λ = 14.2-16 m, similar with RB at 70 cm, both 1D and 3D at 90 cm were primarily affected by elevation variance indicated by the distinct peaks occurring at $f = 0.0781$ (Figure 4.7e).

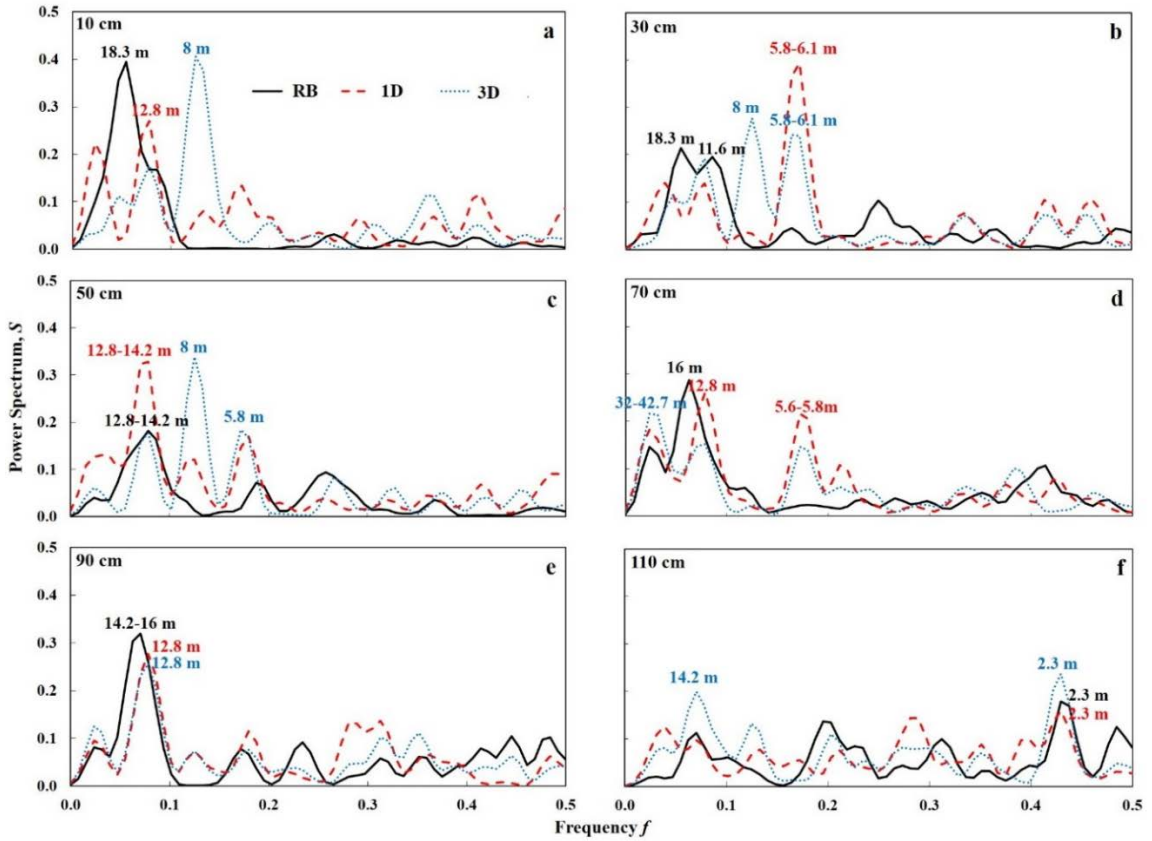

Figure 4.7 Power spectra for matric potential changes from the beginning to the end of irrigation (RB), and from the end of irrigation to one day (1D) and three days after irrigation (3D) at six depths: (a) 10, (b) 30, (c) 50, (d) 70, (e) 90, and (f) 110 cm. The numbers above the peaks indicate the wavelengths λ at corresponding frequencies f.

Co- and quad-spectra were calculated to analyze the spatial associations between each boundary condition and matric potential change during each period. Based on normalized data, the relative importance of these boundary conditions can be compared through the magnitude of the major peaks present in their respective co-spectra. The greater the peak, either positive or negative, the more strongly the boundary condition was spatially correlated with the matric potential change. Figure 4.8 shows the co- and quad-spectra between RB and three boundary conditions at six depths.

The largest peaks in the co-spectra for RB at 10 and 30 cm occurred with irrigation intensity at the frequency around $f = 0.0469$ ($\lambda = 21.3$ m) (Figure 4.8a, d). The strongly negative spatial correlations indicated that with an increase in irrigation intensity, less water was retained in the upper soil layers. At 50 cm, the distribution of matric potential increase was mainly affected by surface roughness as described by elevation variance (Figure 4.8i). The positive peak implied that a rougher soil surface allowed more water to accumulate at this depth. Compared to the other two boundary conditions, the co-spectra for RB had the highest peaks with elevation variance at 70 and 90 cm, as well. Considering the common periodicities revealed in the power spectra with sand content at 60-70 cm, the corresponding co- and quad-spectra were calculated and presented in Figure 4.9. The peaks manifested in the co-spectra for RB at both depths were greater with sand content. And the negative spatial correlations may be explained by the high hydraulic conductivity as a result of increased sand content *in situ* or above under high matric potential, leading to fast movement and little retention of water. At the bottom, application time delay was found to be the dominant factor that affected RB distribution (Figure 4.8q).

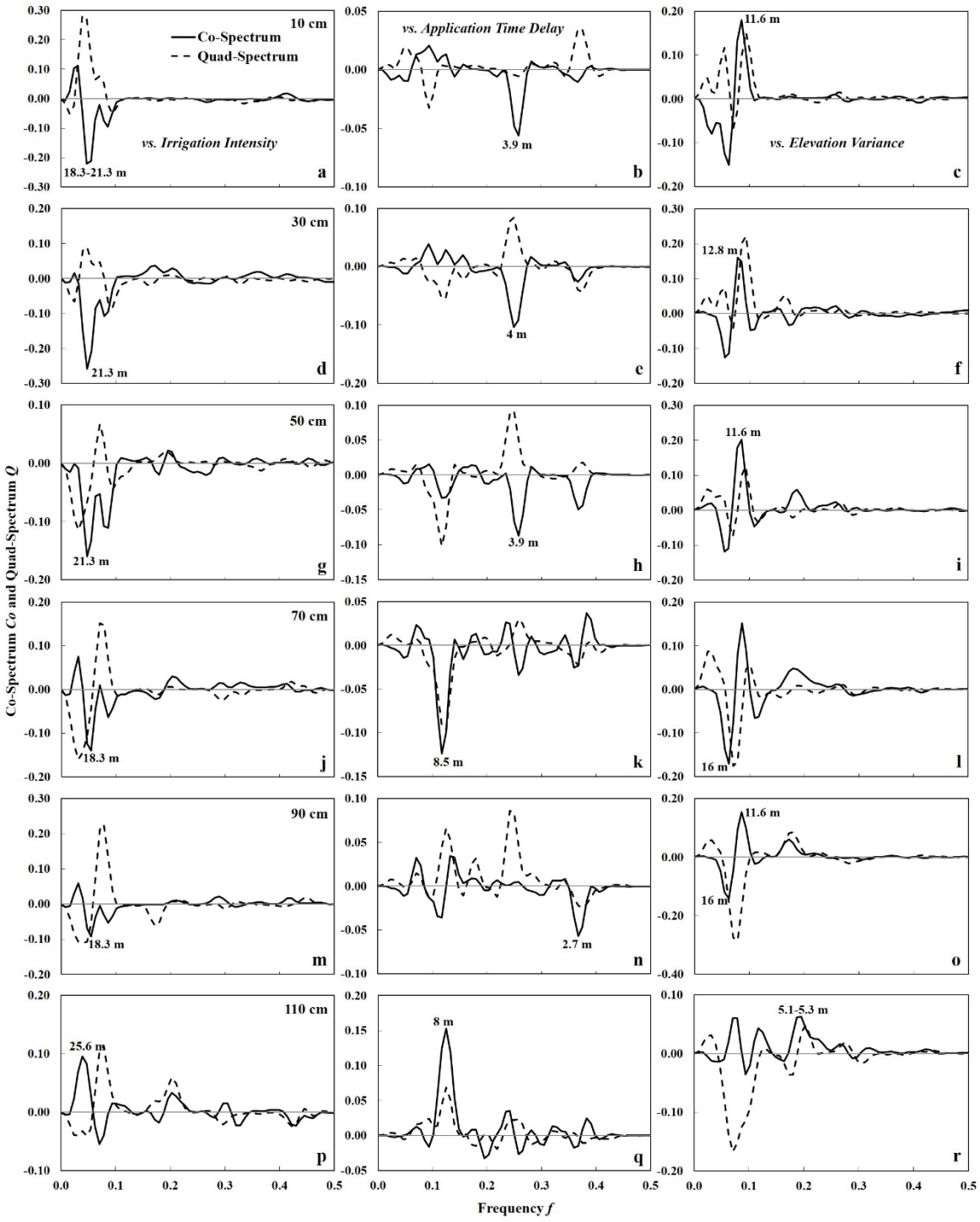

Figure 4.8 Co- and quad-spectra between matric potential change from the beginning to the end of irrigation (RB) and (a, d, g, j, m, p) imposed irrigation intensity, (b, e, h, k, n, q) application time delay, and (c, f, i, l, o, r) investigated elevation variance at six depths.

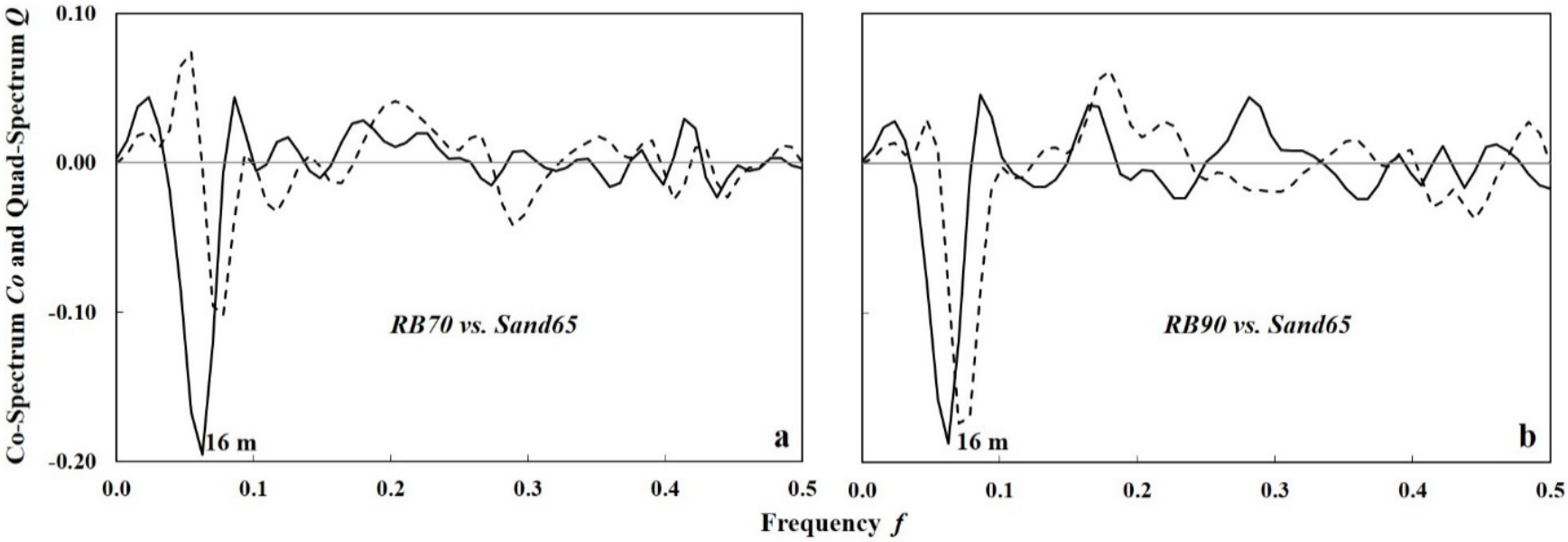

Figure 4.9 Co- and quad-spectra (a) between matric potential change from the beginning to the end of irrigation at 70 cm (RB70) and sand content at 60-70 cm (Sand65), and (b) between RB90 and Sand65.

During the one-day drainage following irrigation, water redistribution was mainly controlled by irrigation intensity and elevation variance. As shown in Figure 4.10, the highest peaks appeared in the co-spectra for 1D with irrigation intensity at 30, 90 and 110cm, at the frequency $f =$ 0.0391 ($\lambda = 25.6$ m). All these peaks were negative, indicating that water accumulated under higher intensity irrigation drained faster once irrigation stopped. At the other three depths, the greatest peaks were revealed in the co-spectra with elevation variance, at the frequency of either 0.0781 ($\lambda = 12.8$ m) or 0.1719 ($\lambda = 5.8$ m). Furthermore, elevation variance contributed to the spatial distribution of 1D at 30 and 90 cm, but with a less extent compared to irrigation intensity. These negative spatial correlations suggested more water drainage under a rougher soil surface during short-term redistribution.

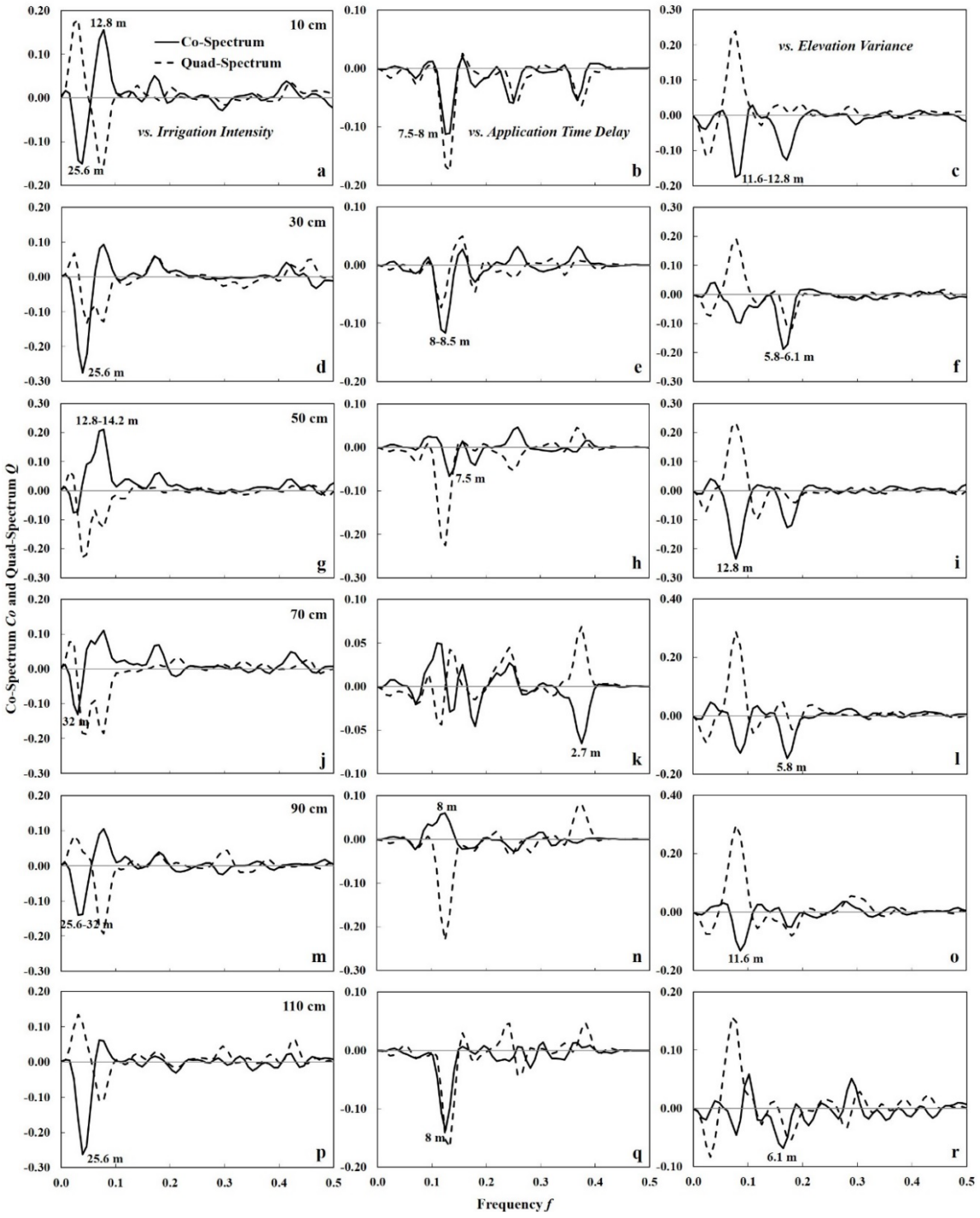

Figure 4.10 Co- and quad-spectra between matric potential change from the end of irrigation to one day after irrigation (1D) and (a, d, g, j, m, p) imposed irrigation intensity, (b, e, h, k, n, q) application time delay, and (c, f, i, l, o, r) investigated elevation variance at six depths.

When the water redistribution lasted for three days, the major factors causing matric potential decrease and water loss were different. The co- and quad-spectra between 3D and the three boundary conditions under investigation at six depths are displayed in Figure 4.11. Irrigation intensity and application time delay became the dominant factors for this period of water movement. Corresponding to the major peaks at $f = 0.125$ ($\lambda = 8$ m) in the power spectra for 3D at 30 and 50 cm (Figure 4.7b, c), the greatest peaks of -0.16 and -0.20 were found at the same frequency in the co-spectra with application time delay, respectively (Figure 4.11e, h). The time delay of irrigation relative to Br^- application was negatively correlated with matric potential change during three days of drainage. In contrast, although a distinct peak at $f = 0.125$ ($\lambda = 8$ m) was also shown in the power spectra for 3D at 10 cm (Figure 4.7a), the co-spectrum at this frequency was only -0.04 (Figure 4 .11b). Compared to the significant quad-spectrum of 0.51 here, a phase lag of 2 m was manifested. It was implied that the matric potential change responded negatively to the solute application time delay applied at 2 m behind. At 70 and 90 cm, 3D was mainly affected by irrigation intensity (Figure 4.11j, m). As with the one-day drainage, the spatial correlations at these two depths were also negative. Intensity also played an important role in the spatial distribution of 3D at the lowest depth of 110 cm as indicated by the negative peak of -0.20 in the corresponding co-spectra (Figure 4.11p); however, the peak in the co-spectra between 3D and application time delay was greater (Figure 4.11q), suggesting the prevailing impact exerted by irrigation timing.

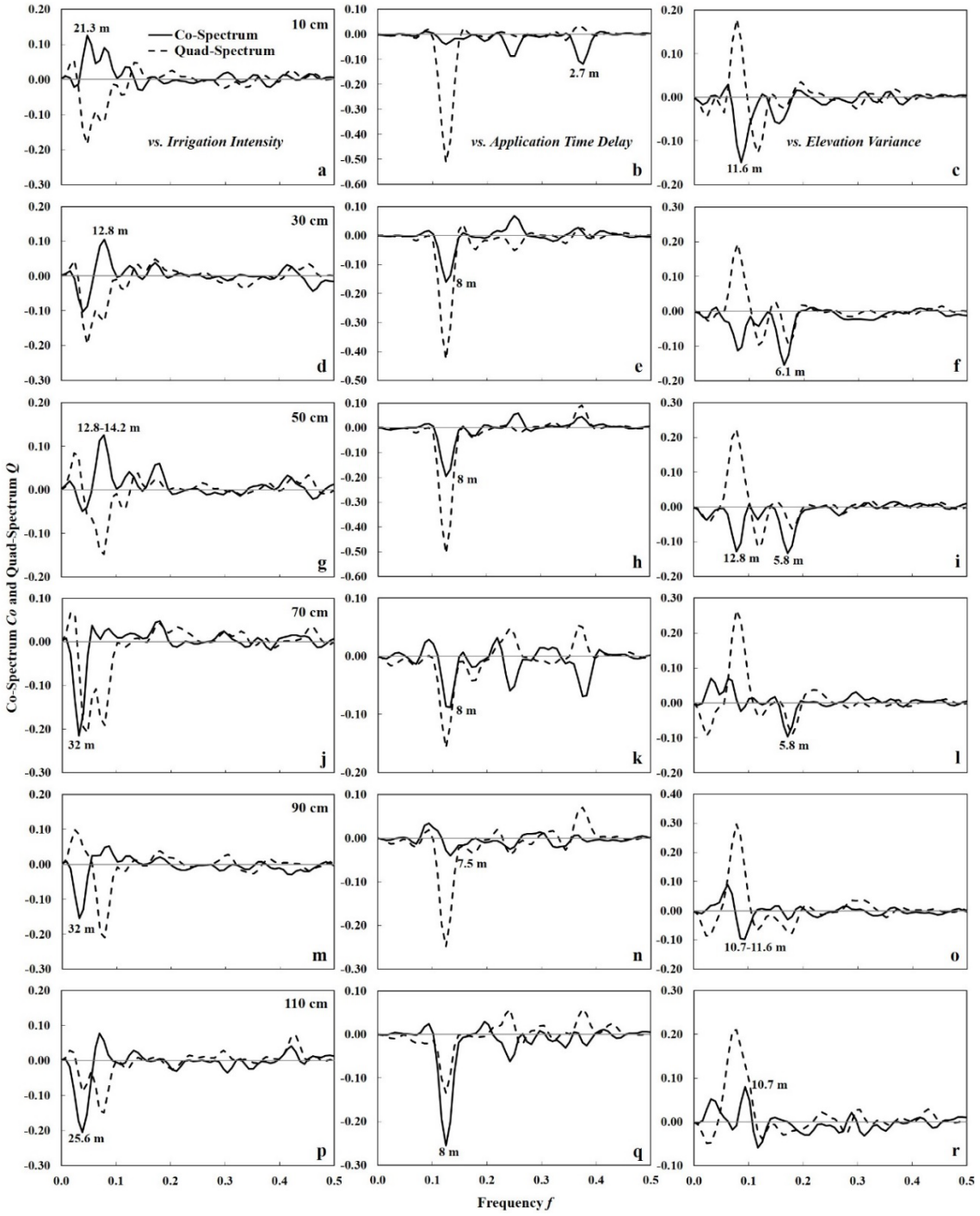

Figure 4.11 Co- and quad-spectra between matric potential change from the end of irrigation to three days after irrigation (3D) and (a, d, g, j, m, p) imposed irrigation intensity, (b, e, h, k, n, q) application time delay, and (c, f, i, l, o, r) investigated elevation variance at six depths.

The dominant boundary condition controlling the spatial distribution of water movement varied with time and depth (Figure 4.8, 4.10, 4.11). During the simulated irrigation, RB at the top two soil depths was most strongly correlated with intensity (Figure 4.8a, d) and the corresponding correlations were negative. Meanwhile, a positive spatial correlation was observed for RB with intensity at the lowest depth of 110 cm, which was only minor compared to the correlation with application time delay. These results were consistent with the more even vertical distribution of RB with soil depth under more intensive irrigation as concluded in Section 4.3.1; and this phenomenon was attributed to the enhancement of preferential flow by increasing intensity. At a high intensity, irrigation water quickly bypassed several subsurface layers and the time allowing water to move from preferential pathways into the soil matrix was limited (Beven and Germann, 1982; Haria et al., 1994; Gazis and Feng, 2004). In addition, the lateral invasion of water can be severely restricted by microbial and root exudates which are commonly present in biopores, typically in grassland, and increase the water repellency of macropore linings (Gerke and Köhne, 2002; Jarvis, 2007). As a result, negative spatial correlations, although not the strongest, were detected between RB and intensity at the soil depths above 110 cm (Figure 8j, m). This causal intepretation is to some extent supported by McIntosh et al. (1999), who found less water and tracer exchange between the macrochannels and soil matrix under simulated heavier rainfalls. Compared to the fast preferential flow and limited lateral infiltration, water slowly moving into the soil matrix and micropores under low intensity irrigation tended to be protected from draining during the process of redistribution. It led to a deduction that more water losses after the cessation of irrigation corresponded with higher

intensity, which was verified by the negative spatial correlations between intensity and 1D as well as 3D in the deep soil (e.g. Figure 4.10j, 4.11j).

Similar with irrigation intensity, soil surface roughness described by elevation variance affected matric potential change and water movement through its impact on preferential flow as well. An increase in soil surface roughness not only raises the amount of water that infiltrates (Cogo et al., 1984; Darboux and Huang, 2005), but also enhances water movement through macropores or other preferential pathways (Weiler and Naef, 2003b). During the irrigation in this experiment, more water applied on a rougher surface was transported downwards and then impeded by the plow pan at 40-50 cm, which was believed to be present as a result of tobacco production in this field site several years ago (Yang et al., 2013; Yang and Wendroth, 2014). Hence, water accumulated at 50 cm and a positive spatial correlation between elevation variance and RB was obtained (Figure 4.8i). The matric potential increase resulting from preferential flow was more prone to loss as discussed above. Therefore, an increased elevation variance corresponded with greater matric potential decrease, or more negative 1D, especially at 50 cm (Figure 4.10i).

No significant spatial correlations were expected between irrigation timing and water infiltration, since the water amount applied together with KBr was very small compared to the irrigation afterwards; and the four levels of delay were primarily designed to study solute transport. However, the spectral and cross-spectral analyses revealed that application time delay was responsible for the main spatial distribution patterns of water movement at 110 cm (Figure 4.8q) during irrigation and at many more depths during the relatively long-

term drainage of three days (Figure 4.11). These results might be explained by the influence of time delay on soil moisture status antecedent to irrigation, which thereby affected soil water repellency and preferential flow (Burcar et al., 1994; Shipitalo et al., 2000; Jarvis, 2007). The relatively drier soil near surface resulting from longer time delay exhibited greater water repellency and tended to limit the infiltration of irrigation water into soil matrix (Weiler and Naef, 2003a). Therefore, more water flowed into macropores and continuous channels, leading to deeper leaching of irrigation water and greater matric potential increase at the bottom (Figure 4.8q). The effect of time delay seemed to last longer than elevation variance, showing a dominant role in the spatial distribution of matric potential decrease during the three-day drainage. At the soil depths of 30, 50 and 110 cm, application time delay was revealed as the most important boundary condition (Figure 4.11e, h, q). At 10 cm, a phase lag of 2 m was indicated in the spatial correlation between 3D and irrigation timing (Figure 4.11b). The shifted response of matric potential decrease may be caused by the gentle slope towards grassland where the experimental transect was located.

4.3.3 Spectral Analysis of Br^- Concentration in Soil Water

Figure 4.12 shows the power spectra for Br^- concentration in soil water sampled one hour and one day after irrigation at five depths. Note that no power spectra is presented for the one at 20 cm for one-day sampling, since the lack of Br^- concentration data at nearly half of the locations precluded either spectral or cross-spectral analysis. The peaks manifested in the power spectra for Br^- concentration were generally smaller and less distinct compared to those for matric potential changes as displayed in Figure 4.7. However, as

with water infiltration, the periodic fluctuations in Br^- leaching varied with depth and time. For the only dataset at 20 cm, the major peak appearing at the frequency f = 0.0547-0.0625 (λ = 16-18.3 m) might be correlated with irrigation intensity (Figure 4.12a); while the minor one at f = 0.4063 (λ = 2.5 m) did not seem to correspond with any spatial scales revealed in the three boundary conditions. At 40 cm, small-scale fluctuations were revealed in the Br^- concentration during one-hour sampling, and the wavelength of 2.1 m corresponded with the plot length of 2 m (Figure 4.12b). After one day, the distribution of soil water Br^- concentration was mainly controlled by elevation variance due to the occurrence of major peak at f = 0.0859 (λ = 11.6 m). Bromide concentrations at 60 cm for both samplings varied at similar scales, corresponding to the minor periodicity in elevation variance (Figure 4.12c). At the soil depth below, 80 cm, besides the common fluctuations at around f = 0.25 (λ = 4 m) correlated with application time delay, Br^- concentration in soil water sampled one hour after irrigation also varied at f = 0.4531 (λ = 2.2 m) probably resulting from the plot length; whereas Br^- concentrations obtained in the later sampling were found to have a cyclic pattern identical with that of elevation variance at f = 0.0781 (λ = 12.8 m) (Figure 4.12d). The variation scales and influencing factors implied were quite different for Br^- concentrations at 100 cm measured at two sampling times (Figure 4.12e). One hour after irrigation, the spatial distribution of Br^- was mainly affected by irrigation intensity and to a smaller extent by application time delay, indicated by the major peak at f = 0.0313 (λ = 32 m) and the minor one at f = 0.125 (λ = 8 m), respectively. On the contrary, a distinct peak at f = 0.1641 (λ = 6.1 m) appearing at the power spectra for Br^- concentration obtained one day after irrigation suggested the impact of elevation variance.

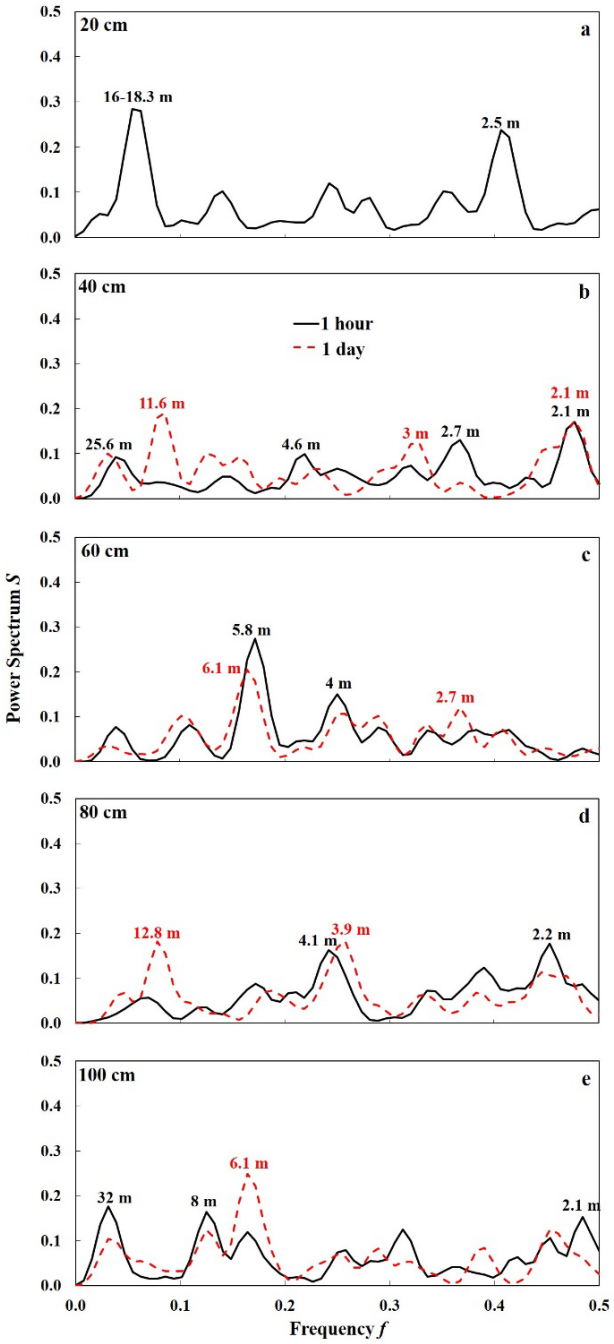

Figure 4.12 Power spectra for Br^- concentration in soil water sampled one hour and one day after irrigation at five depths: (a) 20, (b) 40, (c) 60, (d) 80, and (e) 100 cm. The numbers above the peaks indicate the wavelengths λ at corresponding frequencies *f*. Notice that the samples taken at 20 cm one day after irrigation were not enough to conduct the spectral analysis and in (a) only the result for one-hour sampling is shown.

The co- and quad-spectra for Br^- concentration in soil water sampled one hour after irrigation with three boundary conditions at five depths are shown in Figure 4.13. Irrigation intensity and elevation variance exerted equivalent influence on the spatial distribution of Br^- concentration at 20 cm in view of the similar magnitudes of major peaks appearing in the corresponding co-spectra. The negative peak of -0.14 at f = 0.0469 (λ = 21.3 m) in Figure 4.13a indicated more surface-applied Br^- moving downwards under heavier irrigation; while the positive peak of 0.14 at f = 0.4141 (λ = 2.4 m) appearing in Figure 4.13c suggested that a rougher surface was beneficial for retaining solute in the top soil layers. At the two soil depths below, intensity among the three boundary conditions under investigation was the dominant factor that controlled Br^- distribution. The distinct peaks revealed in the corresponding co-spectra were both positive (Figure 4.13d, g), which means more Br^- has been leached downwards as intensity increased. The peaks in the co-spectra for Br^- at 80 cm with all the three boundary conditions were very small and the one with application time delay was relatively higher (Figure 4.13k). This negative spatial correlation between time delay and Br^- concentration became stronger down to 100 cm (Figure 4.13n), indicating that more solute was protected from leaching when longer time before irrigation was allowed for solute to move into the aggregates near soil surface. Meanwhile, a positive peak of equivalent magnitude, 0.2, was manifested in the co-spectra between Br^- and intensity (Figure 4.13m).

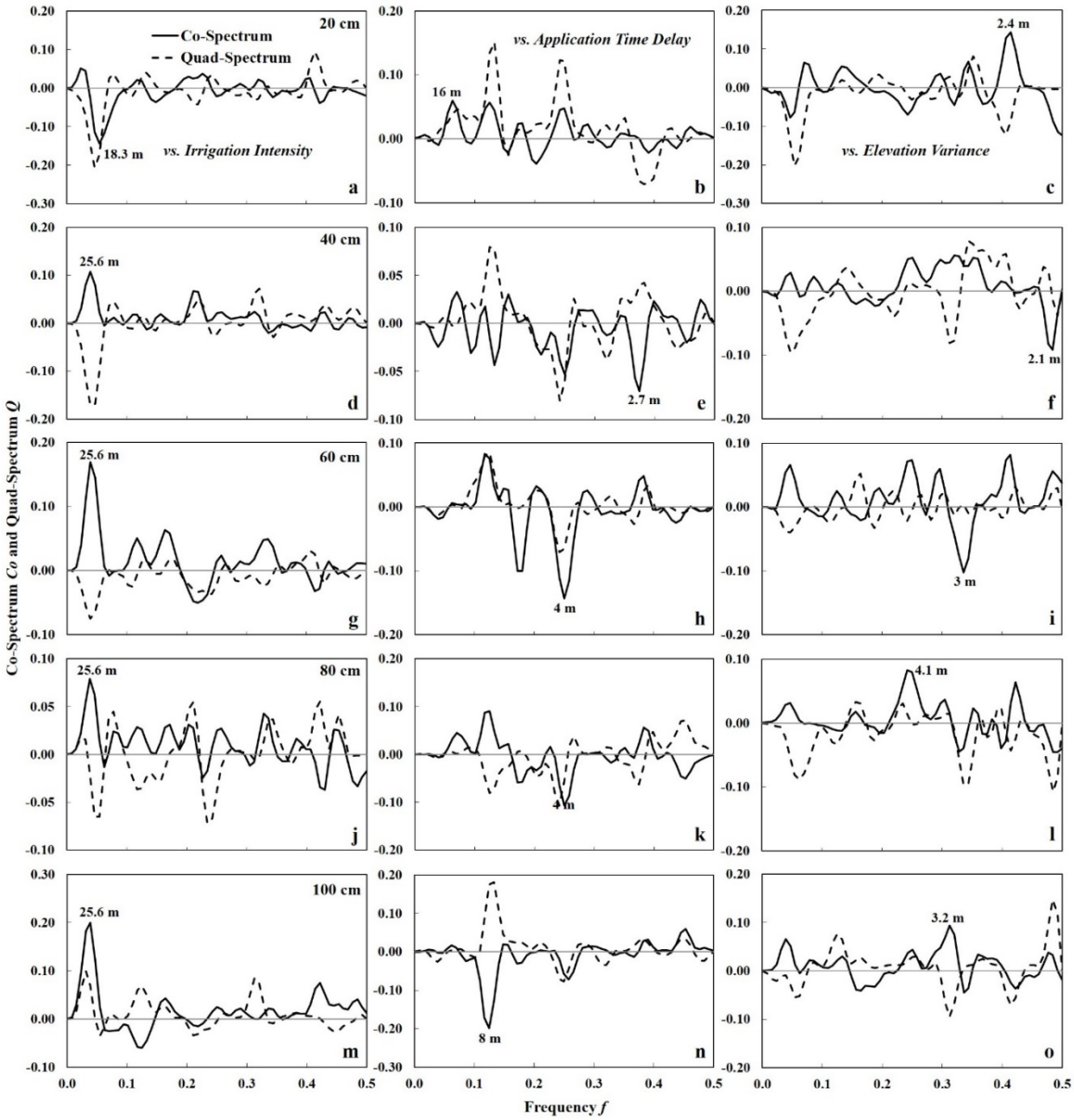

Figure 4.13 Co- and quad-spectra between Br^- concentration in soil water sampled one hour after irrigation and (a, d, g, j, m) imposed irrigation intensity, (b, e, h, k, n) application time delay, and (c, f, i, l, o) investigated elevation variance at five depths.

Analyzing Br^- concentration in soil water samples at different depths provided a consistent result with the Br^- analysis based on soil extracts (Yang et al., 2013) regarding the influence of irrigation intensity. Irrigation at increasing intensity was more capable of transporting

surface-applied solute downwards, resulting in less Br retained above 20 cm and more leached below. However, the impact of either application time delay or elevation variance on Br^- concentration resulting from these two sampling techniques were quite different. At most depths, the spatial correlation scales were disparate. In general, the variation scales revealed here with Br^- concentration in soil water were smaller. And although similar scales were manifested, such as the ones for application time delay with both Br^- concentrations near the bottom of the soil profile studied, opposite spatial associations were detected. The negative correlation here reflected the solute protection function exerted by soil aggregates; while the positive one between time delay and soil Br^- in Yang et al. (2013) probably resulted from the effect of irrigation timing on antecedent soil moisture and preferential flow.

One day later, the spatial patterns of soil water Br^- changed compared to those detected one hour after irrigation (Figure 4.12) because different boundary conditions were found to be more effective in the redistribution process. Instead of irrigation intensity, elevation variance and application time delay became the main factor that affected Br^- distribution at 40 and 60 cm, respectively (Figure 4.14c, e). At the soil depth below, 80 cm, the highest peak was present in the co-spectra for Br^- concentration with irrigation intensity (Figure 4.14g). This positive peak of 0.18 at f = 0.0391-0.0469 (λ = 21.3-25.6 m), together with the positive peak of 0.23 at the similar frequency in the co-spectra between intensity and Br^- at 100 cm (Figure 4.14j), indicated that more Br^- was retained in the deep soil under higher intensity irrigation even after one day of redistribution. Similar to the one-hour sampling

results, a negative spatial correlation between Br^- concentration and application time delay was revealed at 100 cm.

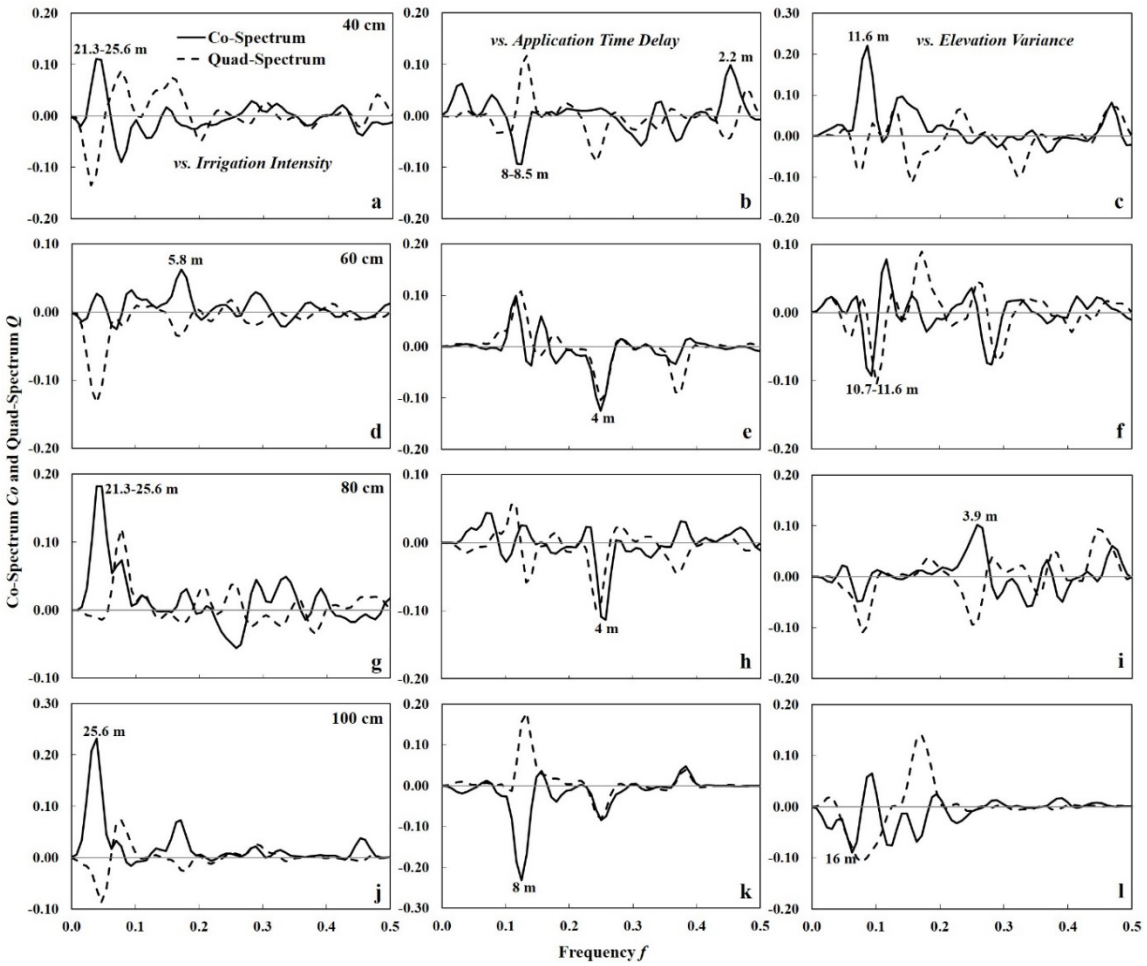

Figure 4.14 Co- and quad-spectra between Br^- concentration in soil water sampled one day after irrigation and (a, d, g, j) imposed irrigation intensity, (b, e, h, k) application time delay, and (c, f, i, l) investigated elevation variance at four depths.

Besides the boundary conditions analyzed in this experiment, there existed other soil properties that contributed to the scale-variant behavior of Br^- leaching, since not all the spatial scales revealed in the power spectra for Br^- concentration in Figure 4.12 have been

explained and related to certain variables. Therefore, cross-spectral analysis between matric potential change and Br^- concentration in soil water was conducted to answer the question: does the change in soil water status contain any other information responsible for the spatial distribution patterns of Br^- leaching?

In some situations, matric potential change helped to explain the horizontal distribution of Br^-. For example, as shown in Figure 4.15a, a distinct positive peak appeared at the frequency $f = 0.4063$ ($\lambda = 2.5$ m) in the co-spectra for Br^- concentration at 20 cm one hour after irrigation with matric potential decrease at 10 cm during three days of drainage. It was implied in these common periodicities that the minor peak shown in the power-spectra for Br^- at 20 cm depth (Figure 4.12a) was correlated with the long-term matric potential decrease since not a single boundary condition investigated here exhibited the fluctuations at the same scale. Surface soil moisture change during two or three days of drainage following a thorough wetting could serve as a good indicator for drainable porosity (van Schilfgaarde, 1957) and has a significant correlation with saturated hydraulic conductivity for a wide range of soil types (Ahuja et al., 1993). Thus a higher (less negative) 3D may indicate a smaller hydraulic conductivity, although the soil in this experiment was not completely saturated during only one irrigation event, which slowed down the leaching of Br^-. However in most cases, the spatial correlation manifested in the co-spectra resulted from the boundary condition which affected both matric potential change and Br^- concentration at the same spatial scale. For example, elevation variance was positively correlated with Br^- concentration at 40 cm one day after irrigation (Figure 4.14c) and negatively correlated with 1D at 50 cm (Figure 4.10i) at a similar frequency $f = 0.0781$-

0.0859 (λ = 11.6-12.8 m), resulting in a significant negative correlation occurring at the same frequency in the co-spectra for solute concentration with water status change (Figure 4.15b). With a higher 1D or in other words, less decrease in matric potential and water content during short-term drainage, Br^- was diluted and the concentration became lower.

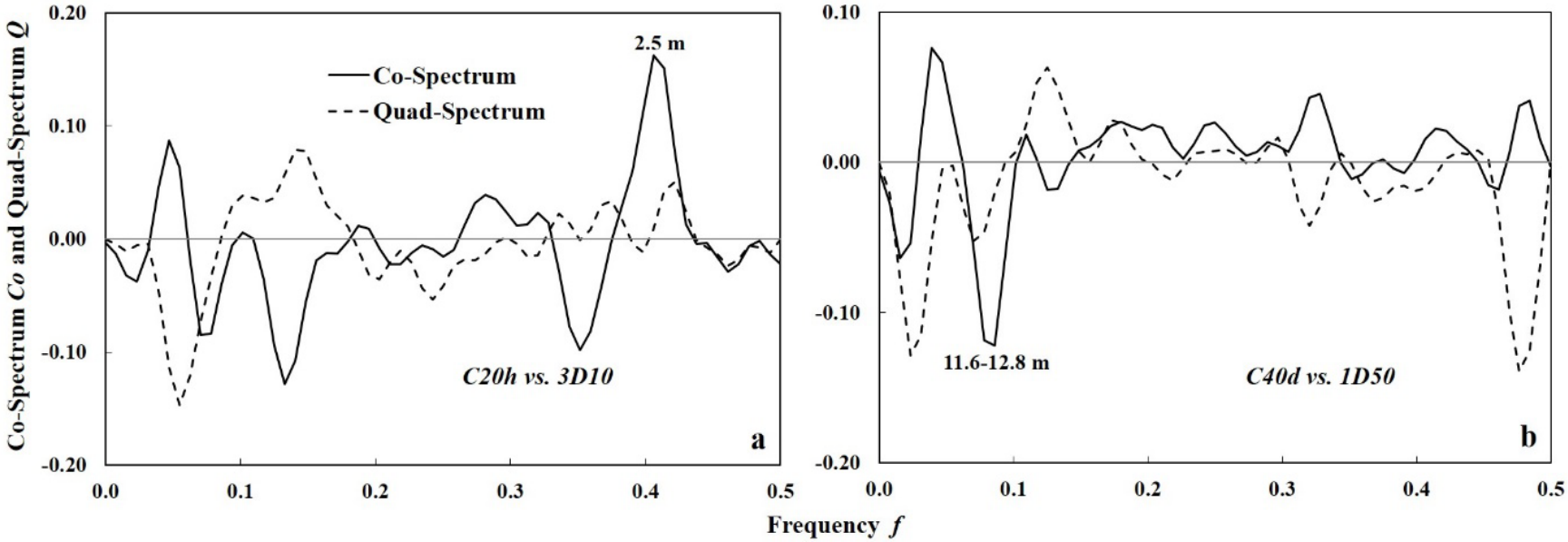

Figure 4.15 Co- and quad-spectra (a) between Br^- concentration at 20 cm one hour after irrigation (C20h) and matric potential change at 10 cm during three days of drainage (3D10), and (b) between Br^- concentration in soil water sampled at 40 cm one day after irrigation (C40d) and matric potential change at 50 cm during one day of drainage (1D50).

4.4 Conclusions

A new experimental design arranging treatments in a periodically repetitive pattern at different spatial scales was employed to analyze the impact of land use, soil surface roughness, irrigation intensity and timing relative to solute application on water infiltration and Br^- leaching. Tensiometers and suction probes were utilized to monitor *in situ* matric potential changes and Br^- concentrations, respectively.

During irrigation, more water and surface-applied Br^- moved downwards at higher intensity, resulting in a more even distribution of Br^- concentration with soil depth, especially in grassland. Preferential flow enhanced by higher irrigation intensity was probably the reason. Spectral analysis also revealed that the spatial correlation between intensity and Br^- was negative at the shallowest depth of 20 cm and positive at greater soil depths. These results were consistent with the observations based on soil coring samples in Yang et al. (2013), suggesting the applicability of suction probes in studying *in situ* solute transport as affected by irrigation intensity at the field scale. However, with respect to the influence of application time delay and elevation variance, these two sampling techniques had different results. One day after the cessation of irrigation, Br^- concentrations determined in soil solution samples became generally lower; and the major factors controlling the spatial distribution of Br^- at each depth changed except at the bottom of 100 cm.

The spatial variation scale of matric potential change varied with time and depth, corresponding with different boundary conditions. Irrigation intensity dominated the spatial distribution of matric potential change at the upper two depths during irrigation and

in the deep soil in the process of redistribution, no matter whether it was one day or three days. Besides that, the matric potential decrease during short-term drainage was mainly influenced by elevation variance; whereas, during the drainage for three days, application time delay was the primary driving force. Both irrigation intensity and elevation variance affected matric potential change and water movement through their impact on preferential flow. Irrigation timing, which was primarily designed to study solute transport, was probably related to the soil moisture antecedent to irrigation, which thereby affected water repellency and preferential flow. Furthermore, it is interesting to discover the phase-shifted response of matric potential change to application time delay at 10 cm depth during the long-term redistribution, which revealed the limited but undoubtedly important role that elevation played in the spatial distribution of water infiltration.

Spatial correlations were detected between matric potential change and Br^- concentration at some depths. It was usually because a boundary condition was spatially correlated with both at the same scale. However under some circumstances, soil properties other than the boundary conditions investigated in this experiment, such as hydraulic conductivity, were embedded in the spatial processes of matric potential change and responsible for the spatial distribution patterns of Br^- leaching. The results of this study not only suggest the applicability of scale-dependent treatment distribution in field experimental design but also provide direct implications for agricultural management and hydrological modelling.

Chapter 5 Conclusions

A novel experimental design was employed to analyze water infiltration and Br^- leaching as affected by land use, soil surface roughness and rainfall characteristics under field conditions. In this rainfall simulation experiment, treatments were arranged in cyclic layout at distinct spatial scales and their impact was manifested in the variance behaviors of temporal matric potential change and Br^- concentration that exhibited common scales. The first analysis (Chapter 2) was based on Br^- concentrations measured in soil core samples collected at different depths along the experimental transect. The results showed that owing to more developed soil structure and more continuous macropores, which enhanced the development of preferential flow, soil Br^- was more evenly distributed with soil depth and leached deeper in grassland than in no-till cropland. Spectral and cross-spectral analyses decomposed variance of soil Br^- at each depth among different scales and revealed its spatial correlations with different boundary conditions, respectively. The dominant factors hence identified were found to vary with soil depth. In the top layer of 0-10 cm, Br^- distribution was primarily controlled by rainfall intensity and to a smaller extent by soil clay content; whereas, in the soil layer immediately below, rainfall timing relative to Br^- application turned to be the main driving force. The impact of rainfall characteristics generally decreased with soil depth. In contrast, the roles of soil properties, i.e., soil texture and surface roughness described by elevation variance, became increasingly important.

Spectral analysis revealed the relative importance of the boundary conditions to Br^- leaching; and in the following chapter, an autoregressive state-space approach was applied

to describe the spatial distribution pattern of soil Br^- site-specifically (Chapter 3). Beginning with spatial associations of Br^- concentrations among different depths, soil Br^- at 20-30, 30-40 and 40-50 cm were found to be most strongly correlated with that in the top layer of 0-10 cm, rather than in the respective neighboring layer above. Similarly, soil Br^- in deeper layers, i.e., 70-80, 80-90 and 90-100 cm, had the strongest spatial correlation with Br^- concentration at 50-60 cm. Therefore, two flow regimes were revealed in the soil profile, i.e., above and below 50 cm. Apparently, the flow dynamics changed when water and solute passed the soil layer of 40-50 cm, where sand content was very low and a plow pan was believed to be still present due to tobacco production several years ago.

The optimal state-space models considering up to three boundary conditions were generated for soil Br^- concentration at each depth. According to the weight of each variable, land use dominated the horizontal distribution pattern of Br^- at shallow depths; while for the soil layers below 40 cm, soil texture was the primary influencing factor and rainfall intensity ranked second. Land use was excluded when comparing the results of state-space analysis to those obtained in Chapter 2, since land use only changed once along the transect and was not treated as a typical cyclic pattern for spectral analysis. It turned out that similar to the findings in Chapter 2, the spatial behavior of soil Br^- in the upper layers was mostly affected by rainfall characteristics when land use was not involved. Furthermore, in contrast to land use, adding Br^- concentration and soil texture of the adjacent layer above as factors in the spatial description mainly improved the prediction quality of state-space models for soil Br^- below 60 cm.

The temporal dynamics of water infiltration and solute leaching were analyzed in Chapter 4. The soil solution samples collected through suction probes one hour after the cessation of rainfall simulation generally had higher Br^- concentrations than those sampled one day later. According to the results of spectral analysis, the major factors controlling Br^- distribution differed between these two sampling times for all the depths investigated except the bottom one of 100 cm.

The spatial variation scale of temporal matric potential change varied with both time and depth, as well, corresponding with different boundary conditions. Rainfall intensity dominated the horizontal distribution of matric potential change at the two shallowest depths, i.e., 10 and 30 cm, during rainfall simulation and in the deep soil during the redistribution process afterwards. Beyond that, the matric potential decreases during one-day and three-day periods of drainage after the rainfall simulation experiment were mainly affected by soil surface roughness and rainfall timing, respectively. Matric potential change was found to be spatially correlated with Br^- concentration at some depths. Usually, it resulted from the boundary condition which affected both at the same spatial scale. However, in some cases, matric potential change did help to explain the scale-variant behavior of Br^- leaching. The impact of soil properties other than the boundary conditions investigated in this experiment, such as hydraulic conductivity, was reflected in the spatial processes of matric potential change and responsible for the major distribution patterns of Br^- concentration.

These results suggest that the experimental design with scale-dependent treatment distribution adopted here may be highly useful in studying hydrological processes under field conditions. With the aid of frequency-domain analysis, this investigation technique overcomes the limitations induced by large spatial variability inherent in soil properties and separates the treatment impacts from the ones exerted by underlying soil processes. Moreover, the findings of this study hold important implications for agricultural management and also for hydrological modelling at the field scale.

References

Ahuja, L.R., O. Wendroth, and D.R. Nielsen. 1993. Relationship between initial drainage of surface soil and average profile saturated conductivity. *Soil Sci. Soc. Am. J.* 57:19-25.

Alberts, E.E., R.E. Burwell, and G.E. Schuman. 1977. Soil nitrate-nitrogen determined by coring and solution extraction techniques. *Soil Sci. Soc. Am. J.* 41:90-92.

Addiscott, T.M., V.H. Thomas, and M.A. Janjua. 1983. Measurement and simulation of anion diffusion in natural soil aggregates and clods. *J. Soil Sci.* 34:709-721.

Afyuni, M.M., D.K. Cassel, and W.P. Robarge. 1994. Lateral and vertical bromide ion transport in a Piedmont landscape. *Soil Sci. Soc. Am. J.* 58:967-974.

Akaike, H., 1969. Fitting autoregressive models for prediction. *Ann. Inst. Stat. Math.* 21:243-247.

Al-Sibai, M., M.A. Adey, and D.A. Rose. 1997. Movement of solute through a porous medium under intermittent leaching. *Eur. J.Soil Sci.*48:711-725

Ashraf, M.S., B. Izadi, and B. King. 1997. Transport of bromide under intermittent and continuous ponding conditions. *J. Environ. Qual.* 26:69-75.

Augustin, S., M. Jansen, E. Priesack, and F. Beese. 1995. Litter decomposition and matter transport in beds of soil aggregates. *In:* Hartge, K.H., B.A. Steward (Eds.), Soil structure: Its development and function. Advances in Soil Science. CRC Press, Inc., Boca Raton.

Barbee, G.C., and K.W. Brown. 1986. Comparison between suction and free-drainage soil solution samplers. *Soil Sci.* 141:149-154.

Barry, D.A., and G. Sposito. 1988. Application of the convection-dispersion model to solute transport in finite soil columns. *Soil Sci. Soc. Am. J.* 52:3-9.

Bazza, M., R.H. Shumway, and D.R. Nielsen. 1988. Two-dimensional spectral analyses of soil surface temperature. *Hilgardia* 56:1-28.

Beven, K., and P. Germann. 1982. Macropores and water flow in soils. *Water Resour. Res.* 18:1311-1325.

Biggar, J.W., and D.R. Nielsen. 1976. Spatial variability of the leaching characteristics of a field soil. *Water Resour. Res.* 12:78-84.

Binley, A., S. Henry-Poulter, and B. Shaw. 1996. Examination of solute transport in an undisturbed soil column using electrical resistance tomography. *Water Resour. Res.* 32:763-769.

Bond, R.D. 1964. The influence of the microflora on the physical properties of soils: II. Field studies on water repellent sands. *Aust. J. Soil Res.* 2:123-131.

Bonnin, G.M., D. Martin, B. Lin, T. Parzybok, M. Yekta, and D. Riley. 2006. NOAA Atlas 14: Precipitation-frequency atlas of the United States, Vol. 2. U.S. Department of Commerce, National Oceanic and Atmospheric Administration, National Weather Service, Silver Spring, MD.

Bouma, J., A. Jongerius, O. Boersma, A. Jager, and D. Schoonderbeek. 1977. The function of different types of macropores during saturated flow through four swelling soil horizons. *Soil Sci. Soc. Am. J.* 41:945-950.

Bowman, R.S. 1984. Evaluation of some new tracers for soil water studies. *Soil Sci. Soc. Am. J.* 48:987-993.

Bresler, E., Kemper, W.D., and R.J. Hanks. 1969. Infiltration, redistribution, and subsequent evaporation of water from soil as affected by wetting rate and hysteresis. *Soil Sci. Soc. Am. Proc.* 33:832-840.

Briggs, L.J., and A.G. McCall. 1904. An artificial root for inducing capillary movement of soil moisture. *Science* 20:566-569.

Brooks, J.R., F.C. Meinzer, R. Coulombe, and J. Gregg. 2002. Hydraulic redistribution of soil water during summer drought in two contrasting Pacific Northwest coniferous forests. *Tree Physiol.* 22:1107-1117.

Buckingham, E. 1907. Studies on the movement of soil moisture. Bulletin 38. USDA Bureau of Soils, Washington, DC.

Burcar, S., W.W. Miller, S.W. Tyler, and D.W. Johnson. 1994. Seasonal preferential flow in two Sierra Nevada soils under forested and meadow cover. *Soil Sci. Soc. Am. J.* 58:1555-1561.

Butters, G.L., W.A. Jury, and F.F. Ernst. 1989. Field scale transport of bromide in an unsaturated soil: 1. Experimental methodology and results. *Water Resour. Res.* 25:1575-1581.

Caron, J., O. Banton, D.A. Angers, and J.P. Villeneuve. 1996. Preferential bromide transport through a clay loam under alfalfa and corn. *Geoderma* 69:175-191.

Cassel, D.K., O. Wendroth, and D.R. Nielsen. 2000. Assessing spatial variability in an agricultural experiment station field: Opportunities arising from spatial dependence. *Agron. J.* 92:706-714.

Clay, D.E., Z. Zheng, Z. Liu, S.A. Clay, and T.P. Trooien. 2004. Bromide and nitrate movement through undisturbed soil columns. *J. Environ. Qual.* 33:338-342.

Cochran, P.H., G.M. Marison, and A.L. Leaf. 1970. Variation in tension lysimeter leachate volumes. *Soil Sci. Soc. Am. J.* 34:309-311.

Cogo, N.P., W.C. Moldenhauer, and G.R. Foster. 1984. Soil loss reductions from conservation tillage practices. *Soil Sci. Soc. Am. J.* 48:368-373.

Cookson, W.R., J.S. Rowarth, and K.C. Cameron. 2000. The effect of autumn applied ^{15}N-labelled fertilizer on nitrate leaching in a cultivated soil during winter. *Nutr. Cycl. Agroecosys.* 56:99-107.

Corwin, D.L., K. Loague, and T.R. Ellsworth. 1999. Assessing non-point source pollution in the vadose zone with advanced information technologies. *In*: Corwin, D.L., K. Loague, and T.R. Ellsworth (Eds.), Assessment of non-point source pollution in the vadose zone. Geophysical Monograph 108. AGU, Washington, DC. pp. 1-20.

Dagan, G. 1987. Theory of solute transport by groundwater. *Ann. Rev. Fluid Mech.* 19:183-215.

Darboux, F., and C. Huang. 2005. Does soil surface roughness increase or decrease water and particle transfers? *Soil Sci. Soc. Am. J.* 69:748-756.

Davis, S.N., G.M. Thompson, H.W. Bentley, and G. Stiles. 1980. Ground-water tracers-A short review. *Ground Water* 18:14-23.

Dekker, L.W., and J. Bouma. 1984. Nitrogen leaching during sprinkler irrigation of a Dutch clay soil. *Agric. Water Manage.* 9:37-45.

De Smedt, F., F. Wauters, and J. Sevilla. 1986. Study of tracer movement through unsaturated sand. *J. Hydrol.* 85:169-181.

Destouni, G., and W. Graham. 1995. Solute transport through an integrated heterogeneous soil-groundwater system. *Water Resour. Res.* 31:1935-1944.

Di, H.J., K.C. Cameron, S. Moore, and N.P. Smith. 1999. Contributions to nitrogen leaching and pasture uptake by autumn-applied dairy effluent and ammonium fertilizer labeled with ^{15}N isotope. *Plant Soil* 210:189-198.

Diez, J.A., R. Roman, R. Caballero, and A. Caballero. 1997. Nitrate leaching from soils under a maize-wheat-maize sequence, two irrigation schedules and three types of fertilizers. *Agric. Ecosyst. Environ.* 65:189-199.

Dourado-Neto, D., L.C. Timm, J.C.M. de Oliveira, K. Reichardt, O.O.S. Bacchi, T.T. Tominaga, and F.A.M. Cássaro. 1999. State-space approach for the analysis of soil water content and temperature in a sugarcane crop. *Sci. Agr.* 56:1215-1221.

Edwards, W.M., M.J. Shipitalo, L.B. Owens, and L.D. Norton. 1989. Water and nitrate movement in earthworm burrows within long-term no-till cornfields. *J. Soil Water Conser.* 44:240-243.

Edwards, W.M., M.J. Shipitalo, L.B. Owens, and W.A. Dick. 1993. Factors affecting preferential flow of water and atrazine through earthworm burrows under continuous no-till corn. *J. Environ. Qual.* 22:453-457.

Ellsworth, T.R., and C.W. Boast. 1996. Spatial structure of solute transport variability in an unsaturated field soil. *Soil Sci. Soc. Am. J.* 60:1355-1367.

England, C.B. 1974. Comments on 'A technique using porous cups for water sampling at any depth in the unsaturated zone' by Warren W. Wood. *Water Resour. Res.* 10:1049.

Ersahin, S., R.I. Papendick, J.L. Smith, C.K. Keller, and V.S. Manoranjan. 2002. Macropore transport of bromide as influenced by soil structure differences. *Geoderma* 108:207-223.

Fairclough, H.R.1999. Virgil, Eclogues, Georgics, Aeneid, Books 1-6. Harvard University Press, Cambridge, MA.

Feyen, J., D. Jacques, A. Timmerman, and J. Vanderborght. 1998. Modelling water flow and solute transport in heterogeneous soils: A review of recent approaches. *J. Agric. Eng. Res.* 70:231-256.

Flury, M., and A. Papritz. 1993. Bromide in the natural environment: Occurrence and toxicity. *J. Environ. Qual*. 22:747-758.

Flury, M., H. Flühler, W.A. Jury, and J. Leuenberger. 1994. Susceptibility of soils to preferential flow of water: A field study. *Water Resour. Res.* 30:1945-4954.

Flury, M., and N. N. Wai. 2003. Dyes as tracers for vadose zone hydrology. *Rev. Geophys.* 41, 1002, doi: 10.1029/2001RG000109.

Flühler, H., W. Durner, and M. Flury. 1996. Lateral solute mixing processes- a key for understanding field-scale transport of water and solutes. *Geoderma* 70:165-183.

Francis, G.S., K.C. Cameron, and R.A. Kemp. 1988. A comparison of soil porosity and solute leaching after six years of direct drilling or conventional cultivation. *Aust. J. Soil Res.* 26:637-649.

Gazis, C., and X. Feng. 2004. A stable isotope study of soil water: Evidence for mixing and preferential flow paths. *Geoderma* 119:97-111.

Gee, G.W., and J.W. Bauder. 1986. Particle-size analysis. *In*: Klute, A. (Ed.), Methods of soil analysis, Part I. Physical and mineralogical methods (2^{nd} ed.). Soil Science Society of America, Madison, WI. pp. 383-411.

Gerke, H.H. 2006. Preferential flow descriptions for structured soils. *J. Plant Nutr. Soil Sci.* 169:382-400.

Gerke, H.H., and J.M. Köhne. 2002. Estimating hydraulic properties of soil aggregate skins from sorptivity and water retention. *Soil Sci. Soc. Am. J.* 66:26-36.

Gerke, H.H., and J.M. Köhne. 2004. Dual-permeability modeling of preferential bromide leaching from a tile-drained glacial till agricultural field. *J. Hydrol.* 289:239-257.

Germann, P.F., W.M. Edwards, and L.B. Owens. 1984. Profiles of bromide and increased soil moisture after infiltration into soils with macropores. *Soil Sci. Soc. Am. J.* 48:237-244.

Ghuman, B.S., S.M. Verma, and S.S. Prihar. 1975. Effect of application rate, initial soil wetness, and redistribution time on salt displacement by water. *Soil Sci. Soc. Am. Proc.* 39:7-10.

Gjettermann, B., K.L. Nielsen, C.T. Petersen, H.E. Jensen, and S. Hansen. 1997. Preferential flow in sandy loam soils as affected by irrigation intensity. *Soil Technol.* 11:139-152.

Grossmann, J., and P. Udluft. 1991. The extraction of soil water by the suction-cup method: a review. *J. Soil Sci.* 42:83-93.

Haines, B.L., J.B. Waide, and R.L. Todd. 1982. Soil solution nutrient concentrations sampled with tension and zero-tension lysimteres: Report of discrepancies. *Soil Sci. Soc. Am. J.* 46:658-661.

Hansen, E.A., and A.R. Harris. 1975. Validity of soil-water samples collected with porous ceramic cups. *Soil Sci. Soc. Am. Proc.* 39:528-536.

Haria, A.H., A.C. Johnson, J.P. Bell, and C.H. Batchelor. 1994.Water movement and isoproturon behavior in a drained heavy clay soil: 1. Preferential flow processes. *J. Hydrol.* 163:203-216.

Heijs, A.W.J., C.J. Ritsema, and L.W. Dekker. 1996. Three-dimensional visualization of preferential flow patterns in two soils. *Geoderma* 70: 101-116.

Ingram, F.M. 1976. Disposition of bromide applied to grass and fallow plots. *Proc. Okla. Acad. Sci.* 56:38-41.

Isaaks, E.H., and R.M. Srivastava. 1989. Applied geostatistics. Oxford University Press, New York.

Janssen, M., and B. Lennartz. 2007. Horizontal and vertical water and solute fluxes in paddy rice fields. *Soil Till. Res.* 94:133-141.

Jarvis, N.J. 2007. A review of non-equilibrium water flow and solute transport in soil macropores: Principles, controlling factors and consequences for water quality. *Eur. J. Soil Sci.* 58:523-546.

Jemison, J.M., Jr., and R.H. Fox. 1992. Estimation of zero-tension pan lysimeter collection efficiency. *Soil Sci.* 154:85-94.

Jiang, Z., Q.J. Wu, L.C. Brown, and S.R. Workman. 1997. Water table depth and rainfall timing effect on Br^- and NO_3^- transport. *J. Irrig. Drain. Eng.*123:279-284.

Jury, W.A. 1985. Spatial variability of soil physical parameters in solute migration: A critical literature review. EPRI EA-4228 Project 2485-6, Riverside, CA.

Jury, W.A., and R. Horton. 2004. Soil physics (6^{th} Ed.). John Wiley & Sons, Hoboken, NJ.

Kachanoski, R.G., and E. De Jong. 1988. Scale dependence and the temporal persistence of spatial patterns of soil water storage. *Water Resour. Res.* 24:85-91.

Kalman, R.E., 1960. A new approach to linear filtering and prediction problems. *Trans. ASME J. Basic Eng.* 82D:35-45.

Kalman, R.E., and R.S. Bucy. 1961. New results in linear filtering and prediction theory. *Trans. ASME J. Basic Eng.* 83:95-108.

Kanchanasut, P., and D.R. Scotter. 1982. Leaching patterns in soil under pasture and crop. *Aust. J. Soil Res.* 20:193-202.

Keller, J., and J.F. Alfaro. 1966. Effect of water application rate on leaching. *Soil Sci.* 102:107-114.

Kessavalou, A., J.W. Doran, W.L. Powers, T.A. Kettler, and J.H. Qian. 1996. Bromide and nitrogen-15 tracers of nitrate leaching under irrigated corn in central Nebraska. *J. Environ. Qual. 25*:1008-1014.

Kluitenberg, G.J., and R. Horton. 1990. Effect of solute application methods on preferential transport of solutes in soil. *Geoderma* 46:283-297.

Köhne, J.M., H.H. Gerke, and S. Kohne. 2002. Effective diffusion coefficients of soil aggregates with surface skins. *Soil Sci. Soc. Am. J.* 66:1430-1438.

Kulli, B., C. Stamm, A. Papritz, and H. Flühler. 2003. Discrimination of flow regions on the basis of stained infiltration patterns in soil profiles. *Vadose Zone J.* 2:338-348.

Kung, K-J.S. 1990. Preferential flow in a sandy vadose zone: 1. Field observation. *Geoderma* 46:51-58.

Li, H., R.J. Lascano, J. Booker, L.T. Wilson, K.F. Bronson, and E. Segarra. 2002. State-space description of field heterogeneity: Water and nitrogen use in cotton. *Soil Sci. Soc. Am. J.* 66:585-595.

Litaor, M.I. 1988. Review of soil solution samplers. *Water Resour. Res.* 24:727-733.

Loague, K., and R.E. Green. 1991. Statistical and graphical methods for evaluating solute transport models: Overview and application. *J. Contam. Hydrol.* 7:51-73.

Matheron, G. 1962. Traité de Géostatistique Appliqué, Tome 1. Memoires du Bureau de Recherches Géologiques et Minières, Paris.

Martin, J.P. 1966. Bromide. *In:* H.D. Chapman (Ed.), Diagnostic criteria for plants and soils. University of California, Berkeley.

McIntosh, J., J.J. McDonnell, and N.E. Peters. 1999. Tracer and hydrometric study of preferential flow in large undisturbed soil cores from the Georgia Piedmont, USA. *Hydrol. Process.* 13:139-155.

McLay, C.D.A., K.C. Cameron, and R.G. McLaren. 1991. Effect of time of application and continuity of rainfall on leaching of surface-applied nutrients. *Aust. J. Soil Res.* 29:1-9.

McMahon, M.A., and G.W. Thomas. 1974. Chloride and tritiated water flow in disturbed and undisturbed soil cores. *Soil Sci. Soc. Am. J.* 38:727-732.

Miller, R., J.W. Biggar, and D.R. Nielsen. 1965. Chloride displacement in Panoche clay loam in relation to water movement and distribution. *Water Resour. Res.* 1: 63-73.

Morkoc, F., J.W. Biggar, D.R. Nielsen, and D.E. Rolston. 1985. Analysis of soil water content and temperature using state-space approach. *Soil Sci. Soc. Am. J.* 49:798-803.

Mulla, D.J., and J.G. Annandale. 1990. Assessment of field-scale leaching patterns for management of N fertilizer application. *In:* K. Roth et al.(Ed.), Field scale water and solute flux in soil. Berkhauser-Verlag, Basel, Switzerland. pp. 55-63.

Murdock, L., J. Grove, and G. Schwab. 2009. A comprehensive guide to wheat management in Kentucky: section 5. Fertilizer management. http://www.uky.edu/Ag/GrainCrops/ID125Section5.html

Netto, A.M., R.A. Pietitz, and J.P. Gaudet. 1999. Field study on the local variability of soil water content and solute concentration. *J. Hydrol.* 215:23-37.

Nielsen, D.R., and M.H. Alemi. 1989. Statistical opportunities for analyzing spatial and temporal heterogeneity of field soils. *Plant Soil* 115:285-296.

Nielsen, D.R., and J.W. Biggar. 1961. Miscible displacement in soils: I. Experimental information. *Soil Sci. Soc. Am. J.* 25:1-5.

Nielsen, D.R., and J.W. Biggar. 1962. Miscible displacement in soils: III. Theoretical considerations. *Soil Sci. Soc. Am. J.* 26:216-221.

Nielsen, D.R., M. Th. van Genuchten, and J.W. Biggar. 1986. Water flow and solute transport processes in the unsaturated zone. *Water Resour. Res.* 22:89S-108S.

Nielsen, D.R., and O. Wendroth. 2003. Spatial and temporal statistics- Sampling field soils and their vegetation. Catena, Reiskirchen, Germany.

Nielsen, D.R., O. Wendroth, and F.J. Pierce. 1999. Emerging concepts for solving the enigma of precision farming research. *In*: Robert, P.C., R.H. Rust, and W.E. Larson (Eds.), Proceedings of Fourth International Conference on Precision Agriculture. Minneapolis, MN. pp. 303-318.

Nimmo, J.R., and E.R. Landa. 2005. The soil physics contributions of Edgar Buckingham. *Soil Sci. Soc. Am. J.* 69:328-342.

Nkedi-Kizza, P., J.W. Biggar, M.T. Van Genuchten, P.J. Wierenga, H.M. Selim, J.M. Davidson, and D.R. Nielsen. 1983. Modeling tritium and chloride 36 transport through an aggregated oxisol. *Water Resour. Res.* 19:691-700.

Olson, G.L., and D.K. Cassel. 1999. Bromide leaching on a piedmont toposequence. *Soil Sci. Soc. Am. J.* 63:1319-1326.

Ottman, M.J., B.R. Tickes, and S.H. Husman. 2000. Nitrogen-15 and bromide tracers of nitrogen fertilizer movement in irrigated wheat production. *J. Environ. Qual.* 29:1500-1508.

Owens, L.B., R.W. Van Keuren, and W.M. Edwards. 1985. Groundwater quality changes resulting from a surface bromide application to a pasture. *J. Environ. Qual.* 14:543-548.

Paramasivam, S., A.K. Alva, A. Fares, and K.S. Sajwan. 2002. Fate of nitrate and bromide in an unsaturated zone of a sandy soil under citrus productions. *J. Environ. Qual.* 31:671-681.

Philip, J.R. 1974. Fifty years progress in soil physics. *Geoderma*, 12:265-280.

Phillips, F.M., J.L. Mattick, T.A. Duval, D. Elmore, and P.W. Kubik. 1988. Chlorine 36 and tritium from nuclear weapons fallout as tracers for long-term liquid and vapor movement in desert soils. *Water Resour. Res.* 24:1877-1891.

Pinner, A., and P.H. Nye. 1982. A pulse method for studying effects of dead-end pores, slow equilibration and soil structure on diffusion of solutes in soil. *J. Soil Sci.* 33:25-35.

Porro, I., P.J. Wierenga, and R.G. Hills. 1993. Solute transport through large uniform and layered soil columns. *Water Resour. Res.* 29:1321-1330.

Radulovich, R., and P. Sollins. 1987. Improved performance of zero-tension lysimeters. *Soil Sci. Soc. Am. J.* 51:1386-1388.

Rao, P.S.C., R.E. Jessup, and T.M. Addiscott. 1982. Experimental and theoretical aspects of solute diffusion in spherical and nonspherical aggregates. *Soil Sci.* 133:342-349.

Rao, P.S.C., D.E. Rolston, R.E. Jessup, and J.M. Davidson. 1980. Solute transport in aggregated porous media: Theoretical and experimental evaluation. *Soil Sci. Soc. Am. J.* 44:1139-1146.

Reynolds, E.R.C. 1966. The percolation of rainwater through soil demonstrated by fluorescent dyes. *J. Soil Sci.* 17:127-132.

Richards, L.A. 1931. Capillary conduction of liquids through porous mediums. *Physics* 1:318-333.

Richards, L.A. 1942. Soil moisture tensiometer materials and construction. *Soil Sci.* 53:241-248.

Richards, L.A., and W. Gardner. 1936. Tensiometers for measuring the capillary tension of soil water. *J. Am. Soc. Agron.* 28:352-358.

Russo, D. 1991. Stochastic analysis of simulated vadose zone solute transport in a vertical cross section of heterogeneous soil during nonsteady water flow. *Water Resour. Res.* 27:267-283.

Russo, D., and M. Bouton. 1992. Statistical analysis of spatial variability in unsaturated flow parameters. *Water Resour. Res.* 28:1911-1925.

Saffigna, P.G., C.B. Tanner, and D.R. Keeney. 1976. Non-uniform infiltration under potato canopies caused by interception, stemflow, and hilling. *Agron. J.* 68:337-342.

Scanlon, B.R. 1992. Evaluation of liquid and vapor water flow in desert soils based on chlorine 36 and tritium tracers and nonisothermal flow simulations. *Water Resour. Res.* 28:285-297.

Schwen, A., Y. Yang, and O. Wendroth. 2013. State-space models describe the spatial variability of bromide leaching controlled by land use, irrigation and pedologic characteristics. *Vadose Zone J.* doi:10.2136/vzj2012.0196.

Schwen, A., Yang, Y., Walton, R.J., Wendroth, O., 2012. A new experimental design reveals the impacts of land use and irrigation characteristics on bromide leaching. *Vadose Zone J.* 11 doi:10.2136/vzj2012.0077.

Shaffer, K.A., D.D. Fritton, and D.E. Baker. 1979. Drainage water sampling in a wet, dual-pore soil system. *J. Environ. Qual.* 8:241-246.

Shillito, R.M., D.J. Timlin, D. Fleisher, V.R. Reddy, and B. Quebedeaux. 2009. Yield response of potato to spatially patterned nitrogen application. *Agr. Ecosyst. Environ.* 129:107-116.

Shipitalo, M.J., W.A. Dick, and W.M. Edwards. 2000. Conservation tillage and macropore factors that affect water movement and the fate of chemicals. *Soil Till. Res.* 53:167-183.

Shipitalo, M.J., and W.M. Edwards. 1996. Effects of initial water content on macropore/matrix flow and transport of surface-applied chemicals. *J. Environ. Qual.* 25:662-670.

Shumway, R.H. 1988. Applied statistical time series analysis. Prentice Hall, Englewood Cliffs, NJ.

Shumway, R.H., and D. Stoffer. 1982. An approach to time series smoothing and forecasting using the EM algorithm. *J. Time Ser. Anal.* 3:253-264.

Shumway, R.H., and D. Stoffer. 2000. Time series analysis and its applications. Springer, New York.

Smith, S.J., and R.J. Davis. 1974. Relative movement of bromide and nitrate through soils. *J. Environ. Qual.* 3:152-155.

Sposito, G. 1986. The "physics" of soil water physics. *Water Resour. Res.* 22:83S-88S.

Starr, J.L., H.C. DeRoo, C.R. Frink, and J.Y. Parlange. 1978. Leaching characteristics of a layered field soil. *Soil Sci. Soc. Am. J.* 42:386-391.

Tamm, C.O., and T. Troedsson. 1957. A new method for the study of water movement in soil. *Geol. För. Stockholm Förh.* 79:581-587.

Timm, L.C., K. Reichardt, J.C.M. Oliveira, F.A.M. Cássaro, T.T. Tominaga, O.O.S. Bacchi, D. Dourado-Neto, and D.R. Nielsen. 2004. State-space approach to evaluate the relation between soil physical and chemical properties. *R. Bras. Ci. Solo* 28:49-58.

Trojan, M.D., and D.R. Linden. 1992. Microrelief and rainfall effects on water and solute movement in earthworm burrows. *Soil Sci. Soc. Am. J.* 56:727-733.

Vachaud, G., A. Passerat De Silane, P. Balabanis, and M. Vauclin. 1985. Temporal stability of spatially measured soil water probability density function. *Soil Sci. Soc. Am. J.* 49:822-828.

Van Alphen, B.J., and J.J. Stoorvogel. 2000. A methodology for precision nitrogen fertilization in high-input farming systems. *Precis. Agric.* 2:319-332.

Vanclooster, M., D. Mallants, J. Vanderborght, J. Diels, J. Van Orshoven, and J. Feyen. 1995. Monitoring solute transport in a multi-layered sandy lysimeter using time domain reflectometry. *Soil Sci. Soc. Am. J.* 59:337-344.

Van der Ploeg, R.R., and F. Beese. 1977. Model calculations for the extraction of soil water by ceramic cups and plates. *Soil Sci. Soc. Am. J.* 41:466-470.

Van Schilfgaarde, J. 1957. Approximate solutions to drainage flow problems. *In*: Luthin, J.N. (Ed.), Drainage of agricultural lands, Agron. Monogr., vol. 7. American Society of Agronomy, Madison, WI. pp. 79-112.

Van Wesenbeeck, I.J., and R.G. Kachanoski. 1990. Spatial scale dependence of *in situ* solute transport. *Soil Sci. Soc. Am. J.* 55:3-7.

Vinogradov, A.P. 1959. The geochemistry of rare and dispersed chemical elements in soil (2nd ed.). Consultants Bureau, Inc. New York.

Webster, R., and M.A. Oliver. 2001. Geostatistics for environmental scientists. Wiley & Sons, LTD, Chichester, England.

Weiler, M., and F. Naef. 2003a. An experimental tracer study of the role of macropores in infiltration in grassland soils. *Hydrol. Process.* 17:477-493.

Weiler, M., and F. Naef. 2003b. Simulating surface and subsurface initiation of macropore flow. *J. Hydrol.* 273:139-154.

Wendroth, O., S. Koszinski, and E. Pena-Yewtukhiv. 2006. Spatial association among soil hydraulic properties, soil texture, and geoelectrical resistivity. *Vadose Zone J.* 5:341-355.

Wendroth, O., S. Koszinski, and V. Vasquez. 2011a. Soil spatial variability. *In:* Huang, P.M., Y.C., Li, and M.E. Sumner (Eds), Handbook of soil science (2nd ed.). CRC Press, Boca Raton, FL. pp. 10.1-10.25.

Wendroth, O., A.M. Al-Omran, C. Kirda, K. Reichardt, and D.R. Nielsen. 1992. State-space approach to spatial variability of crop yield. *Soil Sci. Soc. Am. J.* 56:801-807.

Wendroth, O., W. Pohl, S. Koszinski, H. Rogasik, C.J. Ritsema, and D.R. Nielsen. 1999. Spatio-temporal patterns and covariance structures of soil water status in two Northeast-German field sites. *J. Hydrol.* 215:38-58.

Wendroth, O., H.I. Reuter, and K.C. Kersebaum. 2003. Predicting yield of barley across a landscape: a state-space modeling approach. *J. Hydrol.* 272:250-263.

Wendroth, O., E.L. Ritchey, S. Nambuthiri, J.H. Grove, and R.C. Pearce. 2011b. Spatial variability of soil physical properties. *In:* Gliński, J., J. Horabik, and J. Lipiec (Eds.), Encyclopedia of agrophysics. Springer, Heidelberg, Germany. pp. 827-839.

Wendroth, O., V. Vasquez, and C.J. Matocha. 2011c. Field experimental approach to bromide leaching as affected by scale-specific rainfall characteristics. *Water Resour. Res.* 47 W00L03, doi: 10.1029/2011WR010650.

Whetter, D.A., P.R. Bullock, and R.G. Eilers. 2006. Long-term solute redistribution in relation to landscape morphology and soil distribution in a variable glacial till landscape. *Can. J. Soil Sci.* 86:827-840.

White, R.E., J.S. Dyson, Z. Gerstl, and B. Yaron. 1986. Leaching of herbicides through undisturbed cores of a structured clay soil. *Soil Sci. Soc. Am. J.* 50:277-283.

Yates, S.R., and A.W. Warrick. 2002. Geostatistics. *In:* Dane, J.H., and G.C. Topp (Eds.), Methods of soil analysis, Part 4. Physical methods. SSSA Book Series, no. 5. Madison, WI. pp. 81-118.

Yang, Y., and O. Wendroth. 2014. State-space approach to analyze field-scale bromide leaching. *Geoderma* 217-218:161-172.

Yang, Y., O. Wendroth, and R.J. Walton. 2013. Field-scale bromide leaching as affected by land use and rain characteristics. *Soil Sci. Soc. Am. J.* 77:1157-1167.

Vita

Yang Yang

EDUCATION

M.S. in Physical Geography, Beijing Normal University, Beijing, China, Jun. 2010

B.S. in Geography, Beijing Normal University, Beijing, China, Jun. 2007

RESEARCH EXPERIENCE

Aug. 2010-Present: Research Assistant, Department of Plant and Soil Sciences, University of Kentucky, Lexington, KY

Feb. 2008-Jun. 2008: Teaching Assistant, School of Geography, Beijing Normal University, Beijing, China

AWARDS

2013 Doyle E. Peaslee Outstanding Graduate Student Award, Department of Plant and Soil Sciences, University of Kentucky

2013 1st Place at the First Graduate Student Mini-Symposium, Department of Plant and Soil Sciences, University of Kentucky

PUBLICATIONS

Yang, Y., O. Wendroth, and R.J. Walton. 2014. Field-scale water and bromide transport during and after simulated rainfall. *Soil Sci. Soc. Am. J.* (Under Review)

Wendroth, O., **Y. Yang**, and L.C. Timm. 2014. State-space analysis in soil physics. *In*: Application of soil physics in environmental analysis: Modeling and data integration. Springer, New York. (Accepted)

Yang, Y., and O. Wendroth. 2014. State-space approach to analyze field-scale bromide leaching. *Geoderma* 217-218:161-172.

Yang, Y., Z. Ye, B. Liu, X. Zeng, S. Fu, and B. Lu. 2014. Nitrogen enrichment in runoff sediments as affected by soil texture in Beijing mountain area. *Environ. Monit. Assess.* 186:971-978.

Schwen, A., **Y. Yang**, and O. Wendroth. 2013. State-space models describe the spatial variability of bromide leaching controlled by land use, irrigation and pedologic characteristics. *Vadose Zone J.* doi:10.2136/vzj2012.0196.

Yang, Y., O. Wendroth, and R.J. Walton. 2013. Field-scale bromide leaching as affected by land use and rain characteristics. *Soil Sci. Soc. Am. J.* 77:1157-1167.

Gao, X., **Y. Yang**, Z. Liang, and J. Zheng. 2013. A comparison of three indophenol blue methods for measuring ammonium in five types of soils in China. *Adv. Mat. Res.* 634-638:59-63.

Schwen, A., **Yang, Y.**, Walton, R.J., Wendroth, O., 2012. A new experimental design reveals the impacts of land use and irrigation characteristics on bromide leaching. *Vadose Zone J.* 11 doi:10.2136/vzj2012.0077.

Liu, B., and **Y. Yang**. 2012. Soil water erosion. *In:* Wu, Y., R. Lu, and B. Liu (Eds.), Physical geography. Beijing Normal University Publishing Group, Beijing, China. pp. 387-409. (In Chinese)

Gao, X., **Y. Yang**, J. Han, and H. Yang. 2011. A comparison of two analytical methods for measuring nitrate in five types of soils in China. *Adv. Mat. Res.* 233-235:809-812.

PRESENTATIONS AT SCIENTIFIC CONFERENCES

Yang, Y., O. Wendroth, and R.J. Walton. 2014. Field-scale water and bromide transport during and after irrigation. W-2188 Soil Physics Technical Committee Annual Meeting, Jan. 2-4, Las Vegas, NV.

Wendroth, O., R.J. Walton, and **Y. Yang**. 2013. Spatial range of representativity complements physical sphere of influence of soil water content sensor in spatially variable field soils. ASA, SSA, CSSA Annual Meeting, Nov. 3-6, Tampa, FL.

Yang, Y., O. Wendroth, and R.J. Walton. 2013. Field-scale bromide leaching as affected by land use and rainfall characteristics. ASA, SSA, CSSA Annual Meeting, Nov. 3-6, Tampa, FL.

Wendroth, O., **Y. Yang**, and A. Schwen. 2013. Space-time processes of water and solute transport at different scales. 10th Annual Meeting Asia Oceania Geosciences Society, Jun. 24-28, Brisbane, Australia.

Yang, Y., and O. Wendroth. 2013. State-space approach to describe bromide leaching at a field scale. S-1048 Southern Regional Soil Physics Project Annual Meeting, May 22-24, Lexington, KY.

Wendroth, O., and **Y. Yang**. 2013. State-space analysis in soil physics. Invited keynote presentation, 2nd Brazilian Soil Physics Meeting, May 6-10, Rio de Janeiro, Brazil.

Wendroth, O., **Y. Yang** and A. Schwen. 2013. Frequency domain approach for scale-dependent design and analysis of agricultural experiments, Invited keynote presentation at DAGSTAT (German Society for Statistics), Annual Meeting at University of Freiburg, Mar. 18-22, Freiburg, Germany.

Yang, Y., O. Wendroth, and R.J. Walton. 2012. Spatial variability of soil moisture and its correlation with soil texture as affected by land use. ASA, SSA, CSSA Annual Meeting, Oct. 21-24, Cincinnati, OH.

Schwen, A., **Y. Yang**, R.J. Walton, and O. Wendroth. 2012. State-space modeling allows the separation of small- and large-scale variability components of a field solute leaching experiment. ASA, SSA, CSSA Annual Meeting, Oct. 21-24, Cincinnati, OH.

Schwen, A., **Y. Yang**, R.J. Walton, and O. Wendroth. 2012. Separating small- and large-scale variability components of solute leaching using state-space modeling. 2nd International Conference on Hydropedology, Jul. 22-27, Leipzig, Germany.

Yang, Y., and O. Wendroth. 2011. Spatial variability of wet-range soil hydraulic conductivity as affected by land use. ASA, SSA, CSSA Annual Meeting, Oct. 16-19, San Antonio, TX.

GRANTS

Field-scale Water and Bromide Transport as Affected by Land Use and Rainfall Characteristics. Mar. 2012- Feb. 2013, $5,000

Sponsor: Kentucky Water Resources Research Institute (KWRRI) 104b Student Research Enhancement Project

Investigators: Ole Wendroth (PI), **Yang Yang** (Co-PI)